NTNU

Norwegian University of
Science and Technology

Application of Inviscid Flow CFD for prediction of Motions and Added Resistance of Ships

Jørgen Rørvik

Marine Technology
Submission date: June 2016
Supervisor: Sverre Steen, IMT
Co-supervisor: Jarle Andre Kramer, IMT

Norwegian University of Science and Technology
Department of Marine Technology

NTNU Trondheim
Norwegian University of Science and Technology
Department of Marine Technology

MASTER THESIS IN MARINE TECHNOLOGY

SPRING 2016

FOR

Jørgen Rørvik

Application of inviscid numerical wave tank to prediction of motions and added resistance of ships

It is important to be able to compute the added resistance due to waves on a ship for many reasons, such as calculation of sea margin and dimensioning of propulsion system, optimization of hull form for performance in a seaway, routing studies and much more. Current simplified methods, like the ones found in the ShipX package, give fairly reliable estimates in head seas, but they don't take the above-water geometry into account, making proper hull optimization studies impossible, and they aren't very reliable in following waves. URANS CFD methods give generally better results, but they are very resource-intensive, and not practically applicable for irregular waves, due to extremely long computation time.

The objective of the Msc-thesis shall be to investigate how well the motions and added resistance can be predicted by using URANS CFD without taking viscous effects into account, and to estimate the savings of computational time relative to similar calculation including viscous flow effects. Although it is expected that, due to the available time and validation material, the study will be limited to head seas and to a single ship geometry, the validity of conclusions for other ship designs and other headings shall be discussed.

In the thesis the candidate shall present his personal contribution to the resolution of problem within the scope of the thesis work.

Theories and conclusions shall be based on mathematical derivations and/or logic reasoning identifying the various steps in the deduction.

The thesis work shall be based on the current state of knowledge in the field of study. The current state of knowledge shall be established through a thorough literature study, the results of this study shall be written into the thesis. The candidate should utilize the existing possibilities for obtaining relevant literature.

The thesis should be organized in a rational manner to give a clear exposition of results, assessments, and conclusions. The text should be brief and to the point, with a clear language. Telegraphic language should be avoided.

The thesis shall contain the following elements: A text defining the scope, preface, list of contents, summary, main body of thesis, conclusions with recommendations for further work, list of symbols and acronyms, reference and (optional) appendices. All figures, tables and equations shall be numerated.

NTNU Trondheim
Norwegian University of Science and Technology
Department of Marine Technology

The supervisor may require that the candidate, in an early stage of the work, present a written plan for the completion of the work. The plan should include a budget for the use of computer and laboratory resources that will be charged to the department. Overruns shall be reported to the supervisor.

The original contribution of the candidate and material taken from other sources shall be clearly defined. Work from other sources shall be properly referenced using an acknowledged referencing system.

The thesis shall be submitted electronically (pdf) in DAIM:

- Signed by the candidate
- The text defining the scope (signed by the supervisor) included
- Computer code, input files, videos and other electronic appendages can be uploaded in a zip-file in DAIM. Any electronic appendages shall be listed in the main thesis.

The candidate will receive a printed copy of the thesis.

Supervisor : Professor Sverre Steen
Co-supervisor : Jarle A. Kramer
Start : 18.01.2016
Deadline : 10.06.2016

Trondheim, 18.01.2016

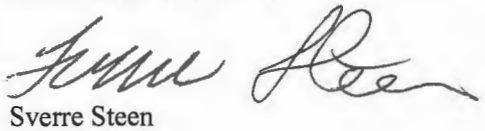

Sverre Steen
Supervisor

Preface

This thesis marks the end of my master degree study at the Norwegian University of Science and Technology (NTNU), where I have studied at the Department of Marine Technology for five years. Hydrodynamics, and especially in connection with ship design caught my interest early in the study. I also found computational fluid dynamics (CFD) very interesting since I first learnt about it in basic hydrodynamic courses. Being able to combine both CFD and ship hydrodynamics in one thesis with an interesting topic have been a great motivation.

Professor Sverre Steen have been an excellent supervisor for my master thesis. He have been very helpful and motivating. The weekly guidance have ensured good progress throughout the thesis.

The idea behind this thesis comes from Jarle Andre Kramer. He have been the co-supervisor of this thesis and I am glad I have been allowed to investigate his idea. Jarle Andre Kramer have also been very helpful when I have encountered problems with my CFD simulations.

Trondheim, 6/10/2016

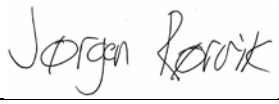

Jørgen Rørvik

Sammendrag

Skip opererer vanligvis I bølger, men likevel blir skipsskrog optimalisert for lavest mulig motstand i stille vann. En grunn til dette er at det er dyrt å gjøre nøyaktige beregninger av motstand på skip i bølger. Modeltest og URANS CFD er de mest nøyaktige metodene for beregning av tilleggsmotstand. URANS er best egnet for optimalisering av skrog design, og kan gi god nøyaktighet, men beregningskostnadene er veldig store.

Denne oppgaven undersøker om det er mulig å beregne tilleggsmotstanden på skip ved å benytte ikke-viskøs CFD kode. Det er en akseptert antakelse at viskositet har liten påvirkning på tilleggsmotstand. Det antas at det er mulig å redusere beregningstiden og samtidig beholde nøyaktigheten CFD beregning har ved å neglisjere viskositet.

Skipet KVLCC2 er brukt for simuleringene. KVLCC2 er en 320m langt VLCC som er utstrakt benyttet i forskning. Både EFD og CFD data er tilgjengelig for stillevann og regulære bølger. Sammenligningsdata benyttet i denne oppgaven er hovedsakelig hentet fra Göteborg 2010 workshop på numerisk skipshydrodynamikk (Larsson, Stern, & Visonneau, 2014).

En ikke-viskøs numerisk bølgetank ble satt opp i STAR CCM+. Tanken ble laget stegvis. En 2D tank ble brukt for å finne et egnet mesh for den frie væskeoverflaten slik at bølger ble korrekt simulert. En stillevannsberegning ble lignende brukt for å sette opp meshet slik at det fanger strømningene rundt skroget. Stillevannsberegningene ble kjørt både med og uten visksositet. Resultatet fra den viskøse beregningen stemte godt overens med resultater fra modelforsøk.

Meshet fra bølgetanken og stillevannsberegningen ble kombinert til en numerisk bølgetank. Både regulære og irregulære JONSWAP bølger ble testet i motsjø. Resultatet fra de regulære bølgene ble sammenlignet med resultater fra modeltest og viskøse CFD beregninger. Den totale motstanden i bølger ble funnet ved å legge sammen trykkmotstanden fra bølgesimuleringen med friksjons- og viskøs trykkmotstand fra viskøs stillevannsberegninger.

Den ikke-viskøse tanken ga resultater med same nøyaktighetsnivå som andre viskøse CFD beregninger sammenlignet mot model test resultater. Det ble gjennomført en sammenligning mellom visøks og ikke-viskøse beregninger med samme simuleringsoppsett i STAR CCM+. Forskjellen mellom disse simuleringene var mye lavere enn forskjellen mellom visøkse CFD beregninger og resultater fra modelforsøk.

Besparingspotensialet ved å benytte ikke-visøkse beregninger fremfor visøkse med en to-lignings turbulensmodell ble funnet til å være mellom 30 og 50 %, avhengig av meshet. Reduksjonen kommer fra to effekter. For det første blir ikke turbulens modelert for ikke-visøkse beregninger, og dermed reduseres antall ligninger som må løses for hver celle med to. For det andre så er det ikke noen grensesjikt som må løses, og dermed trengs det ikke et like fint mesh inntil skroget.

Antagelsen om at viskositet har liten påvirkning på tilleggsmotstanden ble undersøkt. Friksjonsmotstanden og den viskøse trykkmotstanden ble sammenlignet for en simulering i

stillevann og en simulering i bølger. Det ble observert at begge motstandskomponentene økte i snittverdi, samt at begge også oscilerte med møtefrekvensen mellom skipet og bølgene. Dette tyder på at tilleggsmotstand blir påvirket av viskøse effekter.

I denne oppgaven ble det kun gjort tester på et skrog i motsjø. Flere tester er nødvendig før man kan trekke en bred konklusjon. Bølger fra andre retninger kan gi nye utfordringer fordi flere frihetsgrader blir relevant. KVLCC2 er et stort skip, og mindre skip vil ha større relativ bevegelse. Store bevegelser kan skape ustabilitet i CFD beregningene, men kan også føre til fenomener som ikke blir observert på store skrog.

Summary

Ships usually travels in waves, but their hull is normally optimized for calm water. One reason for this is that it is expensive to do accurate calculation of resistance in waves. Model test and URANS CFD is the most accurate methods. URANS is most suited for hull optimization and can give accurate results, but the computational cost is very high.

This thesis investigates if it is possible to calculate the added resistance on ships by applying an inviscid CFD code. It is a commonly accepted fact that viscosity have little effect on added resistance. It is believed that neglecting viscosity can significantly reduce the computational power required to do added resistance calculations, while retaining the good accuracy of CFD calculations.

The ship KVLCC2 was used for simulations. KVLCC2 is a 320m long VLCC which is used extensively in research. Both EFD and CFD data is available for calm water and regular head waves. The comparison data used in this thesis is mainly from the Gothenburg 2010 workshop on ship hydrodynamics (Larsson et al., 2014).

An inviscid numerical wave tank simulation was set up in STAR CCM+. The tank were built stepwise. A 2D tank was used to find a good mesh for the free surface such that the waves were correctly simulated. Similarly, a calm water simulation were used to set up the mesh around the ship hull to correctly capture the flow around the ship. For the calm water resistance study, both viscous and inviscid solvers where used. The calm water resistance from the viscous simulation were compared with model tests data and a good agreement was found.

The meshes from wave tank and clam water resistance were combined into a numerical wave tank. Regular and irregular JONSWAP wave conditions were tested. The result from the regular head wave conditions were compared with model test and viscous CFD results. The total resistance in head waves was found by adding the pressure resistance from the wave simulation with the friction and viscous pressure resistance from the viscous calm water simulations.

The inviscid wave tank gave results with equal order of accuracy as other viscous CFD computations when compared against model test data. A comparison was made between the viscous and inviscid simulation with same simulation setup in STAR CCM+. The difference between these simulations were much lower than the difference between viscous CFD and EFD results.

Saving potential by applying inviscid calculations instead of viscous with a two-equation turbulence model found to be between 30 and 50 %, depending on the mesh. The reduction is due to two effects. First, the turbulence is not modeled for inviscid flow, and that reduce the amount of equations being solved in each cell by two. Secondly, there is no boundary layer so the fine mesh applied to capture the boundary layer can be neglected.

The validity of the assumption that viscosity has little effect on added resistance was investigated. The friction resistance and viscous pressure resistance for a ship in head waves

were compared against the same values for calm water. For both resistance components there was an increase in mean resistance, and both resistances oscillated with wave encounter frequency. This suggests that the added resistance due to waves is influenced by viscous effects.

This thesis only tested one hull geometry in head waves. More tests are necessary before a broader conclusion can be drawn. Oblique waves can give unseen challenges as additional degrees of freedom will be relevant. KVLCC2 is a large ship, and smaller ships will have larger relative motions. Large motions can cause stability problems in CFD, but might also cause phenomena not observed on the larger hull.

Contents

Abbreviations

1D	One dimensional
2D	Two dimensional
3D	Three dimensional
CFD	Computational fluid dynamics
DOF	Degrees of freedom
EFD	Experimental fluid dynamics
EMP	Eulerian multiphase
FFT	Fast Fourier transform
FVM	Finite volume method
GFM	Green function method
HRIC	High Resolution Interface Capturing
JONSWAP	Wave spectra developed by Joint North Sea Wave Observation Project
KCS	Container ship hull used for research
KVLCC2	Very large crude carrier hull used for research
LMP	Lagrangian multiphase
NWT	Numerical wave tank
RANS	Reynolds-averaged Navier–Stokes
RAO	Response amplitude operators
RSM	Rankine singularity method
SIMPLE	Semi-implicit method for pressure linked equations
STAR CCM+	CFD software developed by CD-adapco
TVD	Total variation diminishing

Nomenclature

R_{aw}	Added resistance due to waves
COG	Center of gravity
ω	Circular wave frequency
CFL	Courant–Friedrichs–Lewy condition
ΔX	Discretization size
f_e	Encoutner frequency
FP	Fore perpendicular
C_F	Friction resistance coefficient
Fn	Froude Number
L_{PP}	Length between perpendiculars
γ	Phase
C_{PV}	Pressure resistance coefficient
R	Resistance force
U	Ship velocity
H_S	Significant wave height
S	Spectral density
ΔT	Time step
C_T	Total resistance coefficient
ω-ε	Turbulent frequency and dissipation rate
k-ε	Turbulent kinetic energy and dissipation rate
u	velocity component
V	Velocity vector
μ	viscosity
ρ	Water density
λ	Wave length
T_P	Wave peak period

1 Introduction

Ships operates in wave conditions most of their time, but ships are mainly optimize for calm water resistance. There is many factors influencing this, but one major is the lack of accurate and efficient calculations of resistance in waves. An increasing focus on more environmental friendly shipping pushes hull designers to further decrease ship resistance, and with that pollution. The improvement potential in calm water resistance is reducing and many sees towards optimization of hulls with respect to added resistance as a next step.

Added resistance in wave is of importance also when planning operational routes. Can fuel consumptions be reduced by choosing a longer route with less waves, or waves from a different direction? To answer this question, accurate added resistance calculations for a wide specter of waves and wave directions is needed.

There is many different methods for calculating added resistance. Strip theory is much used, but it has weakness that it is quite inaccurate in oblique waves and it does not take over-water geometry into account. Unsteady computational fluid dynamics (CFD) simulations can compute added resistance with good accuracy, but each simulation is very computational demanding and a lot of simulations is required to calculate added resistance for different waves and headings.

The idea that will be investigated in this thesis is if it is possible to reduce computational time for added resistance calculations by CFD without losing accuracy by assuming inviscid fluid. It is a commonly accepted assumption that viscosity has little effect on the added resistance, and that pressure forces dominates.

> *'From the practical point of view, the added resistance in waves can be considered a non-viscous phenomenon, almost produced by potential effects such as inertial and wave phenomena'*

(Pérez Arribas, 2007)

An investigation of the currently available methods for calculation of added resistance have been performed. It is important to know what have been previously done on the field, such that the same work is not repeated. Knowing about the capabilities and restrictions of other available methods is necessary to evaluate the performance of a new method.

Multiple CFD calculations of ship in an inviscid numerical wave tank (NWT) have been performed to investigate the effect of excluding viscosity. The main data for comparison that have been used is from the Gothenburg 2010 workshop on Numerical Ship Hydrodynamics (Larsson et al., 2014). The calculations have been performed on KVLCC2, which is a 320m long very large crude carrier hull.

Reduction of computational time while maintaining accuracy is the objective. The relative reduction of computational time that is achievable by assuming inviscid fluid is estimated. The validity of this assumption is discussed based on observation in CFD simulations.

2 State of the art study of added resistance calculations

The state of the art study in chapter 2 is originally work performed in the project thesis with some modifications.

2.1 Added resistance

Added resistance due to waves is an increased resistance that occurs on ships in seaways. It is defined as the difference between the mean resistance in calm water and the resistance in waves. The required additional power to maintain speed in waves is called Sea Margin. A common estimate of this margin is 15-30% of calm water power(Pérez Arribas, 2007).

Added resistance, as explained by Pérez Arribas (2007), is due to the energy supplied from the ship to the water. Classical sea keeping divides the effect of added resistance into three main contributors:

- Drifting force
- Diffractions effect
- "Viscous" effect due to damping of vertical motions

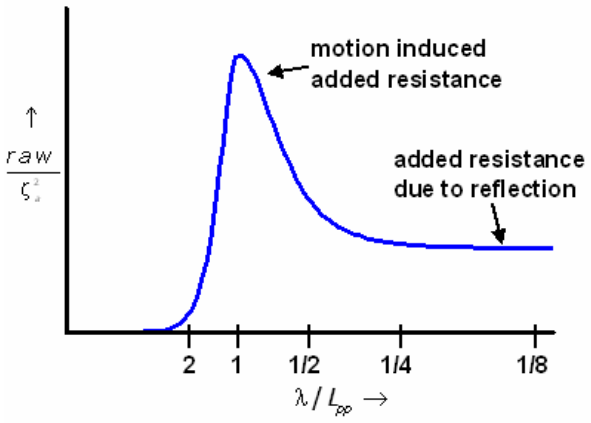

Figure 1 - Added resistance contributors. (van den Boom, van der Hout, & Flikkema, 2008)

Motion induced added resistance is dominating for wave with length about equal to the ship length. This is due to large ship motions. Pitch resonance often occurs at these wave lengths. For shorter waves, there is little to no motions. Then the reflected waves (diffraction) dominates the added resistance. For long waves, the ship do not feel the waves, and is commonly illustrates as a cork floating in waves. This results in low added resistance.

The added wave resistance is according to Gerritsma and Beukelman (1972) proportional to wave amplitude squared. This express the importance of correct modeling of incident waves when doing added resistance calculations. Added resistance is highly dependent on the bow geometry, also the part above mean waterline. For accurate calculations the details of the bow must be taken into consideration.

Head sea waves is traditionally considered the worst condition, and is by far the most investigated condition. Model test experience of oblique wave requires specialized tank, and this have resulted in that a majority of available test results are head (or following) waves only. Calculations in oblique waves is also more demanding because more effects is of relevance such as roll damping.

Bertram and Couser (2014) claims that head sea ways should not in general be assumed most critical. 3D Reynold-averaged Navier Stokes (RANS) calculations on container ships have shown that oblique waves 10°-20° off head waves give more added resistance than head waves.

2.2 Calculations of added resistance

There is three main methods to calculate added resistance on a particular hull. These are experimental, empirical and numerical/theoretical methods.

2.2.1 Experimental methods

A model scale of the ship hull is towed in a tank with waves and in calm water. The difference between mean calm water resistance and resistance in wave is added resistance. This is an extensive test that requires many runs for different conditions. Regular towing tanks with wave-maker and wave-beach could be used, but is then limited to head and following waves. Special facilities exist which can perform experiments in all wave-directions, like the ocean basin at MARINTEK. These test are very expensive and is not commonly performed for commercial ships. Model tests is considered to have the highest accuracy and result from model test is used for verification of other calculation methods.

2.2.2 Empirical methods

There exists many empirical methods for estimation of added resistance. Most of them are based on experimental data from towing tanks. A very simple empirical method is Kreitner (1939), formula (1).

$$R_{aw} = 0.64 g H_s^{\,2} B^2 C_B \rho \frac{1}{L_{wl}} \left(\frac{2}{3} + \frac{1}{3} \cos \beta \right) \tag{1}$$

H_s is significant wave height, B is ship beam, C_B is the block coefficient, ρ is water density, L_{wl} is length in water line and β is the wave encounter angle. All these parameters can be determined in an early design phase, and this have made this formula a popular first estimator.

The accuracy is naturally quite low, when the added resistance is computed based on only a few design parameters. Bertram and Couser (2014) compared Kreitner's empirical method with more accurate CFD calculations on a container ship and found differences of 20-110%.

More recently the Sea Trail Analysis Joint Industry Project (STA-JIP) published two new method to empirical estimate the added resistance of ships on sea trial. These methods are based on model test data from MARIN's Seakeeping and Manoeuvring Basin. The first one is called STAWAVE1 and was developed for trail conditions, which mean mild waves on large ships. At

these conditions only wave reflections is of importance, and this is the only contribution in this calculation method. The parameters used in STAWAVE1 is length of bow section of the ship and the wave height and direction.

The other method suggested by (van den Boom et al., 2008) was STAWAVE2. This method is developed for swell conditions and conditions where the waves are relative long. This method includes both motion induced added resistance and wave reflection added resistance. 'For this method the input should be the wave period, height and direction as well as some ship geometry'(van den Boom et al., 2008). van den Boom et al. (2008) claims that 'The STAWAVE1 and STAWAVE2 method for correcting speed trials for added resistance in waves show great improvement compared to existing methods.' Both of the STAWAVE methods are included in the ISO standard 'Guidelines for the assessment of speed and power performance by analysis of speed trial data' (ISO, 2015) as simplified correction methods for added resistance.

2.2.3 Numerical methods

The first major development of numerical methods started with the potential theory methods in the 1960s. A rapid development throughout the next decades established an efficient way to calculate added resistance of ships. Two branches of methods evolved, with quite different perspective.

2.2.3.1 Far field method

The first branch of methods for calculation of added resistance is far-field methods. These methods considers conservation of diffracted and radiated wave energy and/or momentum flux by considering the velocity potential far away from the ship. Maruo (1957) applied momentum conservation to formulate a method of calculating added resistance. This method has been further elaborated. Joosen (1966) expanded Maruo's formula and included encounter frequency.

Gerritsma and Beukelman (1972) derived formula for added resistance in waves by considering energy of radiated damping wave due to ship motion. The method itself is quite simple, but it requires known ship motions and sectional damping coefficient. The added resistance in their formula varies with V_{za}^2 ,which is the amplitude of vertical relative water velocity This amplitude is proportional to the wave height, and thus added resistance is dependent on the wave amplitude squared.

2.2.3.2 Near field method

Another branch of methods is the near field methods. These methods integrating pressure directly over the wetter surface to find the added resistance. This technique is easy to physically comprehend (Faltinsen, Minsaas, Liapis, & Skjørdal, 1980), while it can be quite difficult to calculate. The accuracy of these methods is very dependent on how fine the bow geometry is resolved, and too coarse grid is suspected to cause errors (Bertram & Couser, 2014). Faltinsen et

al. (1980) derived a direct pressure integration. This method uses the first order velocity potential to integrate the Bernoulli pressure over the instantaneous wetted surface.

2.2.3.3 Strip theory for ship motion calculation

Accurate motion calculations is needed for all the previous mentioned methods. The STF strip method proposed by Salvesen, Tuck, and Faltinsen (1970) made it possible to calculate ship motions with good accurate. Strip theory simplifies the 3D flow problem into many 2D problems by dividing the ship into multiple 2D ship sections (Figure 2). This assumes that the ship is slender, such that the flow variations in cross-sectional planes is much larger that the variation in longitudinal direction (Faltinsen, 1990).

For each section hydrodynamic characteristics such as added mass and damping coefficients are calculated. These was traditionally calculated by close fit conformal mapping (Salvesen et al., 1970), but other methods could be used (Pérez Arribas, 2007). The 3D hydrodynamic coefficients are considered to be the integrated 2D coefficients. Similarly the excitation forces is also calculated for each strip and integrated to find the 3D value. Newton 2nd is then used to calculate the motions of the ship.

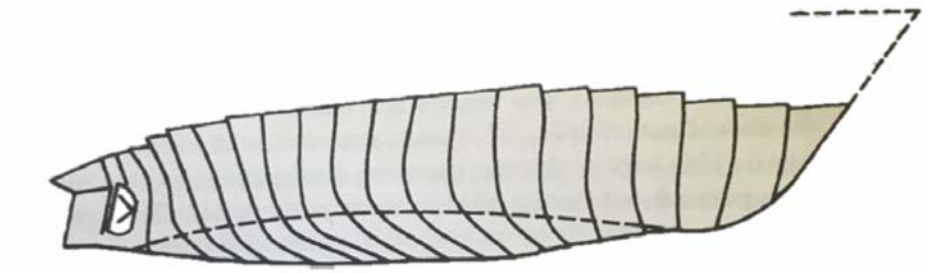

Figure 2 - Ship divided into sections for calculation with strip theory. Fig. 3.7 from (Faltinsen, 1990)

Strip theory is implemented in many software codes, and is according to Bertram and Couser (2014) still the most popular approach for seakeeping problems. Special versions have been developed to also support high-speed vessels with Froude number exceeding the limit of 0.4 from the original strip theory. Other specialized versions are multihull and non-linear for extreme motions.

2.2.3.4 Panel methods

A more comprehensive set of methods for motion calculations is the panel methods. These methods discretizes the body surface into 3D panels. Each panel has a source with strength calculated to maintain body boundary conditions. Two different panel methods exists. The simplest, in terms of source, is the Rankine singularity method (RSM). This method also requires that the free surface is discretized by panels. Another method is the Green function method (GFM). This have a more advance source term, but have the benefit of not having to discretize the free surface.

Panel methods is usually applied for time domain simulations, but could also be used in frequency domain or hybrid. A large amount of studies have investigated near field, radiated energy and far field methods by applying panel methods. In general, they are able to reasonable predict the added resistance quite good compared with model tests.

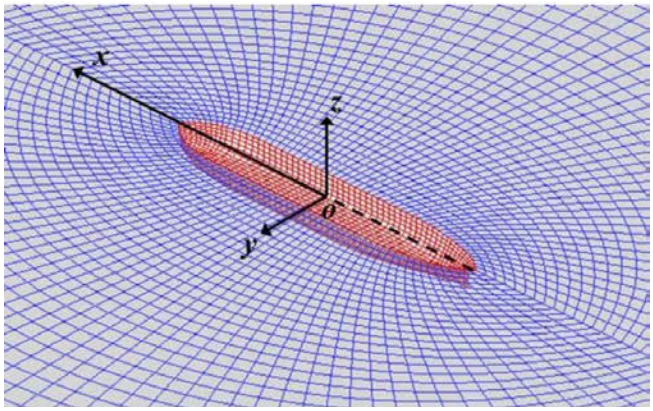

Figure 3 - Rankine panel method mesh. (Seo, Park, Yang, & Kim, 2013)

2.2.3.5 Short waves

In waves with wave lengths shorter than half the ship length ($\lambda/L_{PP} < 0.5$) diffraction force dominates. Ship motions is negligible, and that results in low accuracy for the previous mentioned methods, which is highly dependent on ship motions. Also model test have difficulties measuring added resistance in short waves (B. Guo & Steen, 2010).

Faltinsen et al. (1980) also proposed a method to estimate the resistance in short waves. They assumed and low ship speed ($Fn < 0.2$) and blunt ship forms. The added resistance is considered only due to full wave reflection. The drift force component is integrated over the non-shadowed part of the water line curve. This formula gives an asymptotical value for the added resistance.

Bertram and Couser (2014) presents internal development of the software GL Rankine, which is a 3D RSM. Their code uses semi-empirical methods to extrapolate added resistance for short wave lengths, down to $\lambda/L_{PP} < 0.1$. This gave fairly good agreement with experiments.

B. Guo and Steen (2010) applied a blending of the asymptotic value from Faltinsen et al. (1980) with far field method of Gerritsma and Beukelman (1972) to calculate added resistance for all wave lengths. They compared calculated results with model test data for KVLCC2 and found good agreement for all wave lengths.

2.2.4 Reynolds-Average Navier-Stokes solvers

As computational power is becoming cheaper, the amount of CFD calculations for sea-keeping problems including added resistance has increased. Due to the nature of CFD, the velocity and pressure is calculated everywhere in the fluid. This makes it easy to calculate the resistance on a hull by integrating pressure and friction. Some specific marine challenges had to be overcome to apply CFD to seakeeping and added resistance problems. The main challenge is the free surface.

Special methods have to be applied to track the surface between air and water, and more details on these is found in chapter 3.1.

There have been arranged multiple workshops on ship hull CFD calculations. Added resistance have been a topic at Gothenburg 2010 and Tokyo 2015 workshop. The results from Tokyo 2015 is not yet published. For Gothenburg 2010 (Larsson et al., 2014) test cases was given before the conference. Two of these included added resistance (KCS,KVLCC2) in regular head waves with and without forward speed. Participants presented their results from CFD calculations and model test, and results were compared.

The error for added resistance was in investigated with respect to 0^{th} harmonic, first harmonic and phase(Stern, Sadat-Hosseini, Mousaviraad, & Bhushan, 2014). There is a large variation in how accurate participants have calculated added resistance. The average error for 0^{th} harmonic resistance is 18 % off experimental, while first harmonic was 34 % of experimental.

2.2.5 Euler equation solvers

Added resistance have been calculated by solving the Euler and continuity equation (Yang, Kim, & Nam, 2015). Euler equation is a non-viscous version of the Navier Stokes equation. Yang et al. (2015) applied finite volume method (FVM) to a structured grid. The solid geometry, water and air is distinguished by using volume fraction functions. They calculate the position of the solid body with a level set function. This means that the grid is not directly dependent on the ship geometry, but the geometry is represented as a solid phase. This method is called Cartesian grid method, and is commonly applied in simulations with moving solids. Yang et al. (2015) applied a semi-Lagrangian method to capture free surface. This method is called tangent of hyperbola for interface capturing (THINC).

2.3 Discussion

The most accurate method of calculating added resistance is model test. Stern et al. (2014) compared the model test data for the seakeeping tests presented at Gothenburg 2010 workshop, and calculated the experimental uncertainty. For added resistance the uncertainty was 1.9 % for 0^{th} harmonic amplitude, and 21.5 % for 1^{st} harmonic amplitude. This is much lower than what is possible to achieve with the other methods.

The easiest method calculate added resistance is the empirical methods. One benefit with these methods is that no detailed hull designed is needed to estimate added resistance, just main characteristics. This allow the method to be used in very early design. This is also largest disadvantage for these methods, as they cannot be used to study hull details.

Grin (2015) compares the results obtained with STAWAVE2 method and two other empirical methods with an extensive amount of model tests. The comparison reveals that there is a relative large uncertainty between estimated and measured added resistance.

‘ All three empirical methods show relatively large scatter; this might be explained by the fact that they predict added resistance with only five or six ship parameters without accounting for the actual hull lines.’

(Grin, 2015)

Potential theory methods was compared by Pérez Arribas (2007). He implemented the momentum and energy method, integrated pressure method and radiated energy method with a strip theory method and verified them against model tests. His findings was that the momentum and energy method was robust, but tended to go to zero for short waves due to diffractions effects not being considered. The integrated pressure method estimated well, but could over-estimate at peak value, especially with high Froude numbers. Radiated energy was considered perhaps the better method. It also estimated well, but instabilities was noted for short waves. Calculations of radiated energy method was found to be strongly influenced by calculation of relative motions.

Pérez Arribas (2007) generally suggest to apply integrated pressure or radiated energy method, and apply the one that is most stable for short waves. Pérez Arribas (2007) also concludes that the more accurate prediction of vertical motions is more important than developing more sophisticated added resistance theories.

In a comparative study by Seo et al. (2013), this inviscid Cartesian grid method, two strip theory methods, two Rankine panel methods, formulas for short waves and experimental results in head sea waves was compared. Their comparison of added resistance by 3D panel methods against strip theory methods shows that 3D panel methods is better at predicting the frequency of peak added resistance. It is also noticed that 3D panel methods in general better predicts added resistance than strip theories, especially in short waves.

Comparison of Rankine panel method and Cartesian grid method by Seo et al. (2013) concludes that for blunt ships (KVLCC2) both Rankine panel method and Cartesian grid method gave accurate added resistance. For slender bodies (S175), the Cartesian grid method calculated added resistance with better accuracy then the panel method if high grid resolution was applied.

Stern et al. (2014) concludes after the Gothenburg 2010 workshop that RANS methods is superior to potential flow methods for calculations of added resistance. Note that the shortest waves compared was $\lambda/L_{PP} = 0.6$.

‘The 0^{th} harmonic of the resistance (and added resistance) is predicted by about 18%D for URANS compared to 24% for potential flow for all the wavelengths. Therefore, URANS showed capability for a wide range of head wave conditions covering short, medium and long waves, small and large amplitude waves and including global and local flow variables.’

(Stern et al., 2014)

Short waves have given problems for potential theories. Seo et al. (2013) concludes that short wave formulas in general correctly calculates added resistance for blunt ships, but only one of the investigated formulas accurately calculated added resistance for a slender ship. To achieve a complete series of added resistance, including all wave lengths from very short to very long, it seems like blending or extrapolating can give good results(Bertram & Couser, 2014; B. Guo & Steen, 2010).

RANS methods have different models for modeling free surface. Both VOF and level set methods give equally good results(ITTC, 2011), and the choice of which is used is often decided by which method is available for applied CFD solver. Wave-generation is dependent on which method used for surface modeling. For VOF waves and seakeeping problems, momentum source is a good method (B. Guo & Steen, 2011). Turbulence models applied for seakeeping problems is usually the 2 equation k-ω which accurately predicts ship hydrodynamics (ITTC, 2011). k-ω methods was by far the most used method in Gothenburg 2010 workshop (Larsson et al., 2014).

Computational time for RANS methods is very high. High performance computers is required for complete simulations of added resistance at different waves and directions. In comparison, panel methods can solve the same problem in a few hours on a desktop computer, while strip theory only uses a couple of minutes. The constant evolution in computer hardware will continue to reduce computational time also for RANS methods.

3 Methodology for inviscid numerical wave tank

3.1 Theory of NWT

Some of chapter 3.1 is original work from the project thesis. Additions and modifications have been added. It is estimated that half of the chapter is work from project thesis and half from the master thesis.

3.1.1 Physical assumptions

The basis of this thesis follows the assumptions that added resistance due to waves is independent on viscosity. This allows for simplified calculations when only added resistance and not total resistance is of interest. If added resistance is independent on viscosity it should also be possible to find the total resistance in wave by adding the calm water resistance due to viscosity to the inviscid resistance in head waves. As the ship operates on water, we also assume incompressible fluid.

3.1.2 Governing equations

The governing equation of fluid mechanics is the Navier Stokes equations. Navier Stokes includes continuity equation(2) and momentum equation (3).

$$\frac{\partial \rho}{\partial t} + \nabla \cdot \left(\rho \mathbf{V} \right) = 0 \tag{2}$$

$$\rho \frac{D\mathbf{V}}{Dt} = \rho \mathbf{f} - \nabla p + \frac{\partial}{\partial x_j} \left[\mu \left(\frac{\partial u_i}{\partial x_j} + \frac{\partial u_j}{\partial x_i} \right) - 2\delta_{ij} \mu \frac{\partial u_k}{\partial x_k} \right] \tag{3}$$

Since the fluids are considered incompressible, the continuity equations can be written as (4). The momentum equations can also be rewritten by ignoring viscous terms (5). This equation was first derived by Euler in 1755, and is known as the Euler's equation. These are the two governing equations for the inviscid wave tank.

$$\nabla \cdot \left(\rho \mathbf{V} \right) = 0 \tag{4}$$

$$\rho \frac{D\mathbf{V}}{Dt} = \rho \mathbf{f} - \nabla p \tag{5}$$

3.1.3 Discretization of the Euler equation

The Euler equation (4),(5) have both time derivatives and space derivatives. The equation is discretized on a finite volume mesh. There exists a large number of different schemes. They are characterize by what derivative their solve, the order of accuracy, stability criteria and other properties such as total variation diminishing (TVD). The order of accuracy defines the rate of convergence for a discretization scheme. A n'th order scheme has an error proportional to the discretization variable h to the power of n (6).

$$E = O\left(h^n\right) \tag{6}$$

3.1.4 Discretization of time derivatives

Wave-tank is an unsteady problem, which mean the solution will vary in time. Solutions in time can be found either by explicit or implicit methods. The difference between these methods is that an explicit method uses only values at old time level to calculate at new time level. This simplifies calculations a lot, as values can be computed directly, and no system of equations is needed. Explicit methods weakness is that they have strict stability requirements regarding time step. If this is violated, the solution becomes unstable.

Implicit calculations uses values at new time level to compute at new time level. To manage this a system of equations have to be solved. This require a more advanced solver. The huge benefit is that implicit methods generally is unconditional stable. Good solvers such as the multi-grid type solvers can also solve the system of equations with floating points operations (FLOPS) of order n, where n is number of grid points. This is of the same order as the explicit methods. STAR CCM+ have two implicit temporal discretization scheme, which is first order Euler and second order time discretization (CD-adapco, 2016b). In this thesis the first order scheme is used for calm water simulations, as these simulations are steady. Second order is applied for wave conditions to reduce the amount of wave damping. Higher order schemes is used in other codes for NWT simulations.

3.1.5 Discretization of space derivatives

The convection is calculated at cell faces for a finite volume mesh. Relevant schemes for discretization of the convection terms are first and second order upwind schemes, third order MUSCL scheme and higher order schemes. STAR CCM+ supports first and second order upwind and third order MUSCL, but other codes might use schemes of higher order such as fifth order WENO scheme for NTW simulations.

In a NWT it is important to have a low discretization error to reduce the amount of numerical wave damping. The first order upwind scheme is known to be dissipative. For a steady state simulation, the first order could be beneficial due to faster convergence, but for unsteady simulations as in a NWT, the numerical damping is too big. Second order upwind have much less numerical dissipation. In the project thesis (Rørvik, 2015) the second order upwind scheme was used, and it proved to give satisfactory results for practical applications in a NWT. The second order upwind scheme is applied for all simulations in this thesis.

Some methods have the benefit of being TVD. This means that the scheme is preserving the monotonic of the variable. The MUSCL scheme by van Leer (1979) has this feature. The ENO scheme (Harten, Engquist, Osher, & Chakravarthy, 1987) and the improved WENO scheme uses stencils to construct the variation of variable through the cell based on known values at face. ENO choose the smoothest stencil possible, while WENO weights all possible stencils. Both these schemes is essentially non-oscillatory, and that is how they got their name.

3.1.6 Pressure velocity coupling

Solving the Navier-Stokes equation, or in this case the Euler equation is difficult due to no independent equation for the pressure. In 3D we have three momentum equations and one continuity equation, and three unknown velocities and unknown pressure. This gives four equations with four unknowns. The problem is that when incompressible fluid is assumed, there is no pressure term in the continuity equations.

This problem can be solved in multiple ways, but the most common is coupling the pressure and velocity by combining the momentum equations and the continuity equation to form a pressure equation (Ferziger & Peric, 2012). In cartesian coordinates with constant pressure and no viscosity the pressure correction equation can be written as an Poisson equation(7).

$$\frac{\partial}{\partial x_i}\left(\frac{\partial p}{\partial x_i}\right) = -\frac{\partial}{\partial x_i}\left[\frac{\partial\left(\rho u_i u_j\right)}{\partial x_j}\right] \tag{7}$$

Iterative schemes have been developed to solve the pressure velocity coupling. A much used algorithm is the semi-implicit method for pressure linked equations (SIMPLE) by S. V. Patankar and Spalding (1972). This method iterates with a 'guess-and-correct' approach (Pletcher, Tannehill, & Anderson, 2013). These iterations is called 'inner iterations' in STAR CCM+.

The first step in an SIMPLE algorithm is to guess the pressure. Then momentum equations is solved to find velocity components. Next, the pressure correction equation is solved to find the pressure correction. Pressure and velocity is corrected by adding the intermediate values $\left(u_{i,0}, p_0\right)$ to the corrected values $\left(u_i', p'\right)$. To increase rate of convergence, a under-relaxation factor (α) is multiplied with the correction values, like shown in equation (8) and (9). Then the intermediate values are set to the new corrected values and the iteration starts again if convergence is not reached.

$$p = p_0 + \alpha_p p' \tag{8}$$

$$u_i = u_{i,0} + \alpha_{u_i} u_i' \tag{9}$$

Many variations of the SIMPLE algorithm have been developed. The most noticeable are SIMPLE revised (SIMPLER) by Suhas V. Patankar (1980) and SIMPLE Consistent (SIMPLEC) by Van Doormaal and Raithby (1984). There is also non-iterative method such as Pressure Implicit with Splitting of Operator (PISO) by Issa (1986). PISO applies one predictor step and one or more corrector steps for each time step. STAR CCM+ segregated flow solver, which is applied for the simulations, uses according to the user manual (CD-adapco, 2016b) an algorithm based on SIMPLE, without giving more details.

Another set of method is artificially compressibility. By adding an artificial compressibility (10) to the continuity equation(11), the problem with continuity equation being independent of pressure is solved. The value of β needs to be decided for each case. Adding this artificial term

is only correct when in steady condition. This means that it is not possible to use this method to calculate the intermediate time, but only a steady state solution, thus it could not be used for wave tank simulations.

$$p \sim \frac{\rho^*}{\beta} \tag{10}$$

$$\beta \frac{\partial p}{\partial t} + \nabla \mathbf{V} = 0 \tag{11}$$

3.1.7 Free surface and multiphase flow

CD-adapco (2015) explains that there are two major multiphase models. These are Lagrangian multiphase (LMP) and Eulerian multiphase (EMP). The main difference between these two is that LMP tracks parcels of particle moving through space and time, while EMP considers particles, bubbles or droplets to be a continuum passing through a fixed volume.

When calculating the flow through a fixed volume cell with EMP, a convective cell average have to be used. In their paper on Volume of fluid (VOF), Hirt and Nichols (1981) describes the problem with averaging: 'Convective averaging results in a smoothing of all variations in flow quantities, and, in particular, a smearing of surfaces of discontinuity such as free surfaces'.

VOF is a model for surface tracking between different phases, to avoid the smearing of surfaces of discontinuity. Their method track the position of the free surface and applies special conditions on the free surface to avoid averaging across it. Cells that have a volume fraction between zero and one must have a free surface. Hirt and Nichols (1981) applied a donor-acceptor scheme to track the free surface inside such cells.

More accurate surface tracking methods have been proposed. One commonly used surface tracking scheme is the High Resolution Interface Capturing (HRIC) scheme (Muzaferija, Peric, Sames, & Schellin, 1998). The HRIC scheme was originally developed to capture the free surface in a water entry problem. This scheme uses a blending of upwind and downwind scheme when computing volume fraction flux at cell faces. This give good surface tracking, and also allows for water entry. The HRIC surface tracking scheme is implemented as VOF interface capturing scheme in STAR CCM+, which is used for the simulations in this thesis.

Level set (Osher & Sethian, 1988) is an alternative to VOF. This method track the free surface by defining a smooth function φ, called the level set function. φ has the properties that it is less than zero outside the volume being tracked, larger than zero inside and exactly zero at the boundary. In case of a wave tank, the body will be one of the phases, e.g. water. The value of φ is convected with the velocity field in the simulation. To find the interface at a later time, the φ function can be evaluated equal to zero. Level set is not directly applicable for multi-phase flows, but with the addition of ghost fluid method (GFM) (Fedkiw, Aslam, Merriman, & Osher, 1999) it can be applied.

3.1.8 Wave generation

Different methods for wave generations exists, and they are dependent on which free surface treatment that is used. B. Guo and Steen (2011) investigated three different methods for VOF wave generations, and their strength and weaknesses were discussed.

Lin and Liu (1999) developed the internal wave maker. This wave maker used a mass source function to generate the waves. This wave maker was implemented by changing the continuity equation on the wave generation boundary (12). They were able to generate various wave trains including Stoke waves and irregular waves. Choi and Yoon (2009) modified the internal wave maker method by to instead use momentum source. They verified the method against lab tests and it showed good agreement. The commercial software STAR CCM+ uses momentum source wave maker based on Choi and Yoon (2009).

$$\frac{\partial u_i}{\partial x_i} = f(\mathbf{x}, t) \tag{12}$$

3.1.9 Wave damping

Wave reflections is a challenge in both a physical wave tank and a NWT. In a physical wave tank, wave beach is used to dampen the waves at the end so they do not reflect. The same is necessary in NWTs. One method of damping which is much used is the Sponge layers method by Israeli and Orszag (1981). This method adds a variable damping depending on the position in the sponge layer. For a NWT this translates into an increasing amount of wave damping closer to the boundary, often called artificial wave beach. Damping of waves is achieved by adding a vertical resistance to the vertical velocities of the fluid. This method is utilized by Choi and Yoon (2009) and is also the method implemented in STAR CCM+ (CD-adapco, 2016b).

Another method to achieve wave damping is by gradually coarsening the mesh (Park, Kim, & Miyata, 1999). The coarse mesh gives higher numerical dissipation, which will reduce the wave amplitudes. This method is often combined with an artificial wave beach. It is recommended to increase mesh sizes all the way up to a ship length (CD-adapco, 2016b).

3.1.10 Irregular waves

The waves observed at seas in usually not regular sinusoidal waves. The free surface looks chaotic and highly irregular. This condition can be represented with irregular waves. Irregular waves is a combination of multiple regular waves with different amplitudes, wavelengths and directions. A wave probe can log the wave elevation over time and generate a wave spectra with Fourier transform. This wave condition can then be recreated by an inverse Fourier transform of this spectra. In this thesis only long crested waves are used which mean all waves comes from the same direction.

Standardized wave spectra have been developed. One much used spectra is the Pierson Moskowitz (PM) spectra (Pierson & Moskowitz, 1963). The spectra describes the wave energy in a fully developed sea. The PM spectra was originally expressed as a function of wind velocity

19.5 meter above sea surface, but have been rewritten as a function of peak frequency ω_p and significant wave height H_s (13).

Measurement of waves in the north sea in 1968-1969 by the Join North Sea Wave Project discovered higher peak values then suggested by PM. They modified the spectra to fit their observation, and this spectra is known as the JONSWAP spectra (Hasselmann, 1973). The JONSWAP spectra can be expressed as the modified PM spectra by increasing its peak value (DNV, 2011). The JONSWAP spectra is calculated as (14) where γ is a non-dimensional peak shape parameter, σ is spectral width parameter and A_γ is a normalizing factor.

$$S_{PM}(\omega) = \frac{5}{16}\left(H_S^{\,2}\omega_p^{\,4}\right)\omega^{-5}\exp\left[-\frac{5}{4}\left(\frac{\omega_p}{\omega}\right)^4\right] \tag{13}$$

$$S_J(\omega) = A_\gamma\, S_{PM}(\omega)\gamma^{\exp\left[-\frac{(\omega-\omega_p)^2}{2\sigma^2\omega_p^{\,2}}\right]} \tag{14}$$

$$A_\gamma = 1 - 0.287\ln(\gamma) \tag{15}$$

$$\sigma = \begin{cases}\sigma_a, & \omega \le \omega_p \\ \sigma_b, & \omega > \omega_p\end{cases} \tag{16}$$

DNV (2011) states that the average values for JONSWAP experiment data are $\gamma = 3.3$, $\sigma_a = 0.07$, $\sigma_b = 0.09$. These are the values used in this thesis when JONSWAP spectra are used.

An interesting wave condition is when the mean zero crossing period T_Z corresponds to wave length of $1.2L_{PP}$. Around this wave length there is large motions that results in large added resistance. To find the corresponding spectra a relation between T_Z and T_p is needed. This is given by DNV (2011) and can be seen in formula (17). For $\gamma = 3.3$ the relationship between T_Z and T_P is as given in (18).

$$\frac{T_Z}{T_p} = 0.6673 + 0.05037\gamma - 0.006230\gamma^2 + 0.0003341\gamma^3 \tag{17}$$

$$T_Z = 0.777T_p \tag{18}$$

3.1.11 Turbulence

Turbulence is present in viscous ship calculations. Special considerations have to be taken for modeling this. With the computational performance available today it is not feasible to directly solve the Navier Stokes on all scales (DNS). Also directly solving large eddies, while modeling the

small eddies (LES) is too computational demanding for commercial seakeeping studies. Turbulence is thus modeled completely by Reynold average Navier Stokes (RANS) methods.

Reynolds ansatz is that the turbulent fluid velocities and pressure can be decomposed into a time averaged mean part and a fluctuating part with zero mean. By inserting this into the Navier Stokes equations Reynolds stress tensor is found. The most common way of solving this is by using a two equation model. It is claimed that no visible improvement in accuracy for ship simulations can be seen by using more advance turbulence models than two equations models (Larsson et al., 2014).

K-ε is a turbulence model (Jones & Launder, 1972) which solves two transport equations for estimating local turbulence. These two equations is turbulent kinetic energy k, and dissipation rate ε. This method is improved by Shih, Liou, Shabbir, Yang, and Zhu (1995) with the realizable k-ε model. The realizable k-ε model is superior in many ways, and is much better for marine applications.

K-ω turbulence model(Wilcox, 1988) is an alternative to the K- ε model. K- ω solves one equation for the turbulent kinetic energy k, and one equation for the turbulent frequency ω. This method had better accuracy and robustness then the classical k-ε model. An improved method called shear-stress transport (SST) k-ω was suggested by Menter (1992). This method improved on known short-comings of the first K-ω model.

Both K-ε and K-ω methods and their improved versions are available in STAR CCM+. The realizable K-ε turbulence model was chosen for the simulations containing viscosity as this turbulence model was applied at the Gothenburg 2010 workshop (Larsson et al., 2014) and in the tutorial on ship resistance (CD-adapco, 2016b).

3.1.12 Time-step and CFL-number

The time step is closely related to the damping of wave amplitudes, but does also heavily influence the computational time. Ratio between particle movement for one time step and grid size is an important parameter. This is known as the CFL number after Richard Courant, Kurt Friedrichs, and Hans Lewy. In 1D the CFL number is as described in equation (19). As time-step increases the CFL number increases. Depending on discretization scheme, there could be a limitation where the solution becomes unstable.

$$CFL = \frac{u\Delta t}{\Delta x} \tag{19}$$

Choosing time step for new problems can be difficult. In a NWT the most important factors affecting time step is mesh density, wave length and height, time discretization and surface interface capturing scheme. A trial and error is common if no previous experience with similar problems are available. STAR CCM+ recommends choosing time step such that the CFL number on the free surface is less than 1 with a target value of 0.5 when using VOF waves (Cholleti, 2015). Deng et al. (2010) found that for ship in head waves at least 250 time steps per period is

required to get sufficient accuracy in long waves, but for shorter waves more than 100 time steps per period makes the solution time step independent.

3.2 Wave tank

A physical wave tank have to be able to recreate the conditions a ship meets at sea in a controlled environment. This involves having a large enough tank, but also correct wave generation and wave damping. The same apply for a NWT, but in addition, the numerical model must be sufficiently refined at the correct places to capture the physics.

3.2.1 NWT geometry

A NWT is usually designed as a circulation tank, and not as a traditional towing tank. This greatly reduce the size of the simulation domain. Another benefit is that the simulations can run for as long time as desired without extending the size of the tank. Because a ship in calm water or head waves is a symmetric problem, only half of the tank needs to be simulated.

There is two different ways to set up a wave tank with regard to wave damping. The first, which is often applied in calm water simulations, have damping at both the outlet, inlet and the side of the tank. This requires a wider tank, but the cell could be coarse near the side wall.

This setup can also be applied for incoming waves, but without damping on inlet. Waves will not extend through the entire width of the tank, as seen in Figure 4. The benefit of applying this setup for wave calculations is the additional damping at the side wall which can solve problems with wave reflections across the tank. It is important to calibrate the waves to ensure the ship feels the wave as long crested.

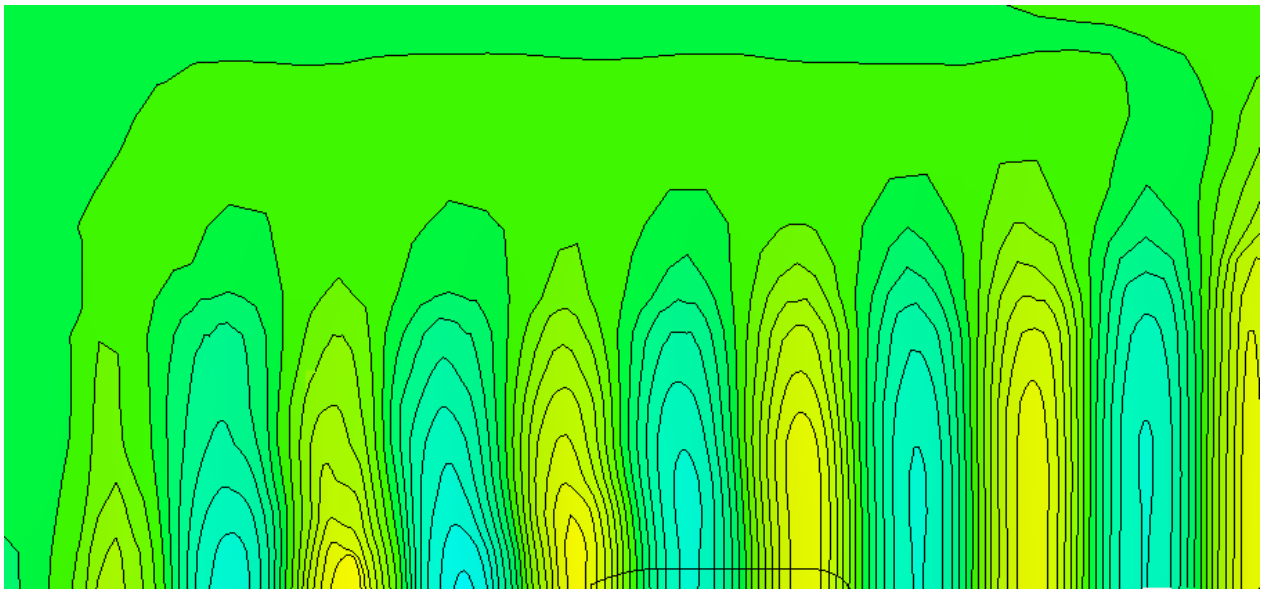

Figure 4 - 3D wave tank with side damping. Contour lines are free surface elevation. Ship is only for reference purpose and not a part of the simulation.

The other method, which is commonly used in head waves simulation, have only damping at the outlet boundary. This reduces the required width of the tank by a large margin. A benefit with a narrow tank is the possibility to have a uniform mesh the whole width of the tank, without a huge increase in number of cells. This is important to simulate uniform incoming waves across the tank width (Figure 5).

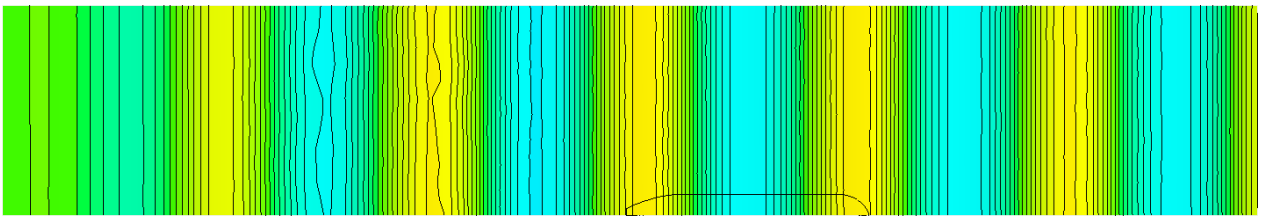

Figure 5 - 3D wave tank without side damping. Contour lines are free surface elevation. Ship is only for reference purpose and not a part of the simulation.

The tank's dimensions should be chosen such that the tank walls does not influence the flow around the ship, but as small as possible to keep number of cells low. Each case must be considered individually, but some general guidelines apply. The water depth should be at least equal to the longest wave length in the tank. Numerical damping beach requires about two wave lengths (Cholleti, 2015; Rørvik, 2015), and thus the distance from the ship and its nearby flow needs to be larger than the wave damping length. This applies to both outlet boundary and side boundary if side damping is enabled. Air gap is not of great importance, but should be larger than the ships over water geometry by some margin. Inlet should be at least one ship length in front of the bow. A long distance can cause problems in some situations with rotating mesh and large ship motions, due to free surface moving outside the refined area.

3.2.2 Boundary conditions

Boundary conditions specify how the boundaries of the simulation domain should be treated. The choice of boundary conditions dictates the flow in the domain. All boundaries must have a boundary condition for the problem to be well posed. Boundary conditions must reflect the physical conditions.

An example is the ship hull. Water can not flow through the hull, so the velocity component normal to the hull is zero. No-slip condition is important for viscous flow, but irrelevant for inviscid. This condition is implemented by forcing zero velocity tangential to the boundary at the boundary.

The other boundary conditions used in inviscid wave tank calculations are velocity inlet, pressure outlet and symmetry plane. Velocity inlet defines a velocity vector entering the fluid at the boundary. This velocity vector can be a function of time, as is the case for wave generation. Pressure outlet is used to allow water to flow out of the tank in a controlled fashion such that the tank does not fill up or get emptied. This is achieved by defining the pressure at the outlet

as a reference pressure and subtract the dynamic pressure due to the normal inflow velocity. For a NWT the reference pressure must be chosen as hydrostatic pressure to avoid water escaping.

Symmetry boundary condition can reduce the simulation domain by applying a symmetry about the centerline of the ship. The symmetry condition applied by enforcing zero shear stress at the boundary. This boundary condition can also be used at the tank side wall. An alternative for side wall is no-slip or slip wall condition.

CD-adapco (2016b) recommends using velocity inlet at as many boundaries as possible, except side wall for a simulation with VOF. This means that wave-generator, top and bottom boundary is velocity inlet. They also recommend using no-slip wall at side wall. Pressure outlet should only be used at the outlet that is the end of the tank.

3.2.3 Wave tank mesh

A fine mesh is required to accurately simulate the free surface waves. A detailed study of which parameters that effects quality of inviscid waves was investigated in the project thesis (Rørvik, 2015). The experience and result from that thesis was applied when generating the mesh for the free surface.

The mesh was generated by using a trimmer mesh with prism layers and volumetric mesh controls. Trimmer mesh is a variant of a structured hexahedral mesher, but with some extra features which is convenient for a NWT. First, it allows anisotropic volumetric refinements. This allows for easy and controlled refinements around the hull, and for the free surface region. Secondly the mesh can be aligned with a user specific coordinate system so all cells align with the inflow. Next to a geometry the cell can't be hexahedral, so they are trimmed by removing one or more corners or edges.

It is important to know how STAR CCM+ trimmer mesher decides cell size when working with it. Cells sizes are chosen by a user specified base size, which is a reference size. This reference size is halved or doubled multiple times to get the desired cell size. If it is impossible to gain the desired cell size with halving or doubling then the size is chosen as the largest size possible that is still smaller than the specified value. This makes it difficult to get the exact sizes you want. As an example, if we want a 5cm long cell and a 3 cm high cell in a region we could specify the base size to be 5 cm. This would give a 5 cm long cell and a 2.5 cm high cell as this is the largest possible cell within the requirements. If base size is chosen as 3 cm this will give a 3 cm long and 3 cm high cell.

Cholleti (2015) suggest that the free surface mesh should have between 40-100 cells per wave length and 20-40 cells per wave height. Rørvik (2015) found that coarser mesh could be applied in a 2D wave tank without increasing damping. For 3D wave tanks there is also a cell length in wave crest direction. This is recommended to be equal to the cell length in wave advancing direction (CD-adapco, 2016b).

3.3 Ship model

3.3.1 Ship mesh refinements

As mention in chapter 3.2.3 the incoming waves need a fine mesh to behave properly. The same applies for waves generated by the ship. The wave length of these waves are relatively short, and that requires a fine mesh. The pressure resistance is highly dependent on correct wave generation so great effort should be invested into capturing all radiated waves near the hull.

3.3.2 Ship motion

The ship is required to move within a simulation to calculate the correct resistance. The motion of the ship is calculated by iterative process. The resulting forces and moments are found by integrating pressure and shear stress over the hull. The equation of motion is solved to achieve equilibrium and the ship is moved accordingly. This process run until equilibrium is found. This process is called dynamic fluid body interaction (DFBI) in STAR CCM+.

A challenge with regard to motion is that the mesh is a fixed grid in space. There are multiple methods to make movement possible. Which method to use is dependent on how the mesh is set up, and the physics involved in the simulation.

One method is to rotate and translate the whole mesh, while maintaining a horizontal free surface. This method works well for small motions, but can be problematic with large motions and especially large rotations. As seen in Figure 6 the free surface almost leaves the refined free surface mesh at inlet, and if the mesh did not rotate the height of the refined area could be much smaller.

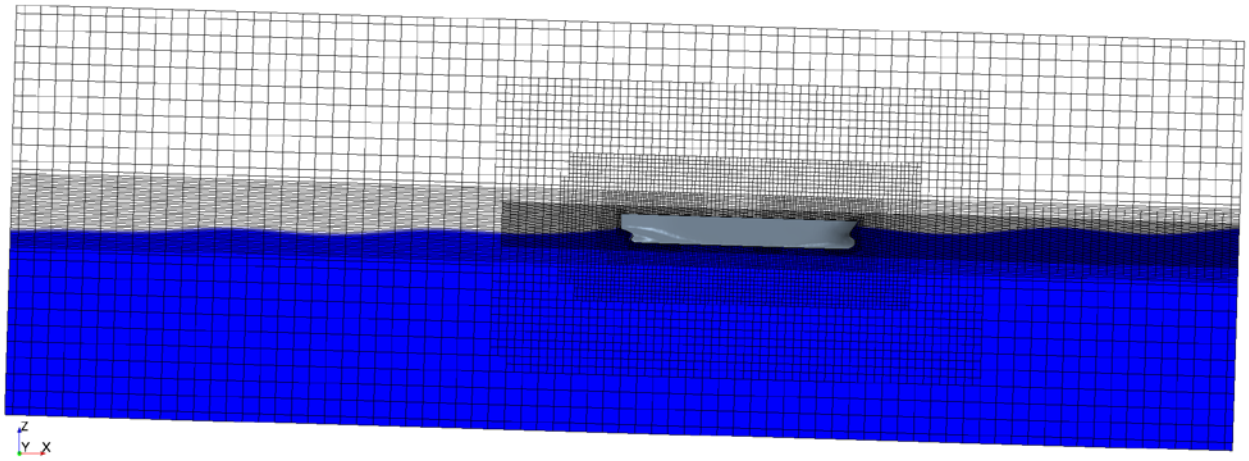

Figure 6 - Mesh rotated to simulate motion in pitch. Free surface is horizontal at all time. Blue is water and white is air

Overlapping mesh (Hadžić, 2006) is a method which can simulate moving bodies by using a background mesh and a body mesh. In a NWT there will be one mesh for the ship and one background mesh of the wave tank. The ship mesh is free to move while the background mesh is stationary. The flow problem is solved on active cells which is the cells belonging to the ship and the non-shadowed background cells. At the boundary between the ship mesh and the

background mesh there is acceptor cells (Figure 7). These cells connect the two solutions by taking an interpolated value from donor cells at the boundaries of each mesh. Which cell that are active changes for each time step as the ship moves.

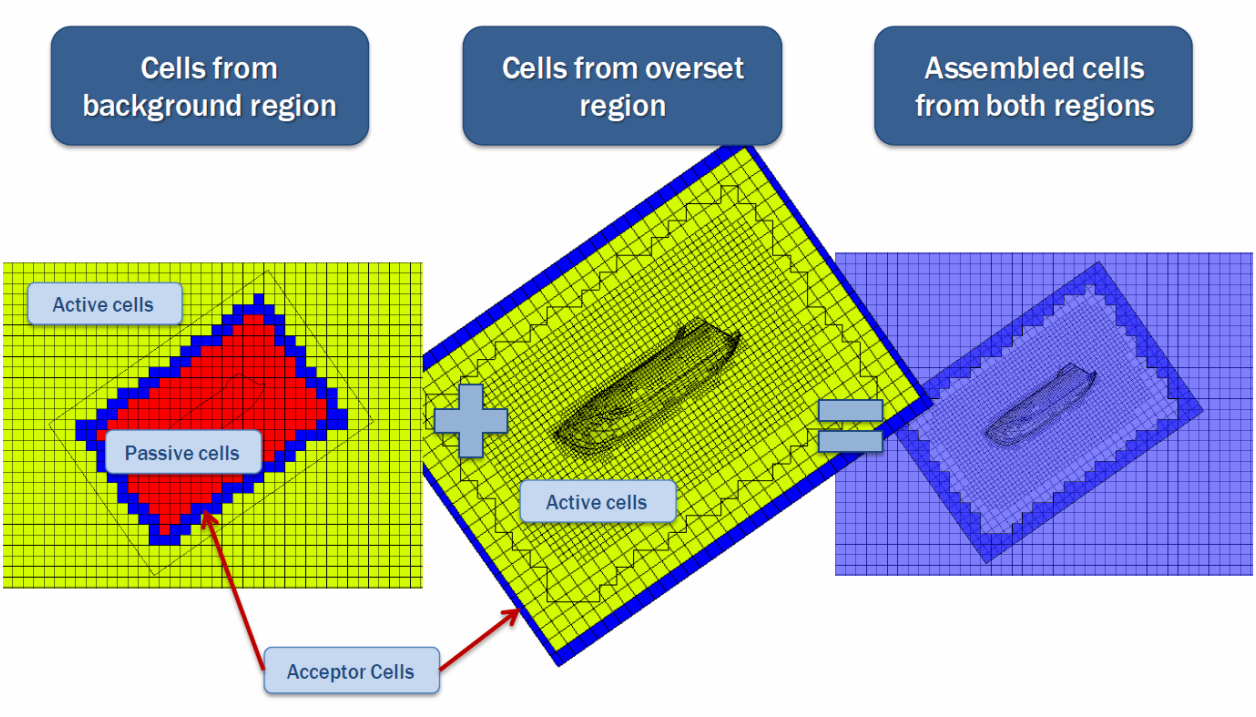

Figure 7 - Example of overlapping mesh for a free fall life boat. Figure by CD-adapco (2016a)

Overlapping mesh has benefits that that it can handle large motions, which for a ship will occur at resonance. Another benefit is that the background mesh can be built as a wave tank independent on the ship mesh and same for ship mesh. Due to the stationary background mesh there would be no problem with free surface moving outside the refined area, and the height of the refined area can be reduced. A disadvantage is that instabilities can occur in the acceptor cells, especially with long time steps. STAR CCM+ have built in support for overlapping mesh and the feature is called overset mesh. Rotating and translating mesh was applied for the simulations, but overlapping mesh could have been interesting to test. Overlapping mesh should be beneficial especially for wave lengths with larger motions than those in the test case and for oblique waves.

3.3.3 Connection

As the ship is not self-propelled it has be to be connected to the tank. In a towing tank it is common to use a setup that restricts sway and yaw while having a spring coupling in surge direction. For a NWT with symmetry plane the only available degrees of freedom is surge, heave and pitch. Surge motion can be modeled with a spring coupling or a fixed connection. Heave and pitch should remain free to correctly represent the physical problem.

At the Gothenburg 2010 workshop (Larsson et al., 2014) the surge was fixed for case 1.4b which have been used for validation in this thesis. It was noted by Larsson et al. (2014) that the experimental fluid dynamics (EFD) data for this case had used a spring connection is surge, and thus the data for amplitude of resistance could not be compared. The properties of the spring system used was not documented, so it could not be modeled to gain comparable data.

3.4 Measurements in simulation

CFD solves the velocities and pressure in each cell for each time step. This is a huge amount of data, and it is not reasonable to store all this data. Ahead of running a simulation one have to define what parameters that are of interest and monitor these in the time domain. For a simulation with ship in waves, interesting parameters is the force and motions for the ship and wave elevations.

Pressure and shear force is found by integrating the pressure and wall shear stress over the hull. Shear forces is not relevant in an inviscid wave tank, but is a large contributor to the total resistance. Position of the free surface can be logged by wave probes. When VOF is used, the free surface is defined as where the volume fraction of water is 0.5. Wave probes are tracking this position and storing the measurements over time.

3.5 Analysis of results

The key parameters for a NWT simulation is resistance and motions. In head waves the relevant motions is heave and pitch. The interesting data is the steady region of the signal. In Figure 8 the signal goes towards a steady state after about 50 seconds and only this part should be used in analyzes.

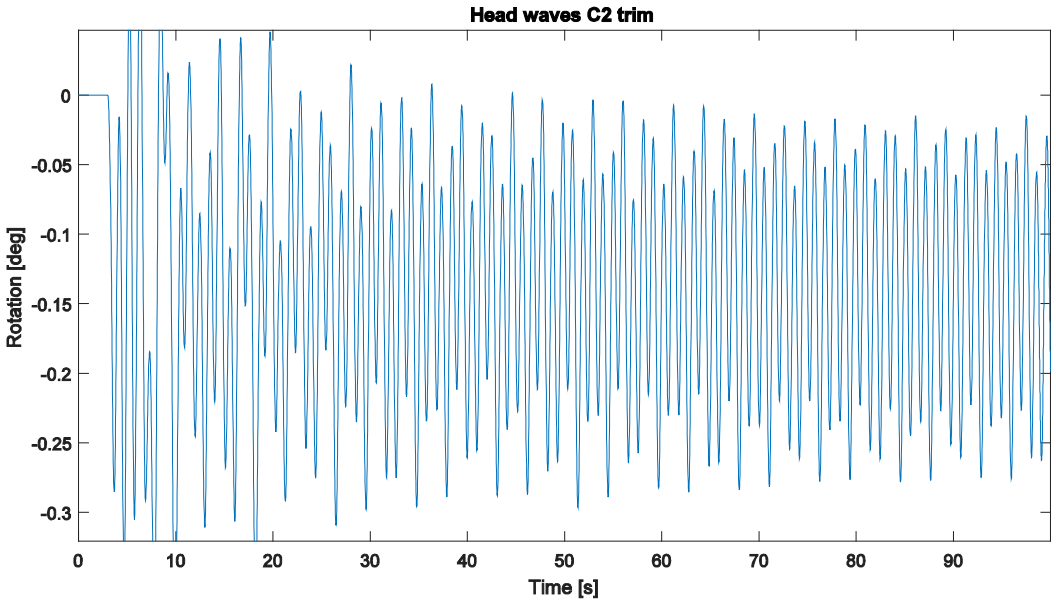

Figure 8 - Trim signal for 100 seconds simulation in head waves. Wave conditions C2

3.5.1 Regular head waves

The main source for comparison data in this thesis is the Gothenburg 2010 workshop (Larsson et al., 2014). The comparison was made on average, first amplitude and phase of the total resistance, heave and pitch. First amplitude is defined as the amplitude of the signal with the frequency equal to the wave encounter frequency f_e. Wave encounter frequency is calculated as in (20) where f_w is the wave frequency, λ is the wave length and U_{ship} is the ship velocity.

$$f_e = f_w + \frac{U_{ship}}{\lambda} \tag{20}$$

Phase (γ_n) is in this case defined as the difference between the input signal (wave) and the response. Time is defined such as there is a wave crest at fore perpendicular (FP) at time zero (Larsson, Stern, & Visonneau, 2010). There is contradicting information on this definition, as according to the assessment by Larsson et al. (2014) the time should be defined such as there is a wave crest at center of gravity (COG) at time zero.

By looking at the result presented in Larsson et al. (2014) it seems like the EFD data might use another time reference than the CFD results, but this was not verified. The CFD results is known to be using the definition with wave crest at FP, and thus the same reference have been applied for simulations in this thesis.

The analysis procedure used is the one suggested for participants at the Gothenburg 2010 conference (21)-(26). The steady part of the time signal is Fourier transformed into a series of cosine functions. γ_I is the initial phase and is zero if the time is defined as above. The comparison values will by this definition be X_0 for the 0th amplitude, X_1 for the first amplitude γ_1 for the phase.

$$X_F(t) = \frac{X_0}{2} + \sum_{n=1}^{N} X_n \cos\left(2\pi n f_e t + \Delta\gamma_n\right) \tag{21}$$

$$\Delta\gamma_n = \gamma_n - \gamma_I \tag{22}$$

$$a_n = \frac{2}{T}\int_0^T X(t)\cos\left(2\pi n f_e t\right)dt \quad (n = 0,1,2,\ldots) \tag{23}$$

$$b_n = \frac{2}{T}\int_0^T X(t)\sin\left(2\pi n f_e t\right)dt \quad (n = 1,2,3,\ldots) \tag{24}$$

$$X_n = \sqrt{a_n^{\,2} + b_n^{\,2}} \tag{25}$$

$$\gamma_n = \tan^{-1}\left(-\frac{b_n}{a_n}\right) \tag{26}$$

3.5.2 Irregular waves

For irregular waves there is a not one encounter frequency, but a large range. This requires a different analyzing procedure than for regular waves. Time series from irregular waves simulations should be transformed into frequency domain by a fast Fourier transform (FFT). One good method for this is the power spectral method by Welch (1967). This method uses a windowing function with overlapping segments that reduce variance.

Time series from wave probes can be compared by the source wave spectra to verify that the waves are correctly generated. If the ship has a forward speed, the spectra must be on the same frequency, either wave frequency or wave encounter frequency. In this thesis the source spectrum (JONSWAP) was converted into encounter frequency domain when compared by the FFT from wave probe. This was achieved by applying the relation (27),(28) given by Faltinsen (1990).

$$S_e(\omega_e) = \frac{S(\omega_0)}{1 + 2U\omega_0 / g} \tag{27}$$

$$\omega_e = \omega_0 + \frac{\omega_0^2 U}{g} \tag{28}$$

Motion spectra's can be used to generate response amplitude operators (RAO) by dividing the response spectra by the wave spectra. It should be noticed that this is only valid for the frequency range which has significant wave energy, and multiple irregular wave conditions is required to gain a complete RAO.

Added resistance due to waves is calculated as the difference between the mean resistance in wave and the mean resistance in calm water. The frequency information is lost when the mean value of the time signal is calculated. It is thus impossible to find added resistance as a function of frequency for one irregular time series.

4 Inviscid wave tank with ship in head waves

4.1 Introduction

An inviscid wave tank was set up to test if added resistance can be calculated without considering viscosity. The hull KVLCC2 was used as an example hull due to good experimental and numerical comparison data. The simulation were performed with STAR CCM+. A large focus was put on reducing simulation time while preserving accuracy.

A ship in waves is a complex problem. First, there is the ship hull with a complex flow field. Then there is the waves and their interactions with the ship hull. These waves then induces motions to the ship hull, which again alters the flow field around the ship. Then there is the task of discretizing this complex problem to use in a CFD simulations. The flow around ship must be sufficient captured, incoming waves must maintain the wave height and the forces on the hull must be calculated. Each of these effects requires individual considerations, but also in combination.

To reduce the amount of error sources, it was decided to build the simulation step by step. The first step was to set up a calm water tank with ship to experiment with mesh refinements around the hull. Then an empty wave tank was used to investigate how the waves behaved in 2D and later expand to 3D. When both the 3D wave tank and the calm water ship simulation had sufficient accuracy the two simulation were combined.

4.2 KVLCC2

Good validation data is essential when testing CFD codes. This is the main reason why KVLCC2 was chosen as a test hull. There is large amounts of experimental and computed results available. The comparison data used in this thesis is mainly experimental and computed results from Gothenburg 2010 workshop (Larsson et al., 2014).

KVLCC2 is a very large crude carrier developed by Korea Research Institute for Ships and Ocean Engineering (now MOERI) and is used as an example hull in research. Its main dimensions is found in Table 1.

Due to calculating without viscosity there should be no different results in model scale or full scale. Model scale of 1/58, which is equal to EFD from Gothenburg 2010, was chosen due to multiple reasons. Firstly, a calm water resistance calculation is needed to find the resistance due to friction. Here the scale does matter. Secondly, comparison data is given in model scale and thus it is convenient to use the same scale.

KVLCC2 geometry is obtained from Professor Sverre Steen at NTNU and is equal to the one used for model tests to the Gothenburg 2010 workshop. This model is equal to the model available from the SIMMAN 2008 web page, but has larger freeboard as described by B. Guo (2011). The larger freeboard is to avoid waves breaking over the bow which could occur in some of the test cases. A comparison by the geometric model provided for the Gothenburg 2010 was not

possible because the web page have been shut down, and the geometry is not included on the proceedings CD.

Table 1 - KVLCC2 main dimensions from Larsson et al. (2014)

Main particulars (Full Scale)		**KVLCC2**
Length between perpendiculars	L_{PP} (m)	320.0
Maximum beam of waterline	B (m)	58.0
Draft	T (m)	20.8
Displacement	Δ (m^3)	312622
Wetted area w/o rudder	S_W (m^2)	27194
LCB (%L_{PP}), fwd +	–	3.48
Vertical Center of Gravity (from keel)	KG (m)	18.6
Metacentric height	GM (m)	5.71
Moment of Inertia	K_{xx}/B	0.40
Moment of Inertia	K_{yy}/L_{PP}, K_{zz}/L_{PP}	0.25
Service speed	U (knots)	15.5
Froude number	Fr	0.142

4.3 Software

The simulations in this thesis have been performed with the software package STAR CCM+ developed by CD-adapco. STAR CCM+ handles the workflow from importing geometry to meshing, solving and post-processing. The software is known for good capabilities with free surface waves, and can solve both viscous flow with RANS and the inviscid Euler equations.

MATLAB have been used for post-processing including FFT and plotting. CSV files of time series were imported from STAR CCM+. Automatic scripts for analyzing and plotting multiple time series were developed to quickly gain comparable results from STAR CCM+ simulations. Results and simulation parameters were logged and compared in a Microsoft Excel spreadsheet.

4.4 Calm water resistance

4.4.1 Setup of calm water tank

First a calm water simulation were set up. A tutorial for a calm water resistance test for KCS was used as a foundation (CD-adapco, 2016b), but adjusted to better fit KVLCC2 geometry and

particulars (Table 1). This simulation was run with turbulence modeled by the realizable K-ε turbulence model (see chapter 2.2.4).

The tank geometries was chosen to fit a damping length of seven meters. This will sufficiently dampen waves up to 3.5 m long, which should include all waves generated by the hull as Froude number is significant lower than 0.35. Wave damping was applied at inlet, side wall and outlet. The damping area should not contain physics of importance for the ship hull, and thus some distance between the hull and the damping area is necessary.

The tank were chosen to be 24.5 m long and 10 m wide. This equals roughly 4.5 L_{PP} long and 2 L_{PP} wide. The tank has a 5 meter water depth and 5 meter air gap. The ship model was places in center of the tank in longitude direction, and with centerline through the symmetry plane.

Trimmed mesher was chosen as it is well suited for ship simulation. Multiple layers of mesh refinement near the hull was applied to capture the hydrodynamics. Closest to the hull prism layers was applied to capture the boundary layer. The thickness of the boundary layer was found to be about 0.02 m. Six prism layers with a relative growth rate of 1.5 was found to nicely capture the velocity gradient next to the hull, and resulted in y^+ value in the desired range between 30 and 50. In Figure 11 the prism layers can be seen as the cells following the geometry of the bow.

Further away for the ship hull the mesh was gradually coarsened (Figure 9, Figure 10). Refinement were set to capture the flow near the hull and in the wake where generated waves travels. Waves should according to Kelvin wake spread with an angle of 19.5° with respect to the centerline so the wake refinement was set up with a larger angle of 26.5° relative to the centerline. The mesh near the free surface was refined in the vertical direction to accurate track the free surface location. With these refinements the total number of cells for the domain was 731 000 cells.

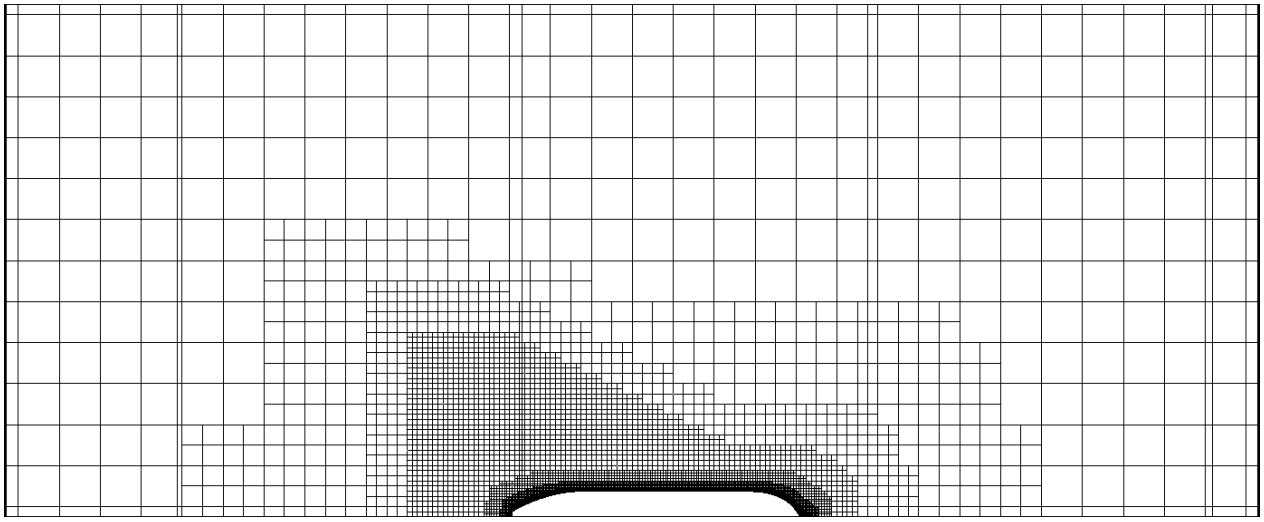

Figure 9 - Mesh of wavetank with KLVCC2 for calm water resistance simulation. Seen from above onto the free surface

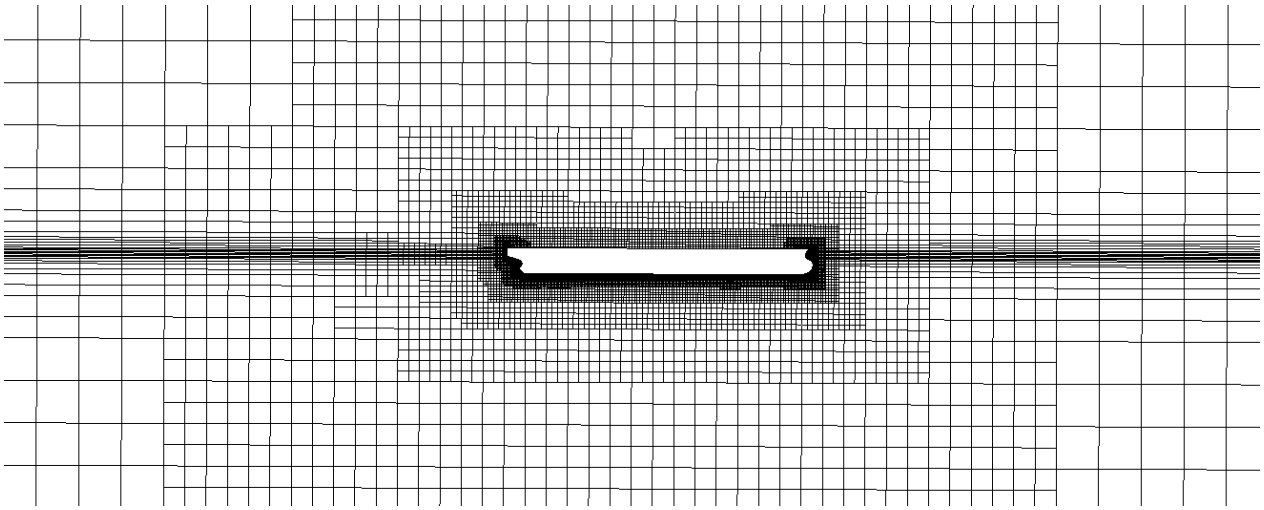

Figure 10 - Mesh of wavetank with KLVCC2 for calm water resistance simulation. Seen from side to a plane midship

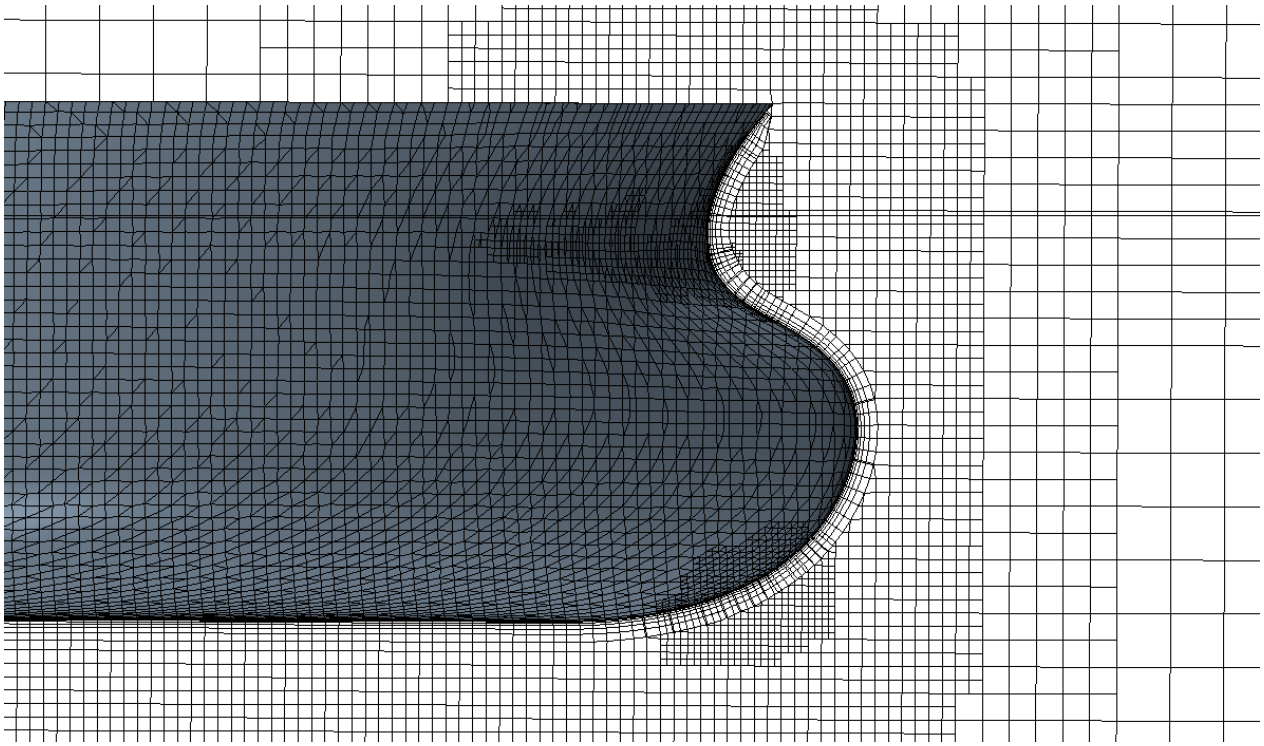

Figure 11 - Mesh around bow of KVLCC2 for calm water resistance simulation

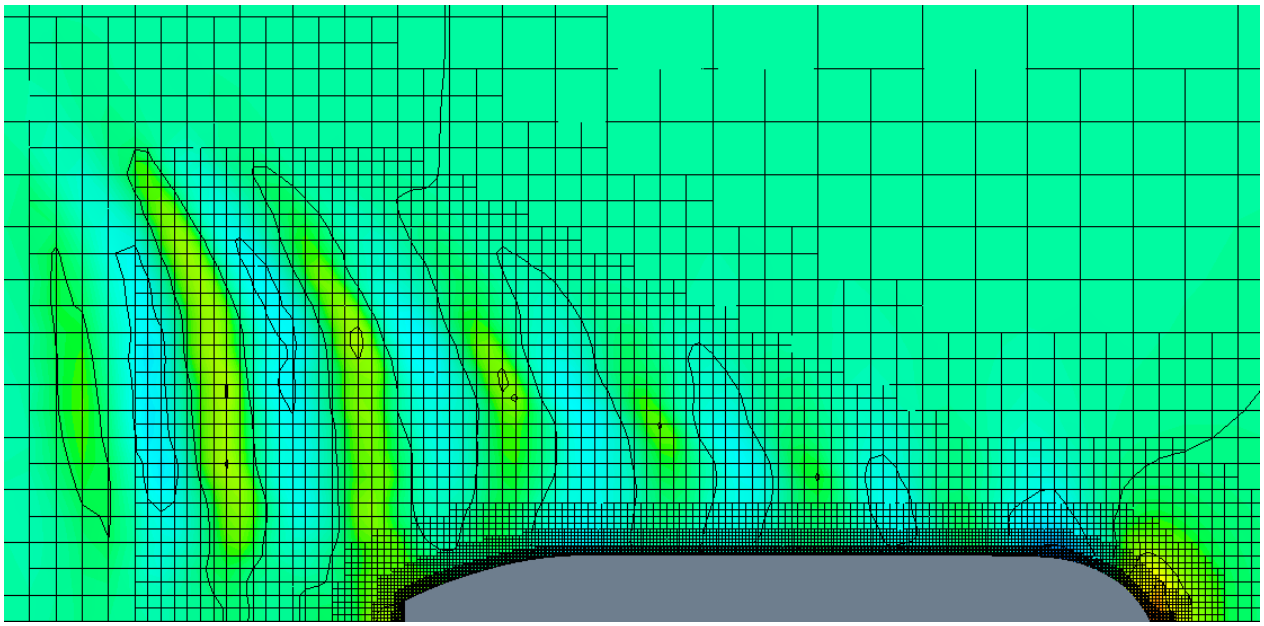

Figure 12 - Free surface with mesh overlay

A time step of 0.03 was found to give a good balance between simulation time and accuracy. First order time scheme was used, as it is more stable then second order and the problem converges to a steady solution. Second order upwind scheme were applied for the convective terms. Inner iterations (SIMPLE iterations) was set to a maximum of 10 per time step which gave lower residuals then the recommended maximum of 10^{-3} (ITTC, 2011). Turbulence was modeled by the realizable K-ε turbulence model.

4.4.2 Result for viscous calm water resistance

The resistance was recorded as time series with an individual recording of pressure resistance and friction resistance. The resulting resistance found in Table 2 is the average of the resistance in steady state. The resistance components were made non-dimensional (Table 3) by the standard procedure (29). Here C_T is the total resistance, C_F is the friction resistance and C_{PV} is the pressure resistance. The results were compared with EFD and CFD data from the proceedings of the Gothenburg 2010 conference (Larsson et al., 2010) case 1.2b for Fr = 0.142 (Table 4, Table 5).

$$C = \frac{R}{\frac{1}{2}\rho v^2 S} \tag{29}$$

Table 2 – Calm water resistance of KVLCC2 in 1/58 model scale in a with viscosity

Froude no	Pressure resistance [N]	Friction resistance [N]
0.142	3.695	13.50
0.182	8.130	21.62

Table 3 - Resistance coefficients for calm water resistance of KVLCC2 in 1/58 model scale with viscosity

Froude no.	$C_T(x10^{-3})$	$C_F(x10^{-3})$	$C_{PV}(x10^{-3})$
0.142	3.898	3.060	0.8377
0.182	4.105	2.983	1.122

Table 4 - Comparision of CT for Fr = 0.142

Organization (Method/Software)	$C_T(x10^{-3})$	E%D
MOERI (EFD)	4.056	NA
MOERI (VAVIS) CFD Grid #1	4.175	-2.93
MOERI (VAVIS) CFD Grid #2	4.181	-3.08
MOERI (VAVIS) CFD Grid #3	4.245	-4.65
This thesis (STAR CCM+)	3.898	3.90

Table 5 - Comparision of CF and CPV for Fr = 0.142

Organization (Method/Software)	$C_F(x10^{-3})$	$C_{PV}(x10^{-3})$	C_F / C_{PV}
MOERI (VAVIS) CFD Grid #1	3.245	0.9292	3.49
MOERI (VAVIS) CFD Grid #2	3.257	0.9240	3.52
MOERI (VAVIS) CFD Grid #3	3.305	0.9393	3.52
This thesis (STAR CCM+)	3.060	0.8377	3.65

4.4.3 Inviscid calm water resistance

The calm water simulation was also run without viscosity. This was done for two reasons. Firstly, we must assure that the waves are generated properly also without viscosity. This should not be a problem, but it was validated as wave generation is essential for correct resistance calculation.

Secondly, it is necessary to be able to compare resistance form an inviscid NWT with EFD data and other viscous CFD results. That is not possible to do directly with an inviscid simulation due to no viscous resistance. The viscous part of the calm water resistance for one velocity can be found by taking the difference between the viscous and the inviscid simulation. By applying assumption that added resistance is independent on viscosity, the total resistance of a ship in waves can be found as the sum of inviscid resistance in waves and viscous resistance in calm water.

The viscous simulation was continued, but the inviscid solver was used. No other parameter or mesh was changed. As expected, the friction resistance disappeared instantly, while the pressure resistance reduced gradually due to reduction in viscous pressure resistance (Figure

13). The same procedure of using the average resistance of steady state was applied to find the inviscid calm water resistance (Table 6).

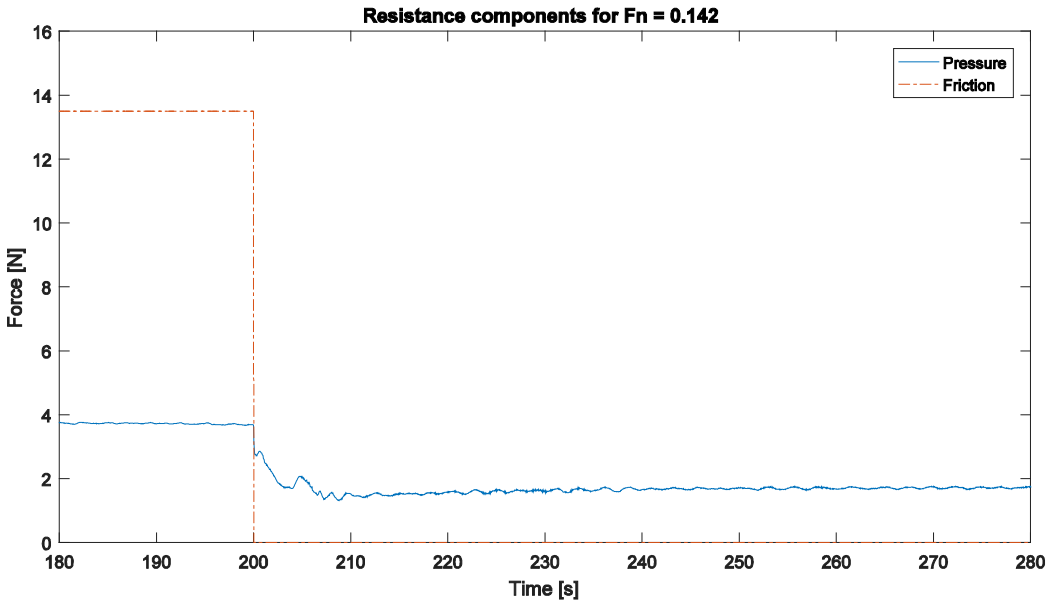

Figure 13 - Time series of resistance components. Viscosity is turned off at time = 200 s.

Table 6 - Calm water resistance of KVLCC2 in 1/58 model scale in a without viscosity

Froude number	Pressure resistance [N]
0.142	1.710
0.182	6.080

Table 7 - Calm water additional resistance due to viscosity

Froude number	Viscous Pressure resistance [N]	$R_{viscous}$-$R_{inviscid}$ [N]
0.142	2.00	15.48
0.182	2.05	23.67

4.4.4 Wave profiles

Test case 1.1b from Gothenburg 2010 workshop included a wave profile comparison at three distances from KVLCC2. Test were performed in calm water with Froude number of 0.142. The EFD data by Kim, Van, and Kim (2001) were used for validation, and raw data were available from the Gothenburg 2010 workshop proceedings CD (Larsson et al., 2010). Wave profiles from both the viscous and inviscid solution was compared (Figure 14, Figure 15 & Figure 16).

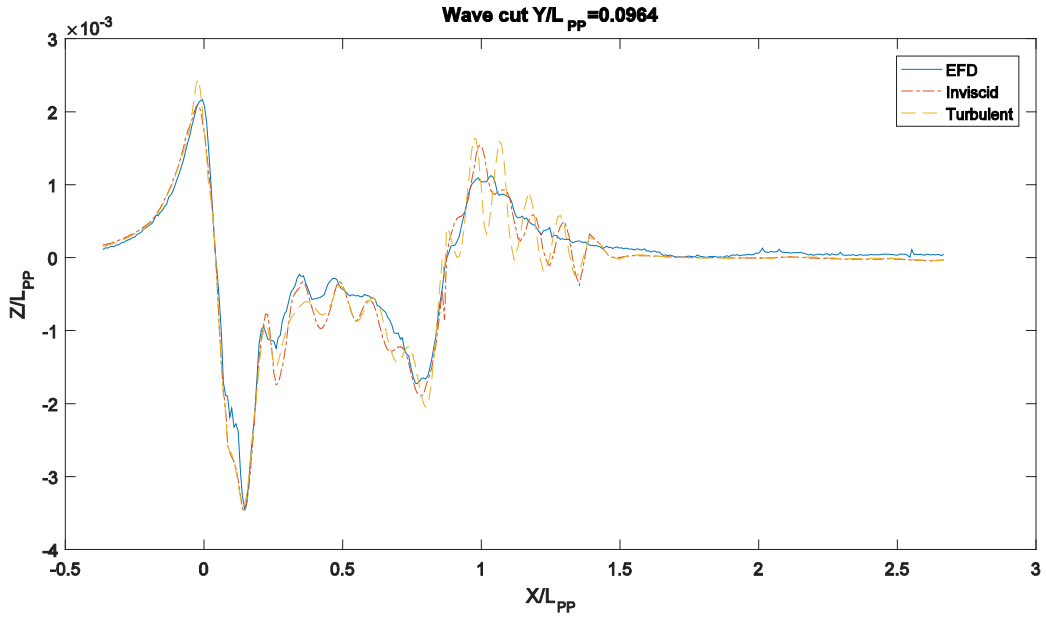

Figure 14 - Wave profiles at y/LPP=0.0964 compared with EFD data (Larsson et al., 2010)

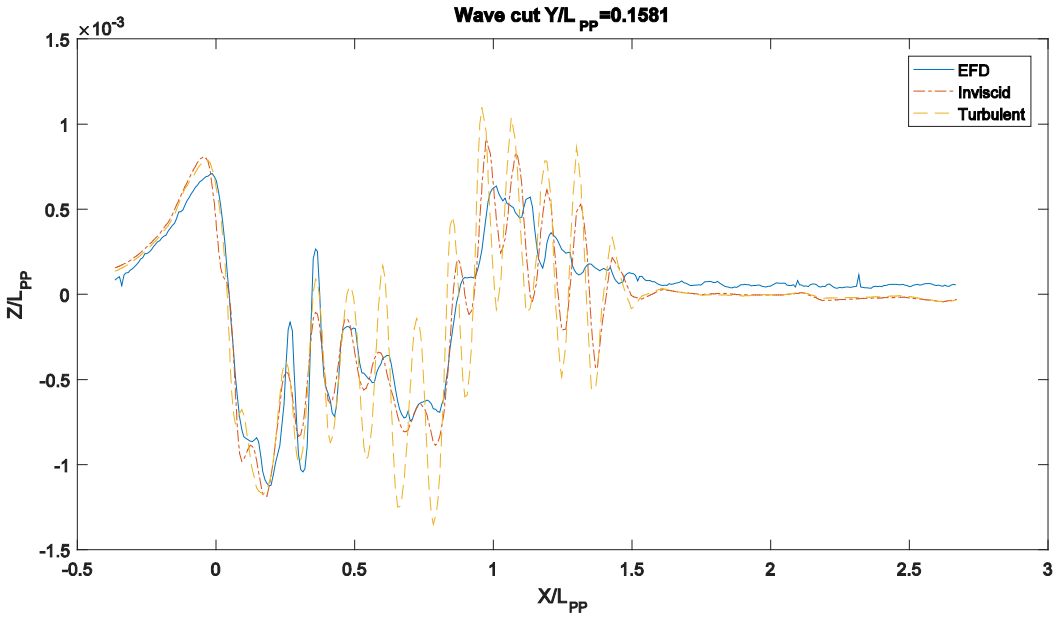

Figure 15 - Wave profiles at y/LPP=0.1581 compared with EFD data (Larsson et al., 2010)

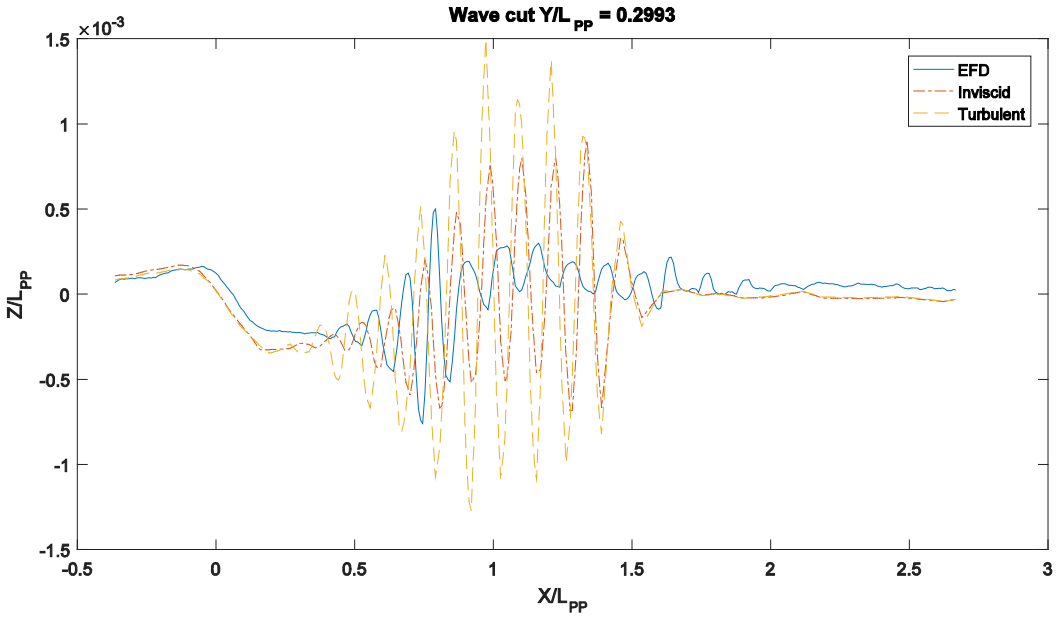

Figure 16 - Wave profiles at y/LPP=0.2993 compared with EFD data (Larsson et al., 2010)

4.5 Wave tank

A wave tank was designed for regular long crested head waves, also known as first order Stoke waves. These are the applied wave conditions at the Gothenburg 2010 workshop. Irregular waves from JONSWAP specter was also tested independent on the workshop.

A high-resolution mesh is needed to capture the free surface accurately and reduce wave damping, but a too fine mesh will give very many cells and a long simulation time. Simulation time can be argued to scale with cell size to the power of four. Dividing a cell in half in each increase the cell count by 2^3. However, to maintain the same CFL number, the time step must also be halved, which would double the simulation time. This shows that it is important with regard to simulation time to find a good balance between cell size and the actual wave conditions being tested.

A good basis knowledge for an inviscid wave tank was established during the project thesis (Rørvik, 2015). Some testing was though required to adjust for the different waves conditions and tank geometries. Another difference was forward velocity, modeled as a current, which was not considered in the project thesis. All results from in the project thesis was for a 2D tank, and this had to be checked in a 3D tank before a ship model could be added to the simulation.

4.5.1 2D wave tank

First, a 2D tank was set up. The benefit of using a 2D tank is that computational time is short compared with a 3D tank, so many different meshes can be tested in a relatively short time. The dimensions of the initial tank was the same as the tank applied for calm water resistance.

Wave-probes logged the free surface height over time at multiple positions along the tank (Figure 17). Grid size and time step was adjusted until a good balance between wave accuracy and computation time were found. It was found that at least 20 cell was needed in wave advancing direction and at least six cells in wave height for the long crested cases.

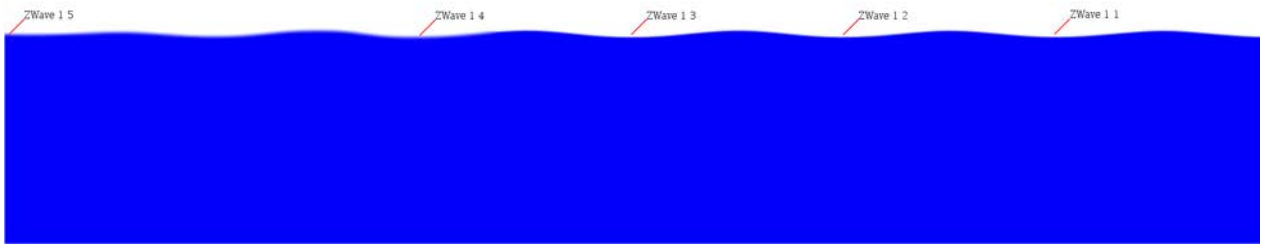

Figure 17 - Wave probe positions

It was noticed that the wave amplitude did increase by a small margin throughout the tank. For a simulation with wave length of 5.06m, wave height of 0.15 m and current of 1.04 m/s the amplitudes were found to increase by about 1 % for each wave length Table 8. The length between the probes was in this case one wavelength, except for probe 1_5 which is at the outlet. The desired wave amplitude was 0.075m, and this is located between wave probe 1_2 and 1_3. This is the area where the ship was placed in the calm water simulation. Due to not getting a constant wave throughout the tank, it would be necessary to calibrate waves for each simulation with ship model.

Table 8 – Measurement from wave probes in 2D wave tank

Probe	0th amp [m]	1th amp [m]
1_1	-0.0005	0.0737
1_2	-0.0003	0.0745
1_3	-0.0003	0.0754
1_4	-0.0007	0.0767
1_5	-0.0006	0.0104

For irregular waves, there is a range of wave lengths where a part of the energy has shorter wave length then the peak value. A minimum of 40 cells per peak wave length and 6 cells per significant wave height gave reasonable results for all but the shortest wave lengths.

Length of time step were tested in the 2D tank, and it was found that for a 2D tank that about 100 time step per wave encounter was sufficient. The encounter frequency is in this case defined as the wave frequency the wave probe sees.

Different mesh refinements distributions were tested. It was found that the free surface needed to be refined through the entire tank to avoid reflections, but a coarser mesh could be used in the wave damping zone.

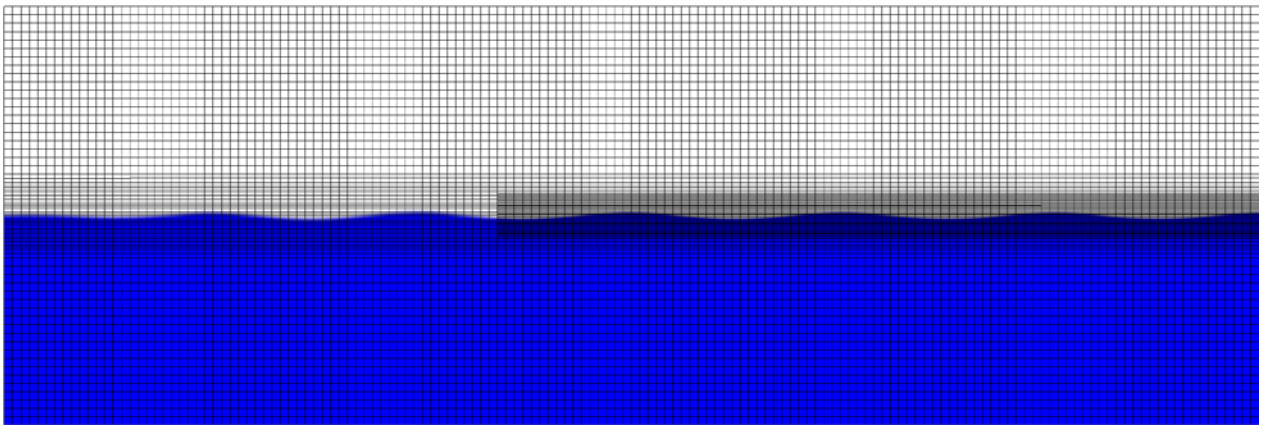

Figure 18 - 2D wave tank mesh with wave

4.5.2 3D wave tank

When satisfying results were found the tank were then extended to 3D, but still without a ship model. The results from 2D tank had to be verified that they also apply in 3D. Effect of side damping was investigated and different mesh strategies in the width of the tank was investigated.

There was great agreement between the results from the 2D tank with the ones observed in the 3D tank. The same phenomena with increasing wave amplitude throughout the tank was observed. There was no noticeable difference between 2D and 3D wave tank.

Simulations in 3D with and without side damping was tested. With side damping it was possible to achieve waves which would seem long crested near the ship, but would dampen out closer to the wall (Figure 4). The mesh in the damping zone could also be coarser without having any negative effect. The results were also very similar to 2D for simulation without side damping. Different cell width were tested, but no effect were found.

4.6 Wave tank with ship

The finding from the wave tanks were implemented in to the calm water resistance simulation. The mesh near the free surface was refined throughout the tank and boundary conditions were changed to generate waves. To reduce the amount of cells the free surface were refined in multiple layers throughout the tank (Figure 19). Side damping was applied due to reflections and/or instabilities in the free surface.

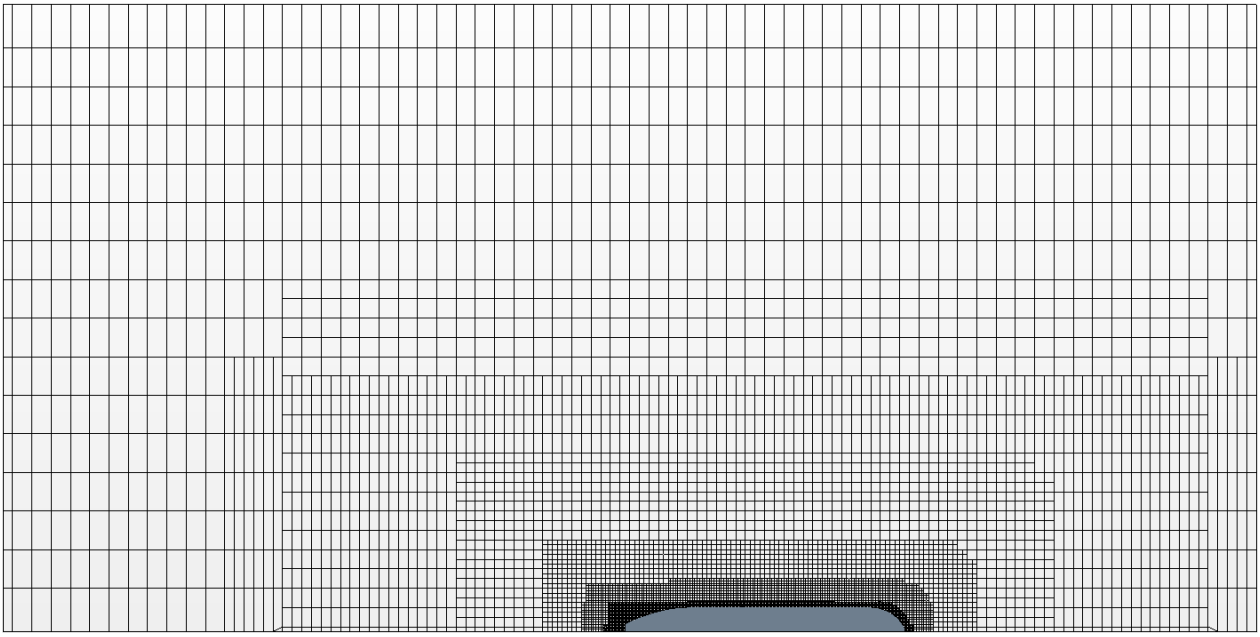

Figure 19 - An early wave tank mesh seen from above

Multiple undesired phenomena was observed in the NTW, which was not observed in either the calm water simulations or the empty wave tank. It was found that most of these errors were connected to ship motions, which is reasonable as that is the main difference between the previous simulation and the NWT. A simulation were set up with fixed ship motions, and the problems disappeared. It was found the pitch motion lead to instabilities and reflections. Having fixed ship motions will not give correct added resistance, so other solutions had to be found.

Low frequency waves were observed traveling through the length of the tank, both with and against the current. The source for this reflection were found to be a too coarse mesh near the outlet. The mesh was especially to coarse in the vertical direction. By refining this area the low frequency waves disappeared.

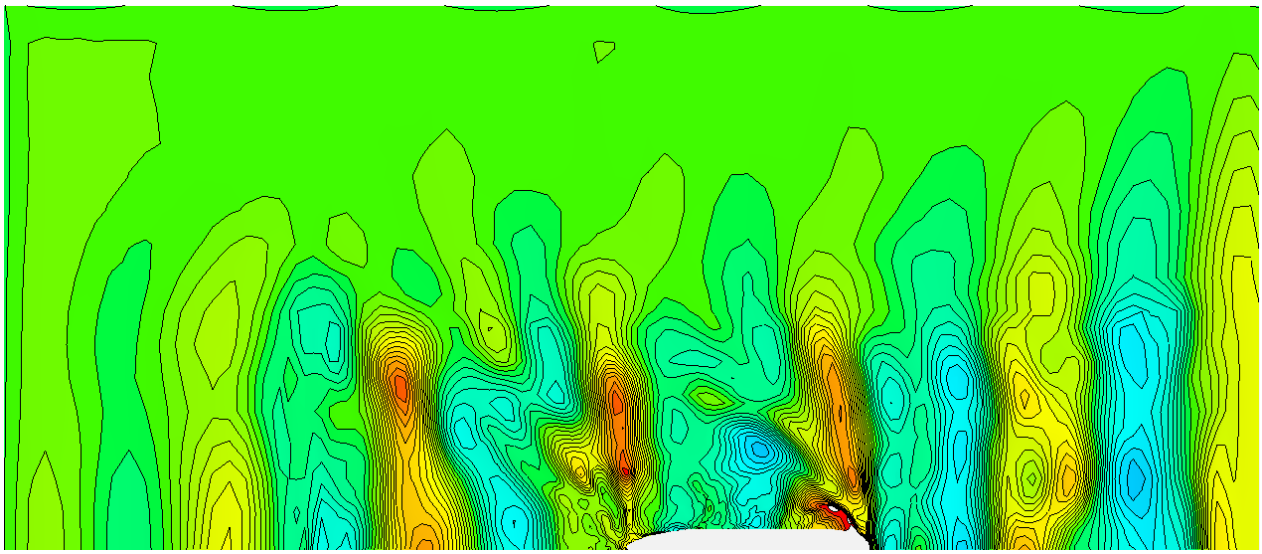

Figure 20 - Wave tank with instabilites causing an unsmooth free surface

The incoming waves was observed to have an unsmooth surface for some simulations. The effect of this varied with the ship motions. Simulations with little motions had realistic waves, while large motions gave waves as seen in Figure 20. Two improvements were implemented to fix this.

First, the ship was moved closer to the inlet. The thought behind this decision was that the speed the free surface traveled through the mesh due to mesh rotation could cause instabilities. Another benefit by moving the ship closer to the inlet was that the height of the refined region in front of the ship could be reduced, as there was less movement of the mesh at the inlet.

Another observation was that the instabilities in the free surface originated from where the mesh changed refinements. A uniform mesh with cell width equal cell length was applied around the free surface and no coarsening except behind the ship. This increased the total number of cells, and the extra width due to side damping was not reasonable. Side damping was removed, and the tank width was reduced from 15 m to 5 m. The final dimensions of the tank was a 30 m long, 5 m wide and 10 m tall.

These changes combined greatly improved the stability of the free surface. Effects as those seen in Figure 20 disappeared and the incoming waves had a uniform profile across the tank. But it was noted on the wave probes that there was a quite large wave damping in the tank, and the measured wave heights had quite large variations. It was known from the 2D wave tank that too few time steps increased the amount of damping. The time step was changed from 100 steps per encounter frequency to 250. This improved the accuracy of the wave, making it near constant through the tank, but the measured wave amplitude did not match the specified wave, and thus the wave needed to be calibrated for each condition. With these improvements, the unstable simulation in Figure 20 changed into a very stable simulation as seen in Figure 21.

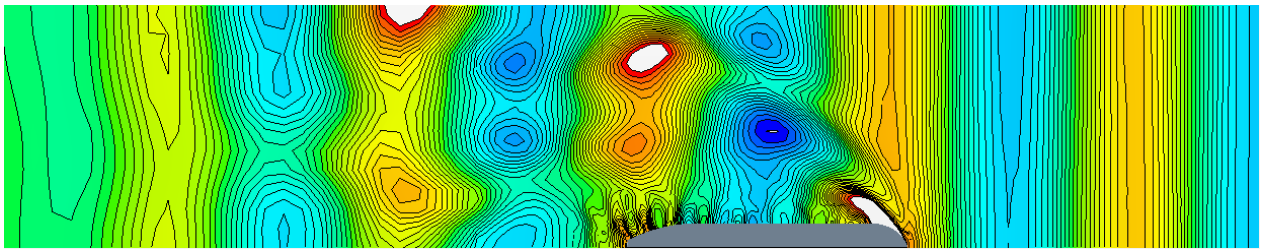

Figure 21 – Simulation of KVLCC2 in head waves with stable long crested head waves

4.7 Regular head waves

Good validation data is essential when testing new methods, such as using inviscid CFD to calculate added resistance. The most complete data and up to date validation data is the results from the Gothenburg 2010 workshop (Larsson et al., 2010, 2014). Test case 1.4b from the workshop used KVLCC2 in head waves. The model was free to move in heave and pitch, but fixed in the other degrees of freedom. Three out of five wave conditions for test 1.4b were tested with the inviscid NWT. The details for these conditions is found in Table 9.

Both EFD and CFD data was available for comparison. The EFD data was provided by NTNU, while four participants delivered CFD results by using five different CFD codes. STAR CCM+ was not one of these codes, so a direct comparison with the same CFD code was not possible.

For each case the same simulation setup were used. Two simulations were documented for each case. One with wave height calibrated as specified in the case, and one with wave height calibrated as the wave height as measured in the EFD. Waves were calibrated by a wave probe two meters in front of FP.

Table 9 - Test cases for KVLCC2 in head waves from Gothenburg 2010 workshop, case 1.4b

Case no.	C3	C4	C5
λ / L_{PP}	0.6364	0.9171	0.6364
H / λ	1/23	1/34	1/23
Fn	0.142	0.142	0.182

The mesh applied for the three simulations were equal, even though the wave lengths were different. This is due to the trimmer mesher, which choose cell lengths relative to a given base size (see chapter 3.2.3). To obtain an equal cell length / wave length ratio the base size must have been changed, which would change the size of every cell in the mesh. This was not tested, as the results were good for all three simulations at the same mesh. This mesh consisted of 433 000 cells and can be seen in Figure 22, Figure 23 and Figure 24.

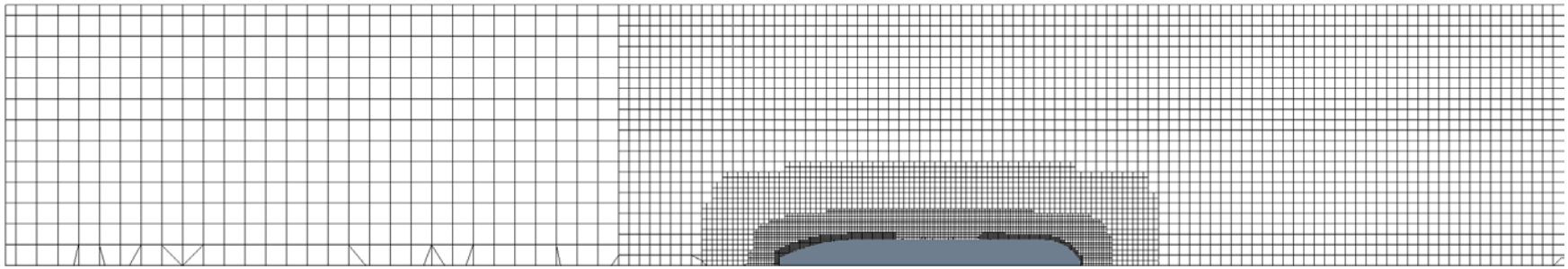

Figure 22 - Mesh KVLCC2 used for head waves. Seen from above onto free surface

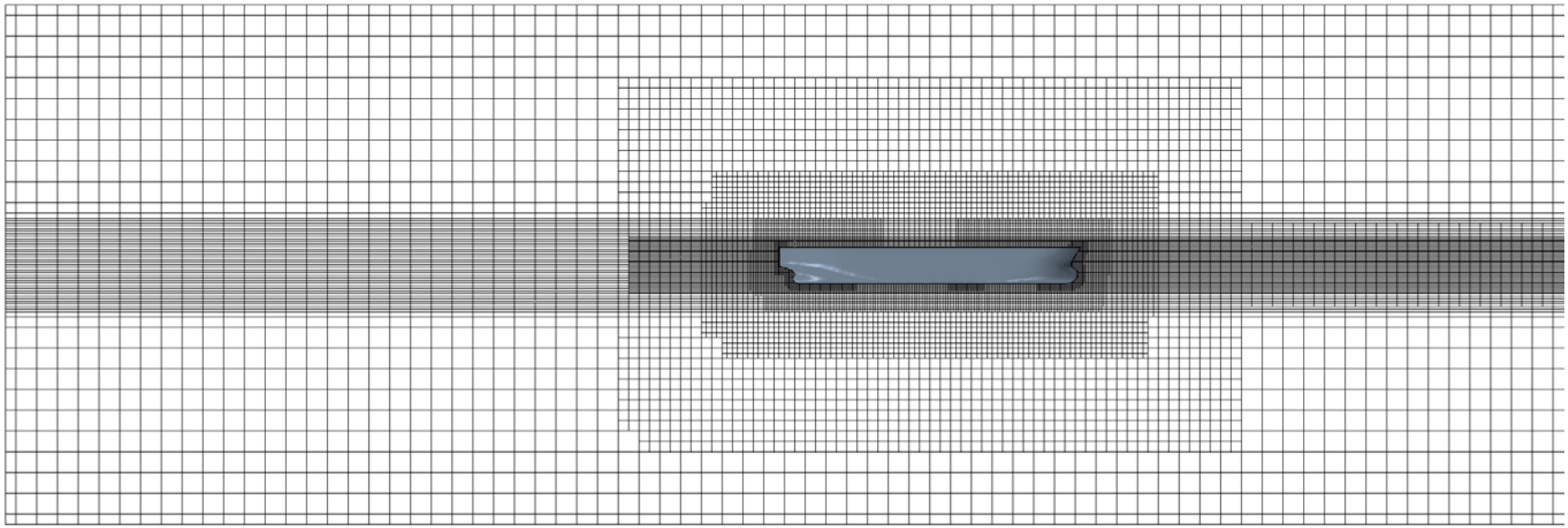

Figure 23 - Mesh KVLCC2 used for head waves. Seen from side onto plane through centerline of ship

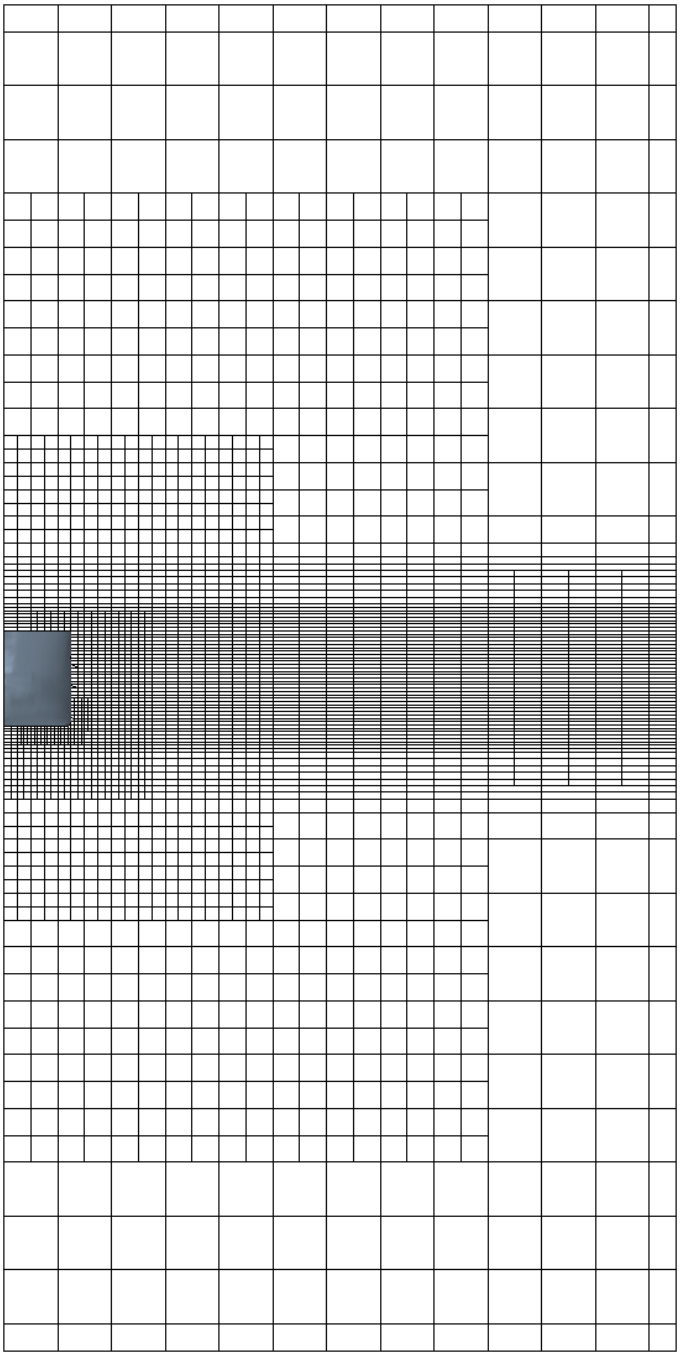

Figure 24 - Mesh KVLCC2 used for head waves. Seen from front onto plane through mid-ship

4.7.1 Result of regular head waves

Results from head wave conditions are presented in Table 10, Table 11 and Table 12. E is the error and is defined as D-S, where D is EFD result and S is simulated result. E%D is error relative to EFD result given as a percentage, and E%360° is phase error relative to 360° also given as a percentage. R_T is total resistance, z is motion in heave and θ is motion in pitch. Time series of resistance, motions and measured wave amplitude for all simulations can be found in appendix A.

Table 10 - Test case C3 from Larsson et al. (2010) compared with inviscid wave tank results

Organization (Code) [Wave height]		R_T			z			θ		
		0th Amplitude (N)	1st Amplitude (N)	1st Phase°	0th Amplitude (mm)	1st Amplitude (mm)	1st Phase°	0th Amplitude°	1st Amplitude°	1st Phase°
EFD (NTNU) [0.140m]	D	40.347	269.354	-	-6.409	5.549	9.141	-0.123	0.147	106.43
ECN/ CNRS (ISISCFD)	S	41.880	252.800	-	-5.910	5.490	-	-0.119	0.155	-
	E%(D/360°)	-3.800	6.146	-	7.786	1.063	-	3.409	-5.442	-
ECN (ICARE)	S	45.000	255.000	22.00	-6.000	5.400	119.00	-0.120	0.160	-139.00
	E%(D/360°)	-11.530	5.330	-	6.380	2.690	-30.516	2.600	-8.840	68.176
GL&UDE (Comet)	S	-	-	-	-6.294	4.743	117.76	-0.181	0.124	-149.67
	E%(D/360°)	-	-	-	1.790	14.530	-30.172	-46.920	15.650	71.140
GL&UDE (OpenFOAM)	S	-	-	-	-4.986	4.464	122.01	-0.109	0.099	-158.05
	E%(D/360°)	-	-	-	22.200	19.550	-31.353	11.530	32.650	73.468
Kyushu University (RIAM-CMEN)	S	50.171	279.172	-18.47	-8.488	4.980	116.32	-0.194	0.208	-153.36
	E%(D/360°)	-24.350	-3.650	-	-32.440	10.250	-29.772	-57.470	-41.500	72.165
(STAR CCM+ Inviscid) [0.147m]	S	40.104	262.488	26.295	-8.200	6.100	151.94	-0.147	0.090	-126.66
	E%(D/360°)	0.603	2.549	-	-27.945	-9.930	-39.666	-19.350	38.776	64.747
(STAR CCM+ Inviscid) [0.141m]	S	38.557	253.521	22.415	-8.100	5.800	148.48	-0.145	0.092	-127.93
	E%(D/360°)	4.437	5.878	-	-26.385	-4.523	-38.705	-17.886	37.211	65.100

Table 11 - Test case C4 from Larsson et al. (2010) compared with inviscd wave tank results

Organization (Code) [Wave height]		R_T			z			θ		
		0th Amplitude (N)	1st Amplitude (N)	1st Phase°	0th Amplitude (mm)	1st Amplitude (mm)	1st Phase°	0th Amplitude°	1st Amplitude°	1st Phase°
EFD (NTNU) [0.138m]	D	59.359	603.078	-	-6.516	12.631	-175.67	-0.137	1.357	-126.001
ECN/ CNRS (ISISCFD)	S	63.960	210.000	-	-5.910	13.230	-	-0.138	1.467	-
	E%(D/360°)	-7.751	65.179	-	9.300	-4.742	-	-0.511	-8.106	-
ECN (ICARE)	S	65.500	230.500	17.000	-6.100	14.350	110.00	-0.145	1.504	174.000
	E%(D/360°)	-10.350	61.780	-	6.380	-13.610	-79.353	-5.920	-10.830	-83.334
GL&UDE (Comet)	S	-	-	-	-6.100	12.482	98.390	-0.191	1.323	160.430
	E%(D/360°)	-	-	-	6.380	1.180	-76.128	-39.520	2.510	-79.564
GL&UDE (OpenFOAM)	S	-	-	-	-3.427	13.079	105.41	-0.118	1.358	163.690
	E%(D/360°)	-	-	-	47.410	-3.550	-78.078	13.810	-0.070	-80.470
Kyushu University (RIAM-CMEN)	S	59.694	206.351	1.827	-8.499	9.929	96.390	-0.186	1.324	156.074
	E%(D/360°)	-0.560	65.780	-	-30.430	21.390	-75.573	-35.870	2.430	-78.354
(STAR CCM+ Inviscid) [0.140m]	S	60.122	208.757	-92.687	-7.600	14.500	-3.632	-0.142	1.487	55.152
	E%(D/360°)	-1.285	65.385	-	-16.636	-14.797	-47.789	-3.869	-9.573	-50.320
(STAR CCM+ Inviscid) [0.149m]	S	65.141	220.096	-92.838	-8.000	15.600	-4.420	-0.153	1.605	54.226
	E%(D/360°)	-9.741	63.505	-	-22.775	-23.506	-47.570	-11.606	-18.254	-50.063

Table 12 - Test case C5 from Larsson et al. (2010) compared with inviscd wave tank results

Organization (Code) [Wave height]		R_T			z			ϑ		
		0th Amplitude (N)	1st Amplitude (N)	1st Phase°	0th Amplitude (mm)	1st Amplitude (mm)	1st Phase°	0th Amplitude°	1st Amplitude°	1st Phase°
EFD (NTNU) [0.140m]	*D*	53.764	247.18	-	-11.162	4.571	154.947	-0.216	0.123	-109.50
ECN/CNRS (ISISCFD)	*S*	53.230	258.27	-	-9.830	4.500	-	-0.205	0.120	-
	E%(D/360°)	0.994	-4.485	-	11.933	1.553	-	5.005	2.123	-
ECN (ICARE)	*S*	65.000	268.00	13.000	-9.850	4.800	122.000	-0.210	0.120	-143.00
	E%(D/360°)	-20.900	-8.420	-	11.750	-5.010	9.152	2.690	2.120	9.305
GL&UDE (Comet)	*S*	-	-	-	-10.252	3.995	113.760	-0.269	0.106	-151.62
	E%(D/360°)	-	-	-	8.150	12.600	11.441	-24.650	13.540	11.699
GL&UDE (OpenFOAM)	*S*	-	-	-	-10.061	3.704	119.710	-0.196	0.083	-162.67
	E%(D/360°)	-	-	-	9.860	18.970	9.788	9.180	32.300	14.769
Kyushu University (RIAM-CMEN)	*S*	80.446	289.29	-25.72	-15.943	3.676	115.482	-0.346	0.123	151.518
	E%(D/360°)	-49.630	-17.030	-	-42.830	19.580	10.963	-60.330	-0.320	-72.506
STAR CCM+ Inviscid [0.143m]	*S*	53.492	259.56	26.065	-12.600	5.000	148.057	-0.240	0.094	-126.41
	E%(D/360°)	0.506	-5.008	-	-12.883	-9.385	1.914	-11.157	23.740	4.697
STAR CCM+ Inviscid [0.147m]	*S*	55.726	266.44	28.630	-12.700	5.100	150.371	-0.240	0.094	-126.87
	E%(D/360°)	-3.649	-7.794	-	-13.779	-11.573	1.271	-11.250	23.415	4.823

4.8 Irregular head waves

Ships usually operates in irregular waves, and thus irregular waves should be used for design optimization. The inviscid wave tank have to be able to handle ship in irregular waves if it should be applied for design optimization. To investigate the capabilities a test with KVLCC2 in irregular head waves were performed.

No comparison data were found for KVLCC2 with forward speed in irregular head waves, so test conditions were selected freely. One condition with short waves and one condition long waves were tested. The long wave condition had a mean zero crossing period corresponding to 1.2 L_{PP} (case JS2). This condition will give large pitch motions, which should result in large added resistance. All wave conditions were head waves and wave profiles were calculated by using the JONSWAP spectra (see chapter 3.5.2). Peak period and significant wave height for each condition is found in Table 13. The combination of significant wave height and peak period was chosen to give conditions regularly seen at sea. Both cases were performed with KVLCC2 at design speed with Fn = 0.142.

Table 13 - Test conditions for irregular waves

Case name		JS1	JS2
Full scale	H_S	7	10
	T_P	9.5	20.2
Model scale 1:58	H_S	0.12	0.17
	T_P	1.2	2.7

The mesh were adjusted slightly compared to the mesh used for regular head waves. 40 cells per peak wave length is necessary to capture the wave components with shorter wave length. This was applied for test case JS2, but for JS1 the peak wave length is only 2.43 m, which would have given unreasonable many cells. 20 cells per peak wave length was chosen to keep the simulation size low. For case JS1 the tank size was reduced by moving the outlet and inlet closer to the ship model, which is possible due to shorter waves. This gave a tank length of 14m. For case JS2 the dimensions were kept the same as for regular head waves. Both meshes had a total number of cells of about 400 000.

A long simulation time is required for irregular waves. This is to capture the irregularities of the wave conditions and get waves in the whole range of frequencies for the spectra. Both conditions were simulated for 300 seconds, but ideally the JS2 conditions should have been simulated for a longer time than the JS1, as the number of wave encounters is what matters.

4.8.1 Results for irregular waves

The free surface elevation due to the incoming waves were measured in front of the model by a wave probe. This time series was converted into the frequency plane (see chapter 3.5.2) and compared against the source JONSWAP spectra (Figure 25, Figure 26).

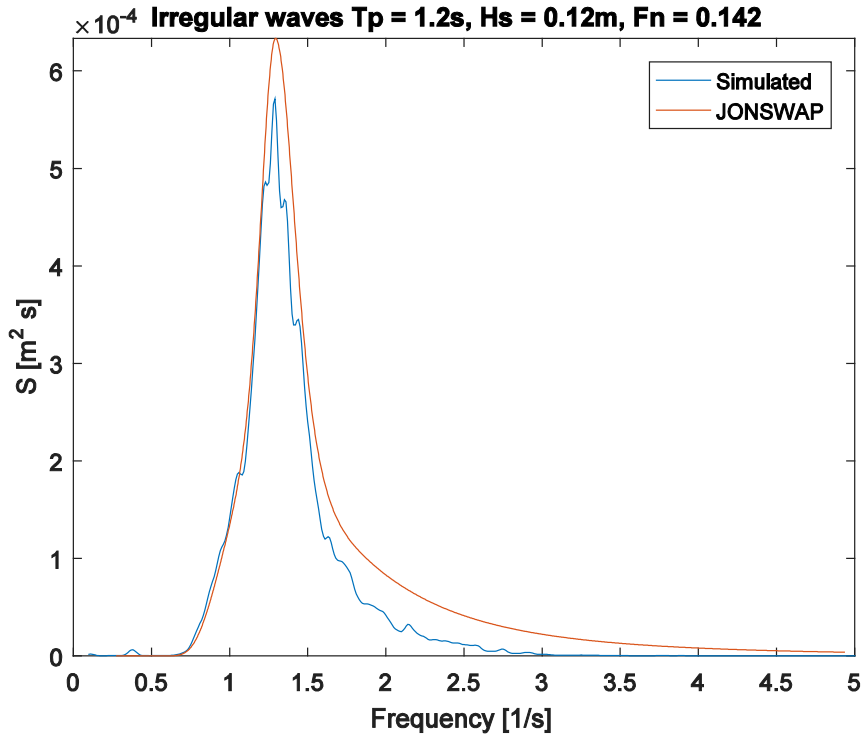

Figure 25 - Measured and source wave spectra for case JS1. Frequency is given as encounter frequency.

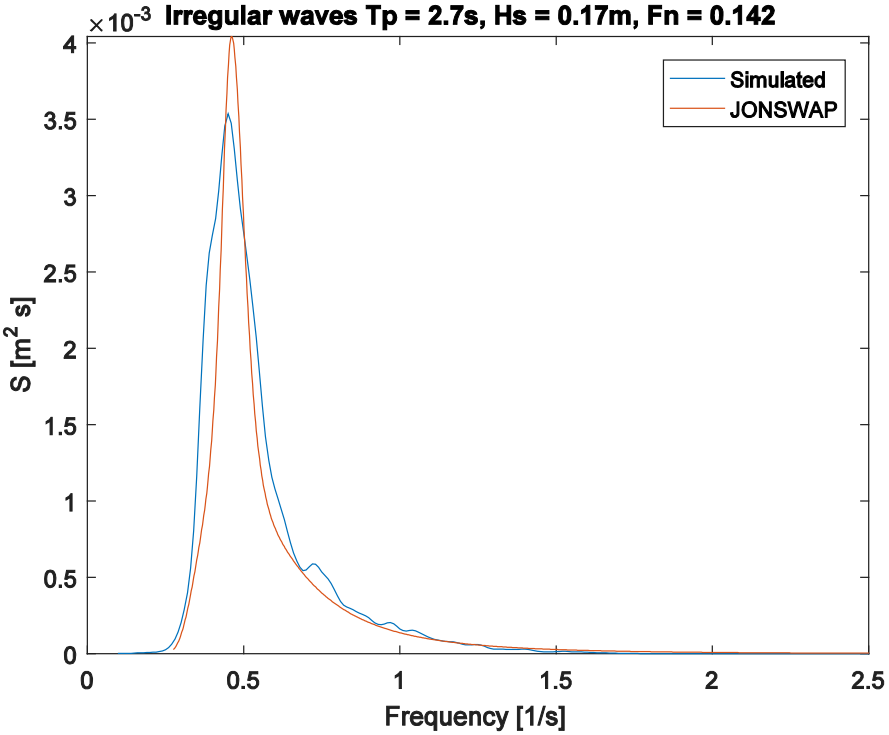

Figure 26 - Measured and source wave spectra for case JS2. Frequency is given as encounter frequency.

Motion and resistance was also measured as time series. The motion series were transformed into frequency domain and RAO's were calculated. The RAO's are only valid for a limited frequency range corresponding to the frequencies that contains significant wave energy. The RAOs for both conditions can be found in Appendix B. The RAO's were compare with RAOS found in B. J. Guo, Steen, and Deng (2012). The figures in the article were not accurate enough for exact comparison, but the RAO were in the same range as in the article.

Added resistance due to waves cannot be calculated in the same manner as the motions. The mean of the resistance time series is calculated and the resistance from the inviscid calm water simulation is subtracted to find the added resistance due to waves (Table 14). A ratio between the calm water resistance from the viscous simulations and the added resistance was calculated.

Table 14 - Added resistance due to waves from inviscid wave tank with irregular JONSWAP waves

Case name	JS1	JS2
Added resistance R_{aw} [N]	5.16	11.58
R_{aw}/R_{Tcalm}	30.0%	67.3%

5 Estimate of saving potential and comparison between turbulence and inviscid NWT

5.1 Saving potential of inviscid solver

Solving the Euler equations is quicker then solving the Navier stokes equations. The reason is that the viscous part of the Navier Stokes equations is disregarded. The savings is depending on which turbulence model that is applied. The most commonly used turbulence models in ship hydrodynamics is 2-equations turbulence models (see chapter 3.1.11).

The 2-equations turbulence models require an additional two equations to be solved for each cell. With Euler there is four equations for each cell, one for pressure and three for velocities. With a turbulence model the total number of equations solved is six. This gives a theoretical saving potential of 33 % by using an inviscid solver instead of a 2-equations turbulent solver, if solution time scales linearly with number of equations. Modern solvers do scale almost linearly, so this is a good assumption.

A test was performed in STAR CCM+ where a ship in calm water was first simulated with a 2-equation $k-\varepsilon$ turbulence model. After the exact same simulation was performed with an inviscid solver. The average solver time / time step was compared (Table 15) and a reduction in simulation time of 34.9 % was observed. This is consistent with the theoretical estimation of 33 %.

Table 15 - Comparison of solver time / time step for a simulation of a ship in calm water with 0.73M cells

Solver	Average Solver time per time step [s]
Inviscid	2.13
2-equation $k-\varepsilon$ turbulence	3.27

5.2 Saving potential due to mesh

A refined mesh close to the ship hull is required to solve the flow in the boundary layer. An accurate boundary layer flow is essential to calculate the viscous drag resistance. This refined mesh increases the total number of cells. If viscosity is neglected then there will not be any boundary layers as boundary layer is a viscous effect. This reduces the number of cells needed for an inviscid simulation, but at the cost of not getting result for friction resistance.

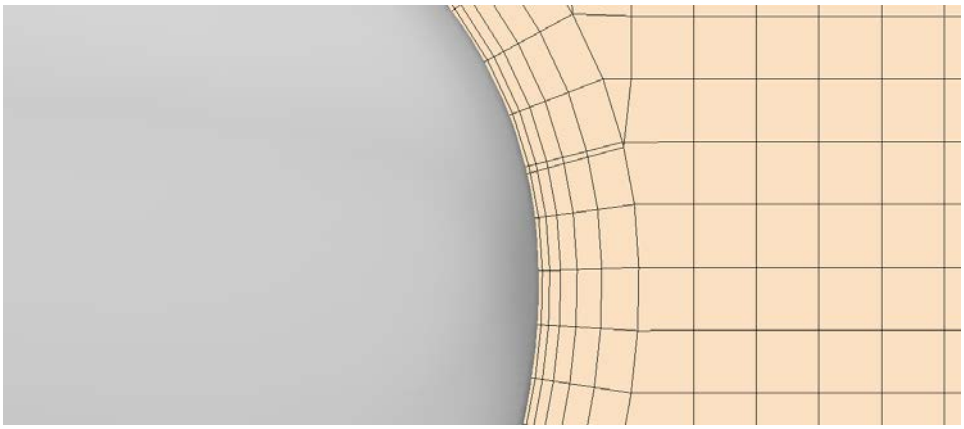

Figure 27 - Refined mesh near ship hull to capture boundary layer flow

It is impossible to give an exact percentage of mesh size reduction. The reduction is very dependent on how fine the ship and boundary layer is meshed compared to the free surface. In the setup used for NWT in this thesis the reduction was between 20 - 30 %, but different results must be expected in other setups.

5.3 Comparison of simulation time for a wave tank simulation with and without viscosity

A complete ship in head waves simulations with viscosity was performed to find the total computational time reduction. Test case C3 (see chapter 4.7) was modified to include viscosity. Realizable $k-\varepsilon$ turbulence model was utilized and six prism layers was added to solve the boundary layer. The mesh increased by 38 % over the inviscid mesh. Both simulations were performed at the same supercomputer with equally allocated resources. A 100 second time simulation in model scale took 5 hours and 33 minutes for the inviscid tank and 10 hours and 1 minute for the viscous simulation. That is a total reduction of 45 % in computational time by using inviscid wave tank.

5.4 Comparison of added resistance and motions for wave tank

The result from the viscous wave tank was analyzed in the same manner as for inviscid wave tank (see chapter 3.5). The results were compared with data from the Gothenburg workshop and the inviscid wave tank (Table 16). Notice that the inviscid simulation have frictional and viscous pressure resistance from calm water simulation added to the inviscid resistance. Also note that the waves was tuned for 0.14m wave height as recorded in model test, and not 0.15m as given in the task before the workshop. This explains the higher results for 0^{th} amplitude of resistance for CFD results at the workshop. A comparison for the same case was also made where the viscous wave tank was used as a reference (Table 17). This was used to show the relative difference between the two methods.

Table 16 - Comparision of EFD, CFD from workshop, inviscid and viscous simulations for case C3

Organization (Code)		R_T		z			θ		
		0th Amplitude (N)	1st Amplitude (N)	0th Amplitude (mm)	1st Amplitude (mm)	1st Phase°	0th Amplitude°	1st Amplitude°	1st Phase°
EFD (NTNU)	*D*	40.35	269.4	-6.409	5.549	9.1	-0.123	0.147	106.4
Average CFD Workshop	*S*	45.68	262.3	-6.336	5.015	118.8	-0.145	0.149	-150.0
	E%D/360	-13.23	2.61	1.15	9.62	-30.45	-17.56	-1.50	71.24
Invisicd	*S*	40.10	262.5	-8.200	6.100	151.9	-0.147	0.090	-126.7
	E%D/360	0.60	2.55	-27.95	-9.93	-39.67	-19.35	38.78	64.75
k-e turbulence	*S*	42.20	258.7	-7.800	5.900	150.4	-0.137	0.104	-118.6
	E%D/360	-4.60	3.95	-21.70	-6.33	-39.25	-11.46	29.18	62.52

Table 17 - Comparision of viscous and inviscid simulations for case C3

Code		R_T		z			θ		
		0th Amplitude (N)	1st Amplitude (N)	0th Amplitude (mm)	1st Amplitude (mm)	1st Phase°	0th Amplitude°	1st Amplitude°	1st Phase°
k-e turbulence	D	42.20	258.7	-7.8	5.9	150.4	-0.137	0.104	-118.6
Invisicd	S	40.10	262.5	-8.2	6.1	151.9	-0.147	0.090	-126.7
	E%*D/360*	4.97	-1.45	-5.13	-3.39	-0.42	-7.08	13.54	2.23

A good agreement between viscous and inviscid simulations were found. With regard to 0th amplitude of resistance the inviscid method gave lower resistance than the viscous. Both results are within a small margin of error, and even though the inviscid is closer to the EFD it does not mean that it is in general more accurate. For a different case, the results may vary.

Regarding the motions the viscous simulation gave results closer to the EFD data than inviscid for both 0th and first amplitude in heave and pitch. A wave probe measured the incoming wave about 0.5 L_{PP} in front of FP. There was no increase in wave amplitude damping due to viscosity for the test case.

Irregular waves was also tested in a 2D wave tank. 300 seconds were simulated on same mesh and time step with the same wave generation seed. The free surface were logged by a wave probe and a FFT transformed the signal back to frequency domain (Figure 28). As with the regular waves no large difference were noted, but at the higher frequencies there seems to be more damping for viscous waves.

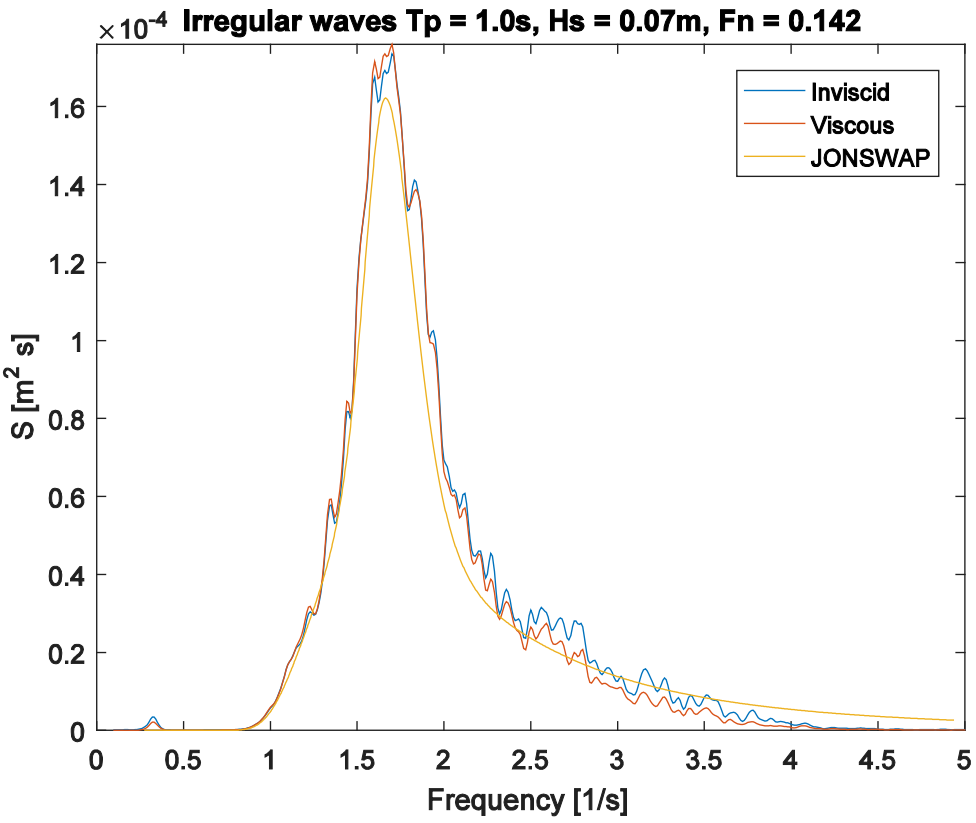

Figure 28 - Wave spectra messured in 2D wave tank and compared with JONSWAP source spectra

5.5 Investigation of inviscid added resistance assumption

The assumption of added resistance being independent on viscosity was investigated. Test case C3 was as mentioned in chapter 5.3 run with and without viscosity. By studying the resistance components, it would be possible to check the validity of the assumption.

If added resistance is an inviscid phenomenon, then friction resistance should remain steady at the calm water friction resistance of 13.50 N. This was plotted (Figure 29) and the friction resistance was found to have a mean of 16.15 N with an amplitude of 2.25 N.

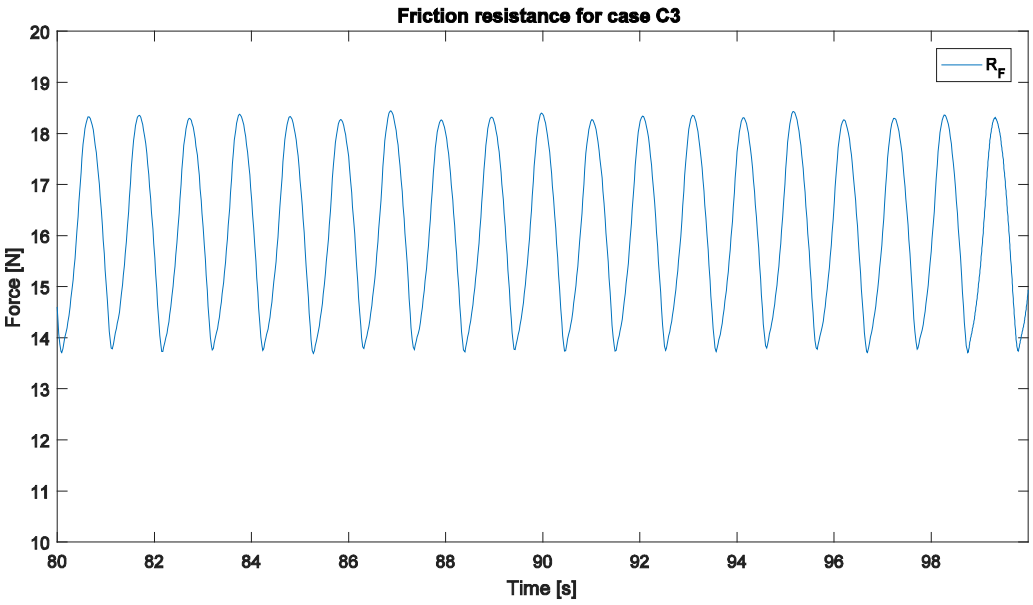

Figure 29 - Friction resistance for viscous wave simulation case C3

The pressure resistance from the viscous simulation should follow the pressure resistance from the inviscid simulation, but have a slightly higher value due to the viscous pressure resistance. The viscous pressure resistance was found to be 2.00 N in calm water (Table 7). Figure 30 shows this trend. If the assumption is correct this also means that if the pressure resistance in the inviscid simulation is subtracted from the pressure resistance in the viscous simulation one should find a steady value of 2.00 N. This difference is plotted in Figure 31. The mean value of the difference is 3.03 N with an amplitude of 4.04 N for the wave encounter frequency.

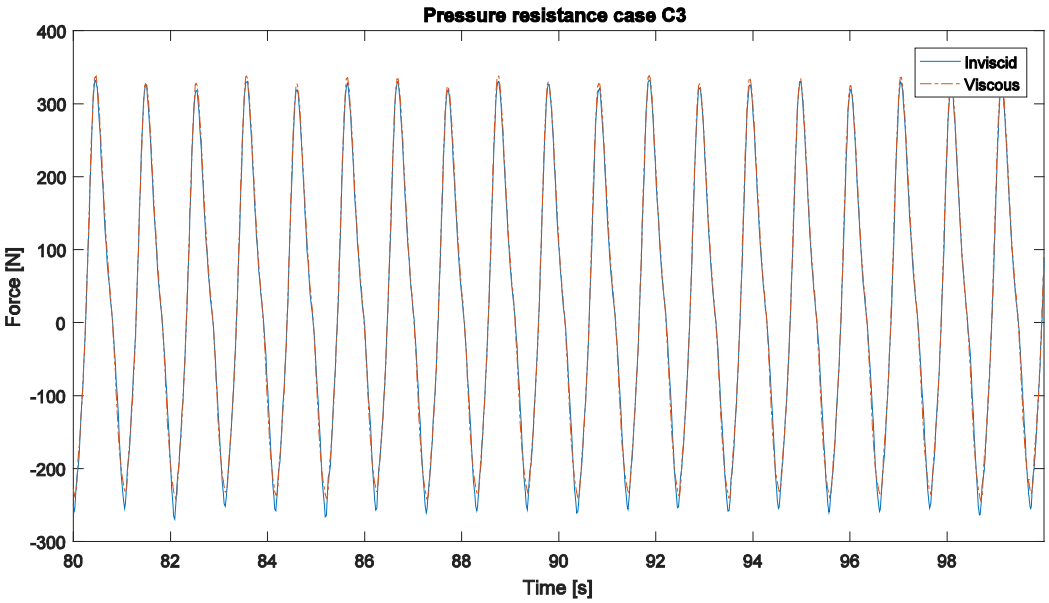

Figure 30 - Pressure resistance for case C3

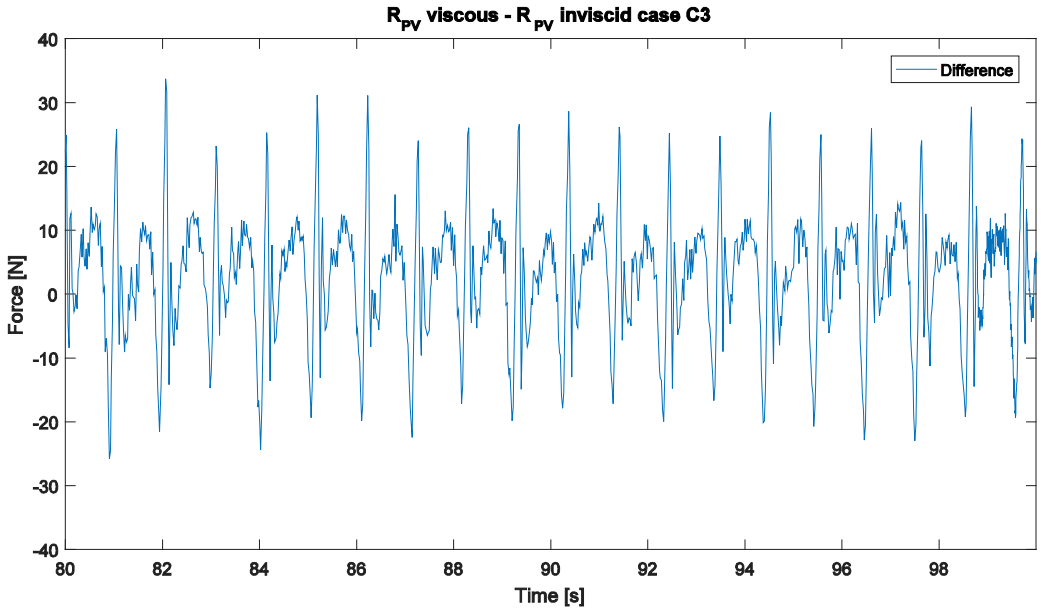

Figure 31 - Inviscid pressure resistance subtracted from the viscous pressure resistance

6 Discussion of results

Calm water resistance was calculated for KVLCC2 for Fn = 0.142 and 0.182 with viscosity enabled. The resistance components converged nicely to a steady value. The results for Fn = 0.142 were compared with results from case 1.2b at the Gothenburg 2010 conference (Larsson et al., 2010). There was a good agreement with the EFD data with an error in total resistance of 3.9 %. This is about the same accuracy as the CFD results submitted by MOERI for the same test case.

When comparing the results against MOERI there is a larger error. MOERI had over-estimated the resistance compared to EFD, while the presented CFD results under-estimated the resistance. Resistance can be measured as a shear force resistance and a pressure force resistance in CFD. Compared against MOERI there were a similar ratio between the shear force resistance and the pressure force resistance.

Wave profiles were recorded for calm water simulation in both inviscid and viscous tank for Fn = 0.142. These were compared with EFD data from test case 1.1b from Gothenburg 2010 workshop (Larsson et al., 2010). An excellent agreement were found near the hull. Further away from the ship the wave amplitudes of the generated waves were overestimated. The profiles from the inviscid wave tank had better agreement with EFD results than from the viscous tank. It is unknown what causes these larger amplitudes away from the ship.

Regular head waves was tested for KVLCC2 by applying an inviscid NWT. Calm water resistance due to viscosity was added to the measured results to find total resistance. The results were compared with case C3, C4 and C5 from test case 1.4b from the Gothenburg 2010 workshop (Larsson et al., 2010). Data from the workshop consisted of 0^{th} amplitude, first amplitude and phase of resistance, heave and pitch motions.

Compared with the other CFD results there is in general an equally good accuracy for the inviscid calculations. The largest errors is found for phase, 0^{th} amplitude of heave and first amplitude of pitch. All CFD participant have large errors for phase calculations, and there is reason to believe that different reference systems could have been used for EFD and CFD data (see chapter 3.5.1).

Both the large 0^{th} amplitude error in heave and the error in phase should not be linked directly to the use of an inviscid wave tank, as similar errors were observed when a turbulence model was applied. There is more reason to believe that the errors is connected to the computational setup. Results from the inviscid tank was compared with results from viscous wave tank where a similar mesh and computational setup was applied. Small differences were noticed, but much smaller than the error compared with EFD data. It was noticed that the mean resistance was almost 5 % lower for inviscid calculations compared with viscous calculations.

Short and long irregular head waves from the JONSWAP spectra was tested. No comparison data was found, so it was not possible to validate the results. The generated waves were measured and compared with the applied JONSWAP spectra. There was in general good agreement, but the peak is not as high as in the JONSWAP spectra. For short waves there is a lower energy in the high frequency range. This is not observed for the long waves. The number of cells per peak wave length was only 20 for the short waves compared with 40 for the long wave. This was changed to maintain a similar total amount of cells. It is believed that this causes the increased damping for the high frequency waves.

A 45 % reduction in computational time is achieved by applying inviscid wave tank compared to a viscous tank with a two-equation turbulence model. The reduction is both due to fewer solved equations and less cells, as the boundary layer do not need to be resolved. The reduction in computational time is significant, but probably not large enough to make hull optimization based on added resistance viable with today's price for computational power.

A brief investigation of the assumption that added resistance is an inviscid phenomenon was performed. If the assumption is true, then the friction resistance and viscous pressure resistance should be equal for simulations in waves and calm water. Both the friction resistance and the viscous pressure resistance was found to increase and oscillate with wave encounter frequency. The large peaks in the viscous pressure resistance should be ignored as they are due to a small phase difference between pressure resistance in the viscous and inviscid simulation. The difference in average friction resistance could be due to different meshes. The mesh used for calm water resistance was more refined near the hull. The oscillations of both friction resistance and viscous pressure resistance with encounter frequency should not occur if added resistance is purely an inviscid phenomenon. However, the added resistance due to the viscous effect is small relative to the inviscid effects.

7 Conclusions

This thesis have investigated if added resistance and motions on a ship in head waves can be accurately calculated with inviscid CFD. Tests on KVLCC2 have been performed in regular head waves, and the results have been compared with both EFD and CFD results.

Application of inviscid CFD to calculate the added resistance and motions of ship in regular head waves can give equal accuracy as viscous CFD. Total resistance in wave can be found by adding the friction and viscous pressure resistance from calm water simulations with the pressure resistance from an inviscid wave simulation.

Computational time can be reduced by 30-50% by applying inviscid CFD instead of viscous CFD with two-equation turbulence model. The reduction is due to not solving the equation for turbulence and a reduction in mesh size as the boundary layer do not need to be resolved.

Added resistance due to waves seems to have a small dependency on viscosity, as both friction resistance and viscous pressure resistance increased slightly in a viscous wave tank simulation compared with calm water. Both resistances was also observed to oscillate with wave encounter frequency, which suggest that viscosity does effect added resistance.

7.1 Suggestion for further work

Validation with other hulls is necessary before general conclusions can be drawn on accuracy of inviscid CFD. KVLCC2 is a large ship with relative small motions. For smaller ships with larger relative motions there might be a higher resistance due to viscous effects. It was harder to get stable results from the CFD calculation in conditions with large motions, and getting stable simulations on smaller ships might be challenging.

Only head waves was tested in this thesis. Resistance in oblique waves is important for ship performance, and should be considered when designing a hull. Oblique waves can give challenges not seen in this thesis. One concern is the increased motions due to roll. Applying overset mesh instead of rotating and translating mesh for handling the motion of the ship could help with this, but overset mesh has its own challenges that must be considered.

The achieved reduction of computational time is not enough to make design optimization based on resistance in wave resistance viable, but it is a step in the right direction. Further reduction of simulation cost is needed if CFD should be viable for optimization studies.

More accurate viscous simulations is required to be able to tell if added resistance is an inviscid phenomenon. The difference between viscous CFD and EFD is much larger than the difference between viscous and inviscid CFD, which makes it hard to say if a result is off due to computational setup or the assumption of inviscid added resistance.

8 Bibliography

Bertram, V., & Couser, P. (2014). *Computational Methods for Seakeeping and Added Resistance in Waves.* Paper presented at the 13th International Conference on Computer and IT Applications in the Maritime Industries (COMPIT'14), Redworth.

CD-adapco. (2015). Spotlight on Multiphase Flow. Retrieved from https://steve.cd-adapco.com/articles/en_US/FAQ/Spotlight-on-Multiphase-Flow

CD-adapco. (2016a). Spotlight on Overset Meshes. Retrieved from https://steve.cd-adapco.com/articles/en_US/FAQ/Spotlight-on-Overset-Meshes

CD-adapco. (2016b). *STAR CCM+ User Guide*.

Choi, J., & Yoon, S. B. (2009). Numerical simulations using momentum source wave-maker applied to RANS equation model. *Coastal Engineering, 56*(10), 1043-1060.

Cholleti, P. (2015). How do I setup my mesh to best capture VOF Waves? Retrieved from https://steve.cd-adapco.com/articles/en_US/FAQ/How-do-I-setup-my-mesh-to-best-capture-VOF-Waves

Deng, G. B., Leroyer, A., Guilmineau, E., Queutey, P., Visonneau, M., & Wackers, J. (2010). *VERIFICATION AND VALIDATION FOR UNSTEADY COMPUTATION*. Paper presented at the A Workshop on Numerical Ship Hydrodynamics, Gothenburg.

DNV. (2011). Modelling and Analysis of Marine Operations (Vol. DNV-RP-H103). http://www.dnv.com.

Faltinsen, O. M. (1990). *Sea loads on ships and offshore structures*. Cambridge: Cambridge University Press.

Faltinsen, O. M., Minsaas, K., Liapis, N., & Skjørdal, S. O. (1980). *Prediction of Resistance and Propulsion of a Ship in a Seaway. In Proceeding of 13th Symposium on Naval Hydrodynamics.* Paper presented at the 13th Symposium on Naval Hydrodynamics, Tokyo.

Fedkiw, R. P., Aslam, T., Merriman, B., & Osher, S. (1999). A non-oscillatory Eulerian approach to interfaces in multimaterial flows (the ghost fluid method). *Journal of computational physics, 152*(2), 457-492.

Ferziger, J. H., & Peric, M. (2012). *Computational Methods for Fluid Dynamics* (3rd ed. ed.). Berlin: Springer Berlin Heidelberg.

Gerritsma, J., & Beukelman, W. (1972). Analysis of the resistance increase in waves of a fast cargo ship. *International Shipbuilding Progress, 19*(217), 285-293.

Grin, R. (2015). On the Prediction of Wave-added Resistance with Empirical Methods. *J. Ship Prod. Des., 31*(3), 181-191.

Guo, B. (2011). *Numerical and experimental investigation of added resistance in waves.* (2011:329), Norwegian University of Science and Technology, Faculty of Engineering Science and Technology, Department of Marine Technology, Trondheim.

Guo, B., & Steen, S. (2010). *Added resistance of a VLCC in short waves.* Paper presented at the ASME 2010 29th International Conference on Ocean, Offshore and Arctic Engineering.

Guo, B., & Steen, S. (2011). Comparison of numerical methods for wave generation by VOF-based numerical wave tank (Vol. 6, pp. 575-584).

Guo, B. J., Steen, S., & Deng, G. B. (2012). Seakeeping prediction of KVLCC2 in head waves with RANS. *Applied Ocean Research, 35*, 56-67. doi:http://dx.doi.org/10.1016/j.apor.2011.12.003

Hadžić, H. (2006). Development and application of finite volume method for the computation of flows around moving bodies on unstructured, overlapping grids: Hamburg Arbeitsbereiche Schiffbau, Techn. Univ. Hamburg-Harburg.

Harten, A., Engquist, B., Osher, S., & Chakravarthy, S. R. (1987). Uniformly high order accurate essentially non-oscillatory schemes, III. *Journal of computational physics, 71*(2), 231-303. doi:10.1016/0021-9991(87)90031-3

Hasselmann, K. (1973). *Measurements of wind-wave growth and swell decay during the joint North Sea wave project (JONSWAP)* (Vol. 12). Hamburg: Deutsches Hydrographisches Institut.

Hirt, C. W., & Nichols, B. D. (1981). Volume of fluid (VOF) method for the dynamics of free boundaries. *Journal of computational physics, 39*(1), 201-225.

ISO. (2015). ISO 15016:2015 *Ships and marine technology -- Guidelines for the assessment of speed and power performance by analysis of speed trial data*.

Israeli, M., & Orszag, S. A. (1981). Approximation of radiation boundary conditions. *Journal of computational physics, 41*(1), 115-135. doi:http://dx.doi.org/10.1016/0021-9991(81)90082-6

Issa, R. I. (1986). Solution of the implicitly discretised fluid flow equations by operator- splitting. *Journal of computational physics, 62*, 40-65.

ITTC. (2011). Recommended Procedures and Guidlines - Practical Guidelines for Ship CFD Applications. Retrieved from http://ittc.info/downloads/Archive%20of%20recommended%20procedures/2011%20Recommended%20Procedures/7.5-03-02-03.pdf

Jones, W., & Launder, B. (1972). The prediction of laminarization with a two-equation model of turbulence. *International journal of heat and mass transfer, 15*(2), 301-314.

Joosen, W. P. A. (1966). *Added Resistance in Waves 6th Symposium on Naval Hydrodynamics*. Paper presented at the 6th Symposium on Naval Hydrodynamics, Washington.

Kim, W. J., Van, S. H., & Kim, D. H. (2001). Measurement of flows around modern commercial ship models. *Experimental Methods and their Applications to Fluid Flow, 31*(5), 567-578. doi:10.1007/s003480100332

Kreitner, J. (1939). Heave, Pitch and Resistance of Ships in a Seaway. *Transactions of the Royal Institute of Naval Architects,'London, 87*.

Larsson, L., Stern, F., & Visonneau, M. (2010). *Proceedings, Volume II.* Paper presented at the A Workshop on Numerical Ship Hydrodynamics, Gothenburg.

Larsson, L., Stern, F., & Visonneau, M. (2014). Numerical Ship Hydrodynamics.

Lin, P., & Liu, P. L. F. (1999). Internal wave-maker for Navier-Stokes equations models. *Journal of Waterway, Port, Coastal and Ocean Engineering, 125*(4), 207.

Maruo, H. (1957). The excess resistance of a ship in rough seas. *International Shipbuilding Progress, 4*(35), 337-345.

Menter, F. R. (1992). Improved two-equation k-omega turbulence models for aerodynamic flows. *NASA STI/Recon Technical Report N, 93*, 22809.

Muzaferija, S., Peric, M., Sames, P., & Schellin, T. (1998). *A two-fluid Navier-Stokes solver to simulate water entry.* Paper presented at the Proceedings of the 22nd symposium on naval hydrodynamics, Washington, DC.

Osher, S., & Sethian, J. A. (1988). Fronts propagating with curvature-dependent speed: algorithms based on Hamilton-Jacobi formulations. *Journal of computational physics, 79*(1), 12-49.

Park, J. c., Kim, M. h., & Miyata, H. (1999). Fully non-linear free-surface simulations by a 3D viscous numerical wave tank. *International Journal for Numerical Methods in Fluids, 29*(6), 685-703. doi:10.1002/(SICI)1097-0363(19990330)29:6<685::AID-FLD807>3.0.CO;2-D

Patankar, S. V. (1980). *Numerical heat transfer and fluid flow*. Washington: Hemisphere Publ.

Patankar, S. V., & Spalding, D. B. (1972). A calculation procedure for heat, mass and momentum transfer in three-dimensional parabolic flows. *International journal of heat and mass transfer, 15*(10), 1787-1806. doi:10.1016/0017-9310(72)90054-3

Pérez Arribas, F. (2007). Some methods to obtain the added resistance of a ship advancing in waves. *Ocean Engineering, 34*(7), 946-955.

Pierson, J. W. J., & Moskowitz, L. (1963). *A Proposed Spectral Form for Fully Developed Wind Seas Based on the Similarity Theory of S. A. Kitaigorodskii*. Retrieved from

Pletcher, R. H., Tannehill, J. C., & Anderson, D. A. (2013). *Computational fluid mechanics and heat transfer* (3rd ed. ed.). Boca Raton, Fla: CRC Press.

Rørvik, J. (2015). *Investigation of inviscid water waves in numerical wave tank.* (Project thesis), NTNU.

Salvesen, N., Tuck, E., & Faltinsen, O. (1970). Ship motions and sea loads. *Trans. SNAME, 78*, 250-287.

Seo, M.-G., Park, D.-M., Yang, K.-K., & Kim, Y. (2013). Comparative study on computation of ship added resistance in waves. *Ocean Engineering, 73*, 1-15.

Shih, T.-H., Liou, W. W., Shabbir, A., Yang, Z., & Zhu, J. (1995). A new k-ϵ eddy viscosity model for high reynolds number turbulent flows. *Computers & Fluids, 24*(3), 227-238.

Stern, F., Sadat-Hosseini, H., Mousaviraad, M., & Bhushan, S. (2014). Evaluation of Seakeeping Predictions. In L. Larsson, F. Stern, & M. Visonneau (Eds.), *Numerical Ship Hydrodynamics*.

van den Boom, H. H., van der Hout, I. I., & Flikkema, M. M. (2008). *Speed-Power Performance of Ships during Trials and in Service*.

Van Doormaal, J., & Raithby, G. (1984). Enhancements of the SIMPLE method for predicting incompressible fluid flows. *Numerical heat transfer, 7*(2), 147-163.

van Leer, B. (1979). Towards the ultimate conservative difference scheme. V. A second-order sequel to Godunov's method. *Journal of computational physics, 32*(1), 101-136. doi:http://dx.doi.org/10.1016/0021-9991(79)90145-1

Welch, P. (1967). The use of fast Fourier transform for the estimation of power spectra: A method based on time averaging over short, modified periodograms. *Audio and Electroacoustics, IEEE Transactions on, 15*(2), 70-73. doi:10.1109/TAU.1967.1161901

Wilcox, D. C. (1988). Reassessment of the scale-determining equation for advanced turbulence models. *AIAA journal, 26*(11), 1299-1310.

Yang, K.-K., Kim, Y., & Nam, B.-W. (2015). Cartesian-grid-based computational analysis for added resistance in waves. *Official Journal of the Japan Society of Naval Architects and Ocean Engineers (JASNAOE), 20*(1), 155-170.

9 List of appendices

Time series for regular head wave conditions

Case C3

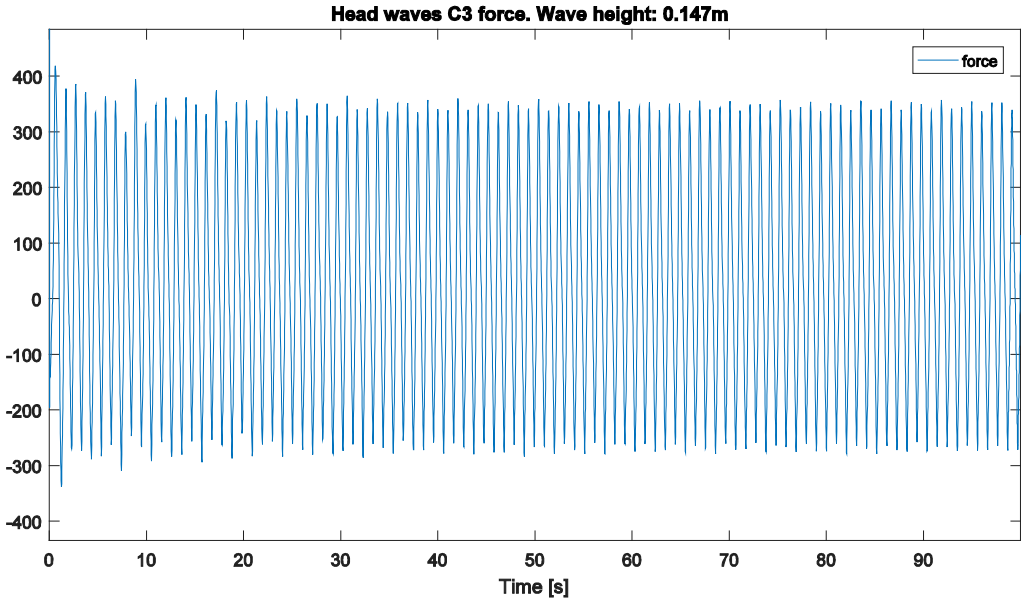

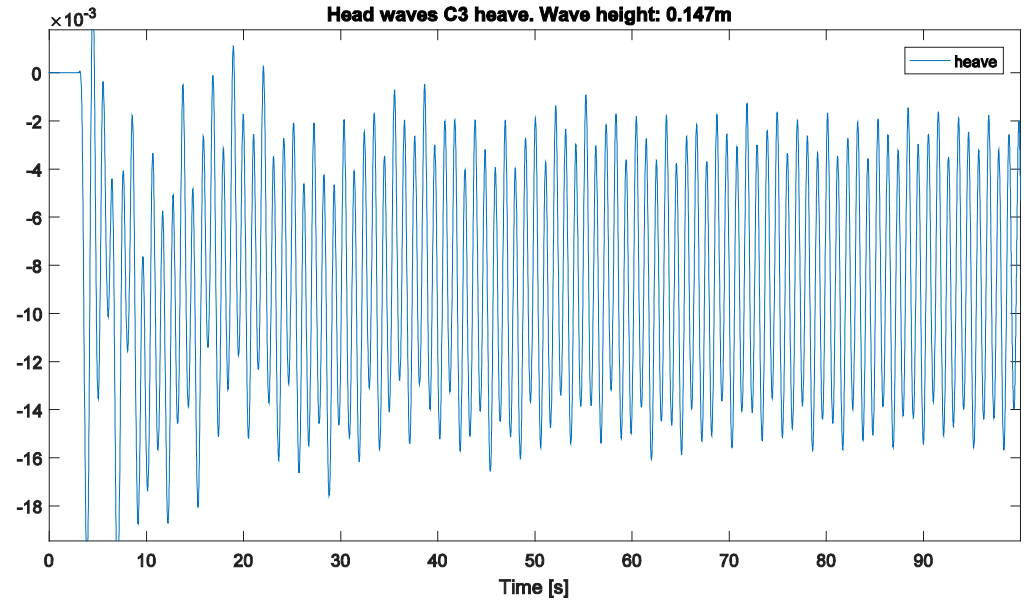

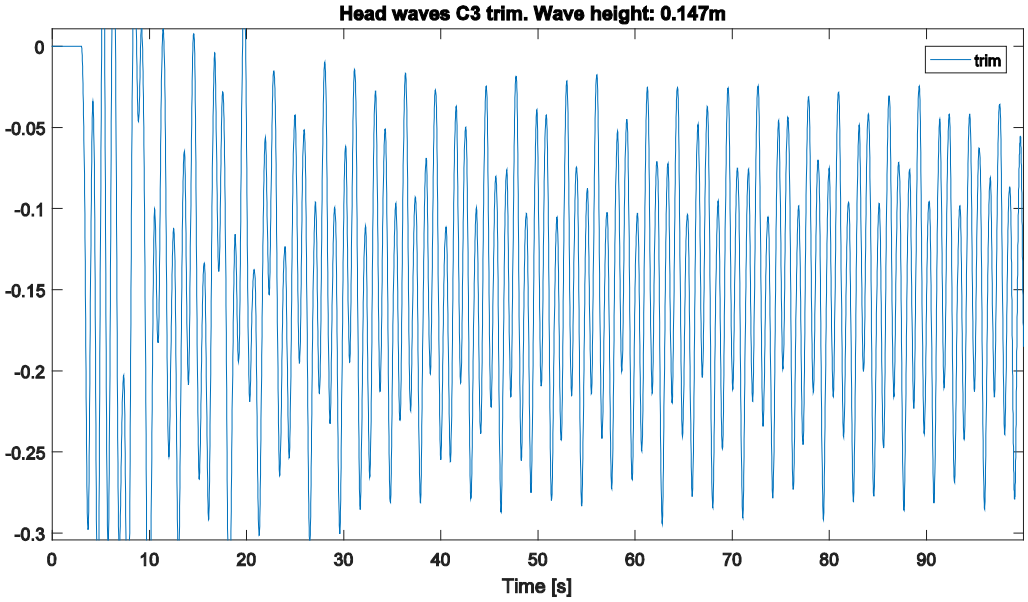
Head waves C3 trim. Wave height: 0.147m
trim
0
-0.05
-0.1
-0.15
-0.2
-0.25
-0.3
0
10
20
30
40
50
60
70
80
90
Time [s]

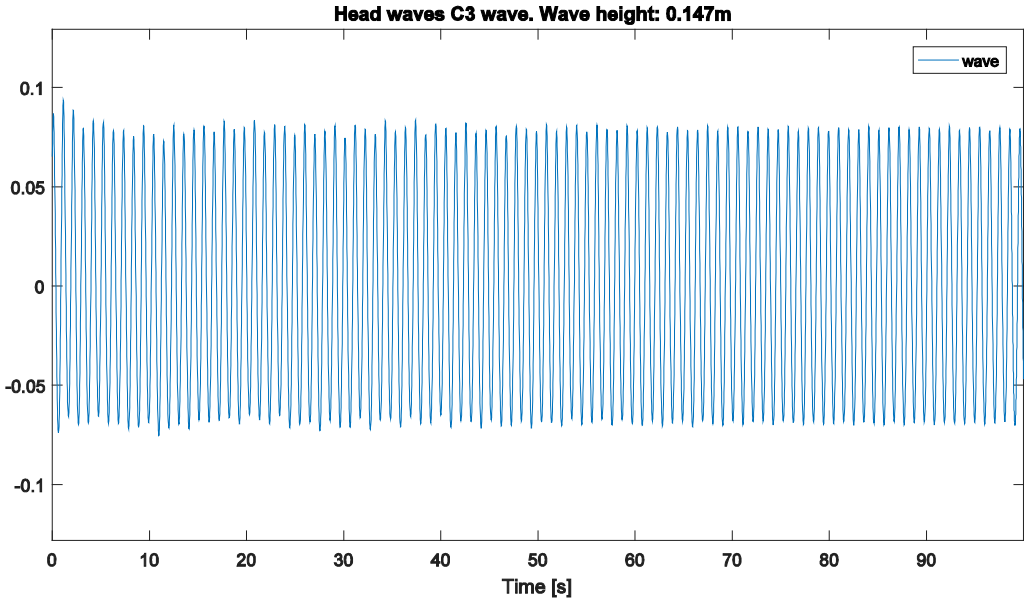
Head waves C3 wave. Wave height: 0.147m
wave
0.1
0.05
0
-0.05
-0.1
0
10
20
30
40
50
60
70
80
90
Time [s]

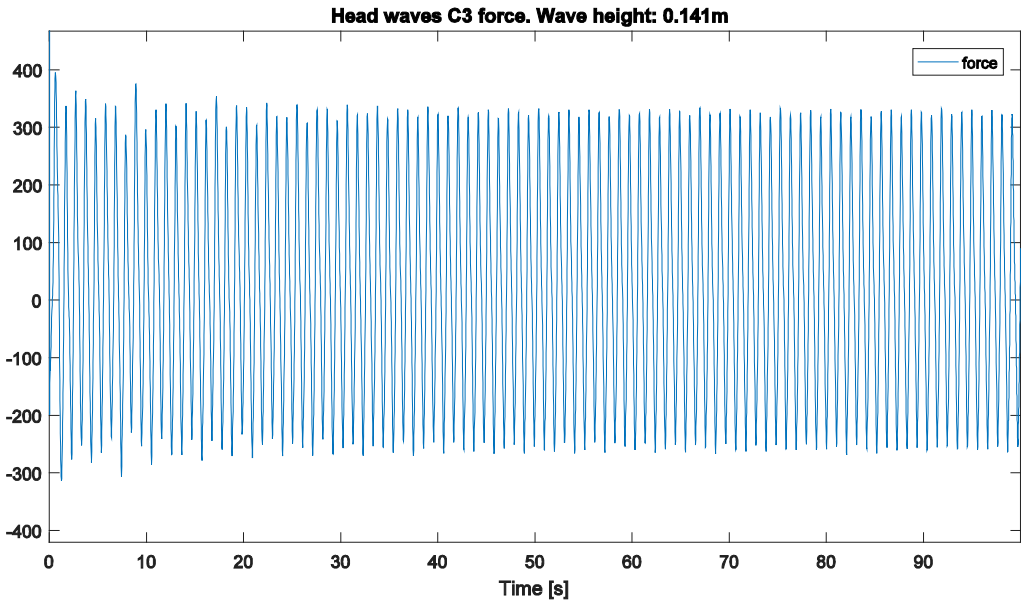
Head waves C3 force. Wave height: 0.141m
force
400
300
200
100
0
-100
-200
-300
-400
0
10
20
30
40
50
60
70
80
90
Time [s]

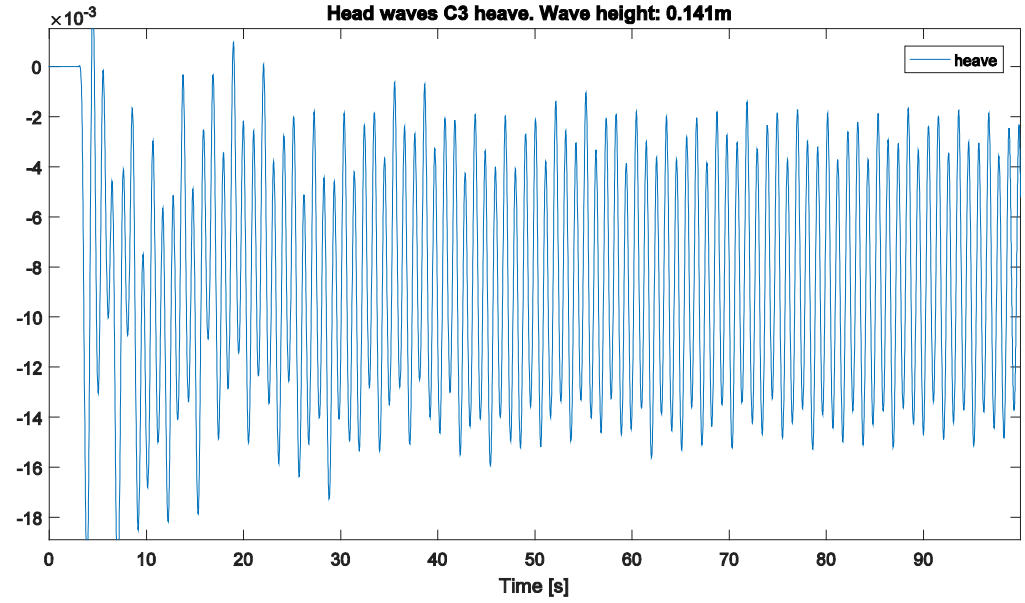
Head waves C3 heave. Wave height: 0.141m
×10-3
heave
0
-2
-4
-6
-8
-10
-12
-14
-16
-18
0
10
20
30
40
50
60
70
80
90
Time [s]

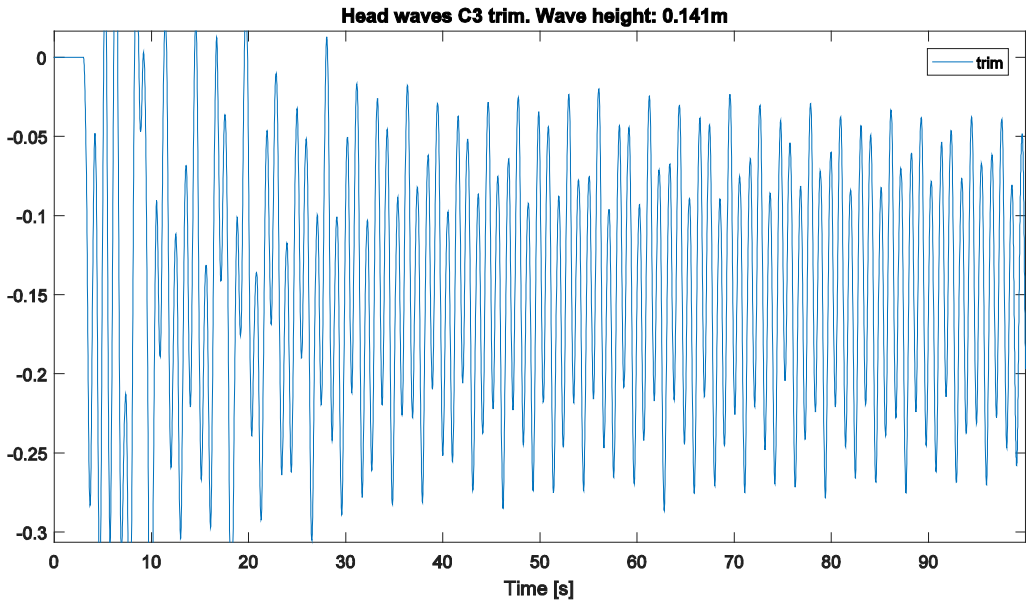
Head waves C3 trim. Wave height: 0.141m
trim
0
-0.05
-0.1
-0.15
-0.2
-0.25
-0.3
0
10
20
30
40
50
60
70
80
90
Time [s]

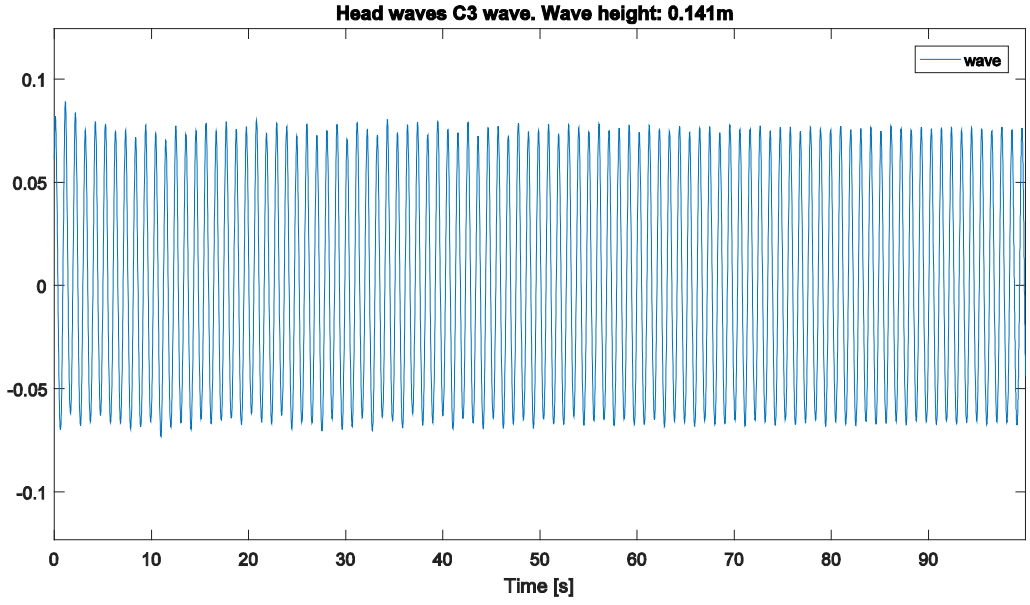
Head waves C3 wave. Wave height: 0.141m
wave
0.1
0.05
0
-0.05
-0.1
0
10
20
30
40
50
60
70
80
90
Time [s]

Case C4

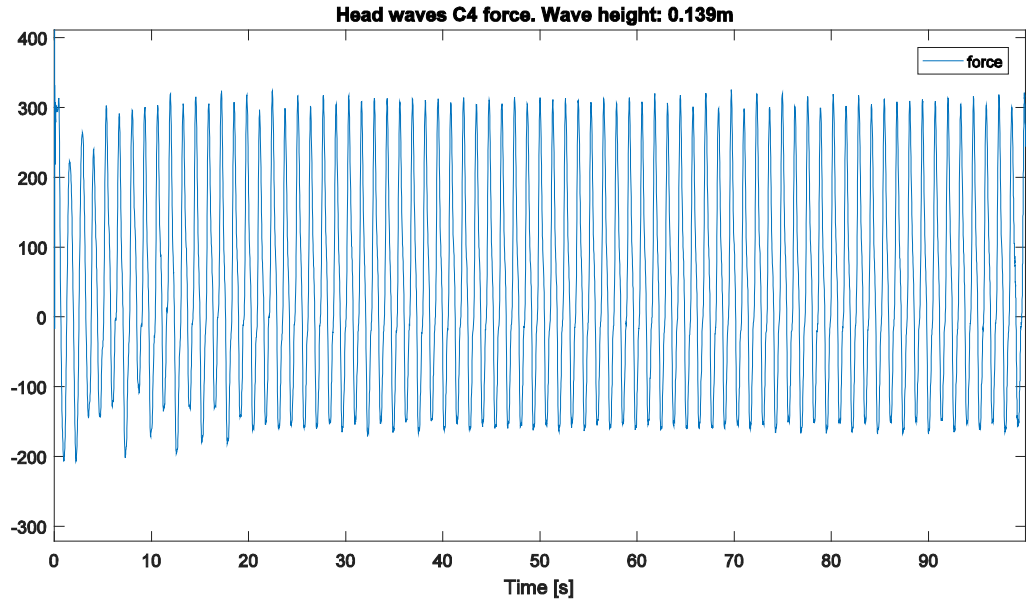
Head waves C4 force. Wave height: 0.139m
force
400
300
200
100
0
-100
-200
-300
0
10
20
30
40
50
60
70
80
90
Time [s]

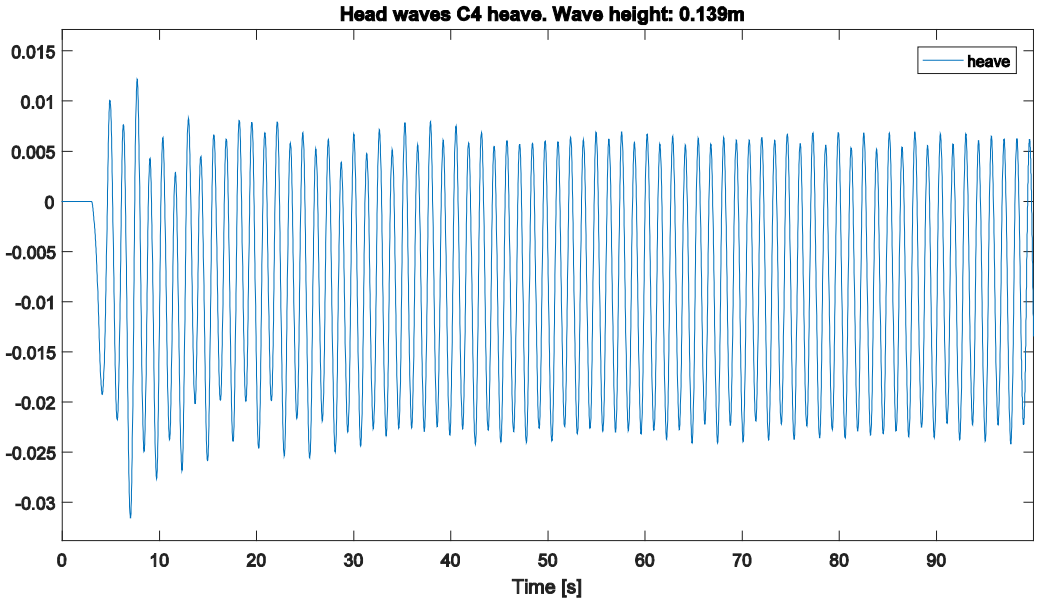
Head waves C4 heave. Wave height: 0.139m
heave
0.015
0.01
0.005
0
-0.005
-0.01
-0.015
-0.02
-0.025
-0.03
0
10
20
30
40
50
60
70
80
90
Time [s]

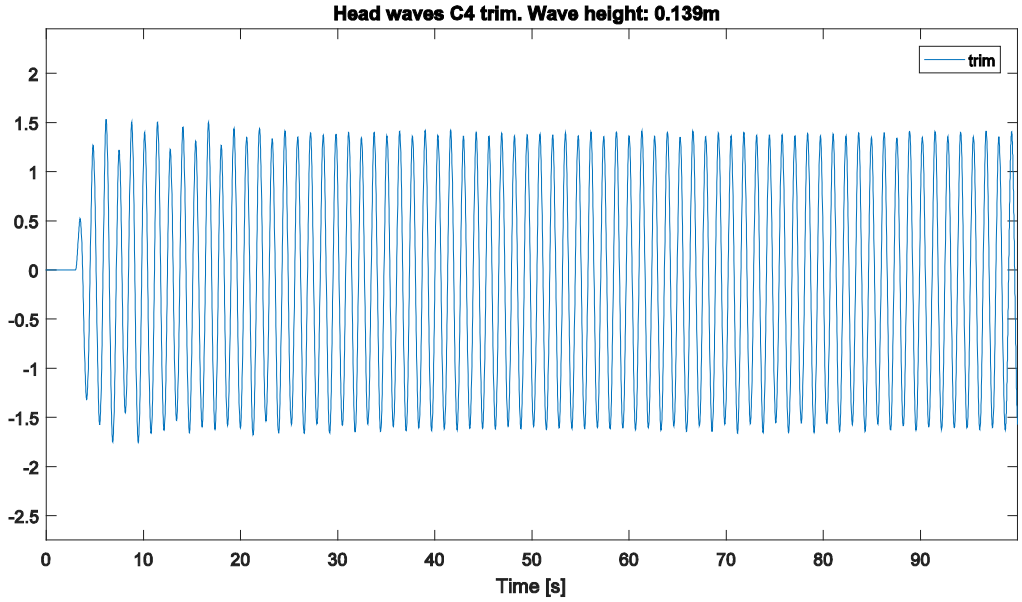
Head waves C4 trim. Wave height: 0.139m
trim
2
1.5
1
0.5
0
-0.5
-1
-1.5
-2
-2.5
0
10
20
30
40
50
60
70
80
90
Time [s]

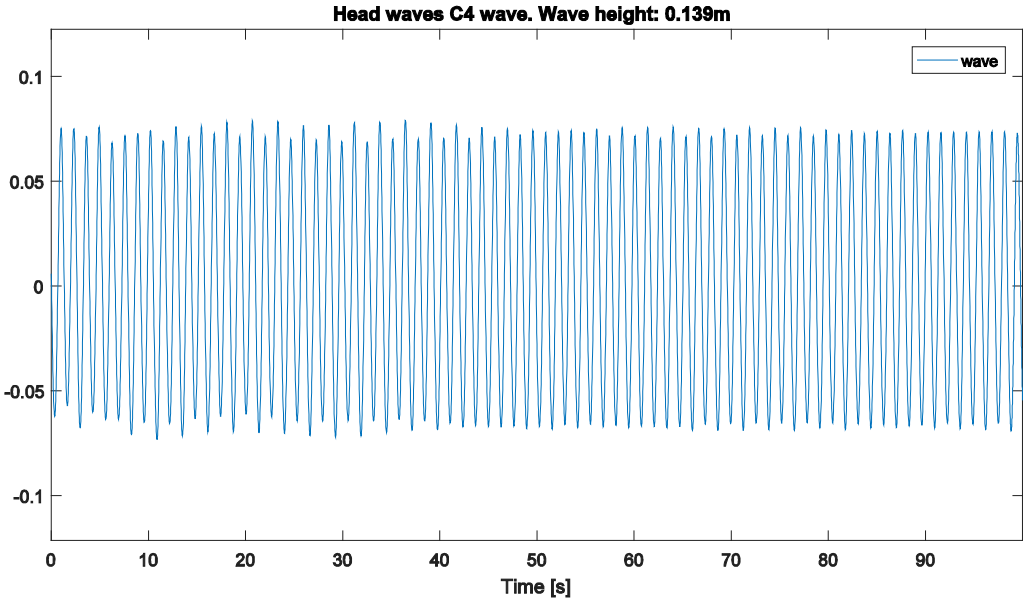
Head waves C4 wave. Wave height: 0.139m
wave
0.1
0.05
0
-0.05
-0.1
0
10
20
30
40
50
60
70
80
90
Time [s]

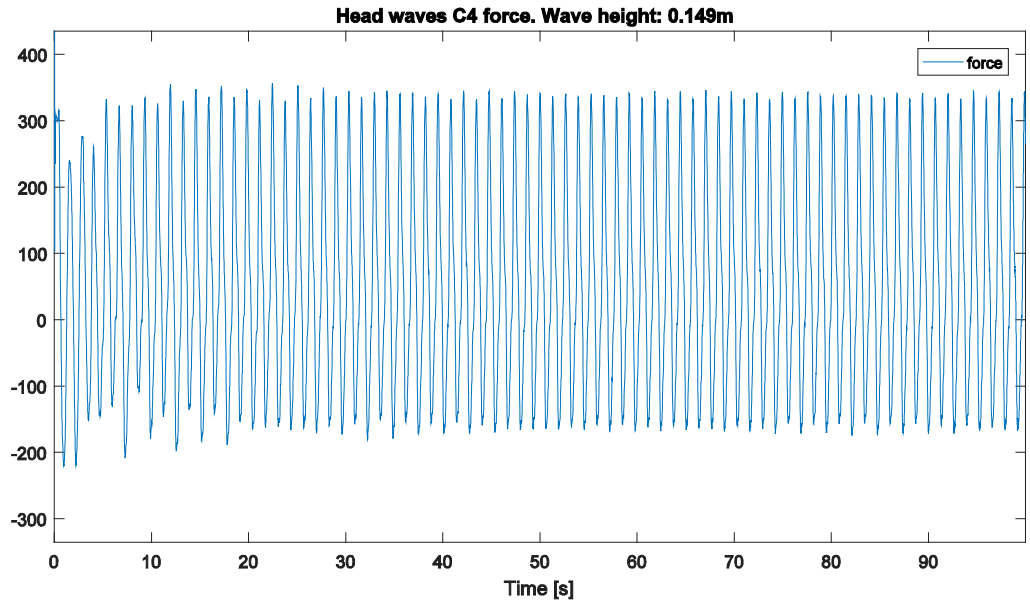
Head waves C4 force. Wave height: 0.149m
force
400
300
200
100
0
-100
-200
-300
0
10
20
30
40
50
60
70
80
90
Time [s]

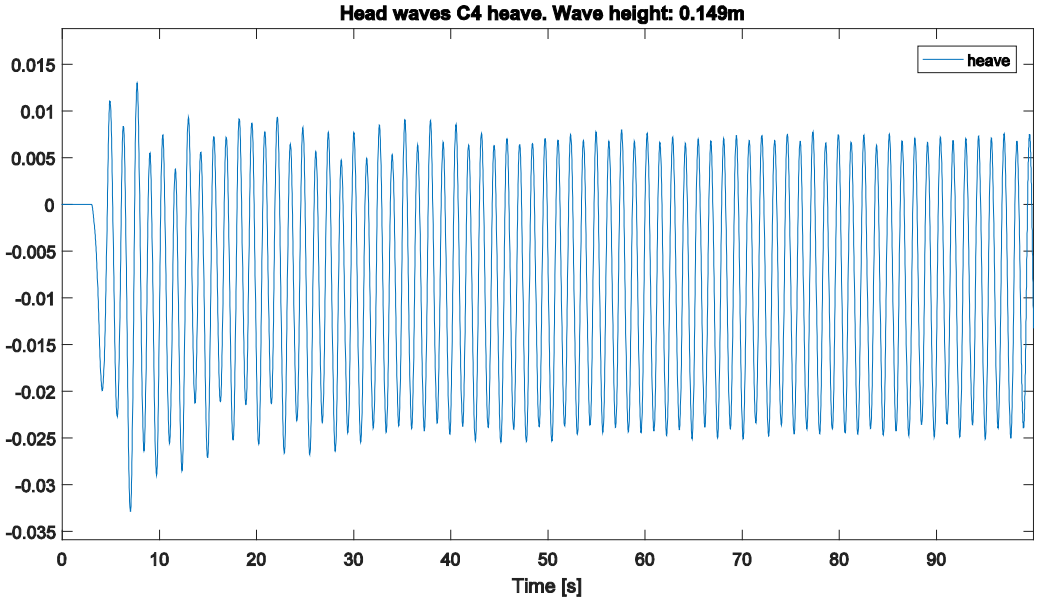
Head waves C4 heave. Wave height: 0.149m
heave
0.015
0.01
0.005
0
-0.005
-0.01
-0.015
-0.02
-0.025
-0.03
-0.035
0
10
20
30
40
50
60
70
80
90
Time [s]

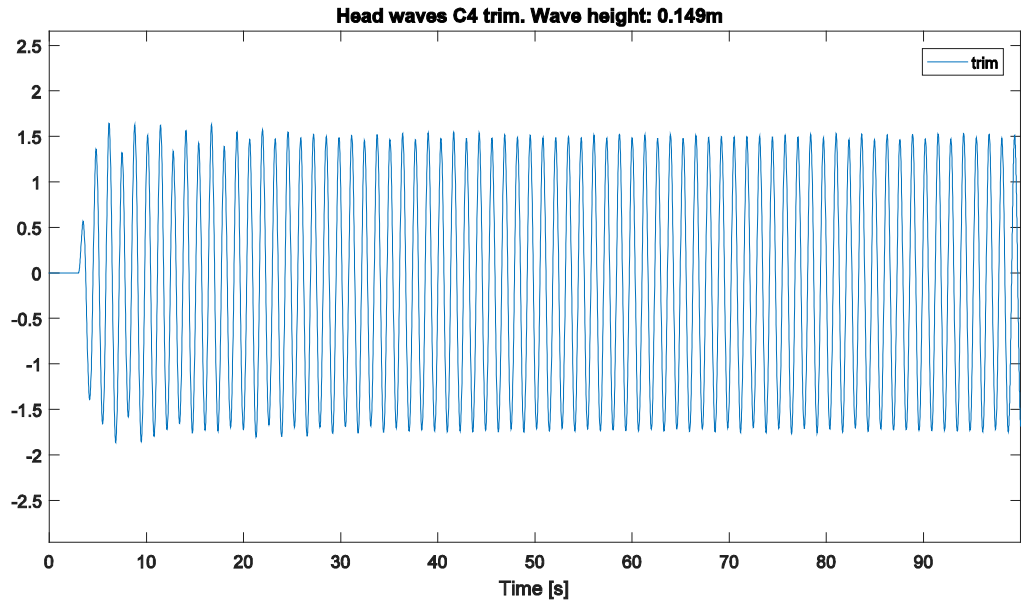
Head waves C4 trim. Wave height: 0.149m
trim
2.5
2
1.5
1
0.5
0
-0.5
-1
-1.5
-2
-2.5
0
10
20
30
40
50
60
70
80
90
Time [s]

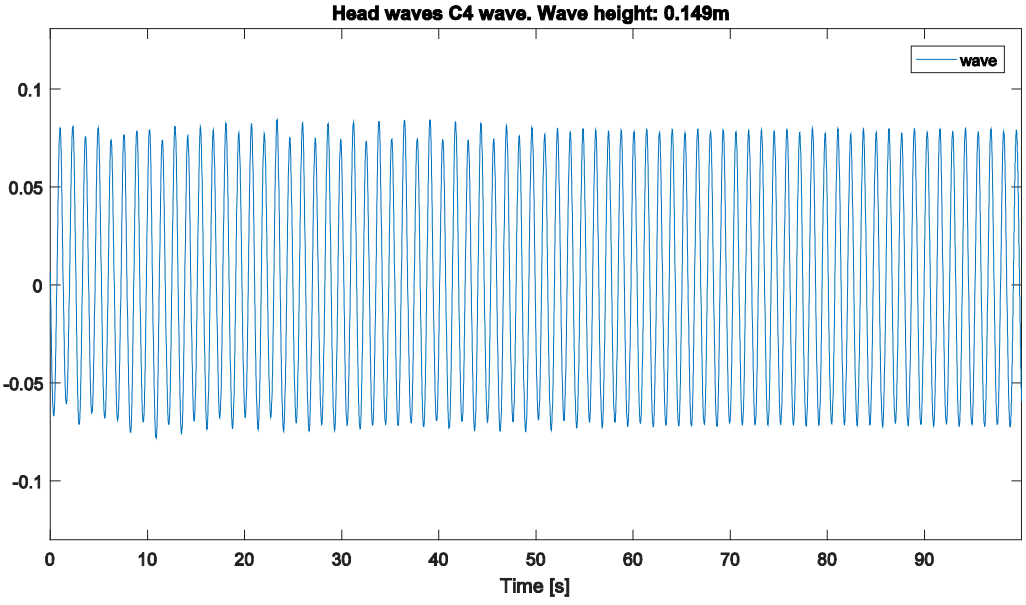
Head waves C4 wave. Wave height: 0.149m
wave
0.1
0.05
0
-0.05
-0.1
0
10
20
30
40
50
60
70
80
90
Time [s]

Case C5

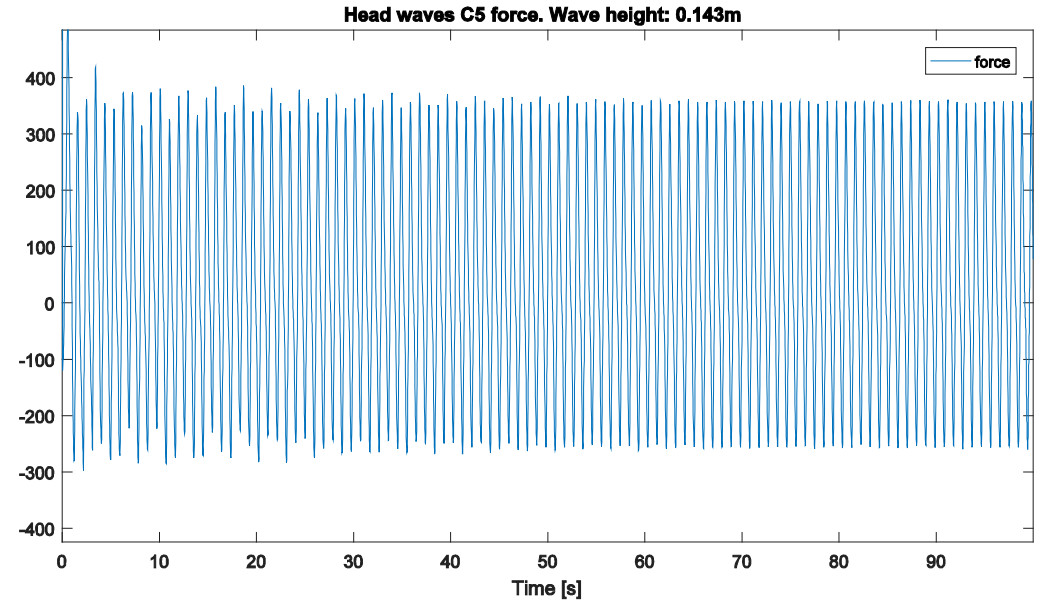
Head waves C5 force. Wave height: 0.143m
force
400
300
200
100
0
-100
-200
-300
-400
0
10
20
30
40
50
60
70
80
90
Time [s]

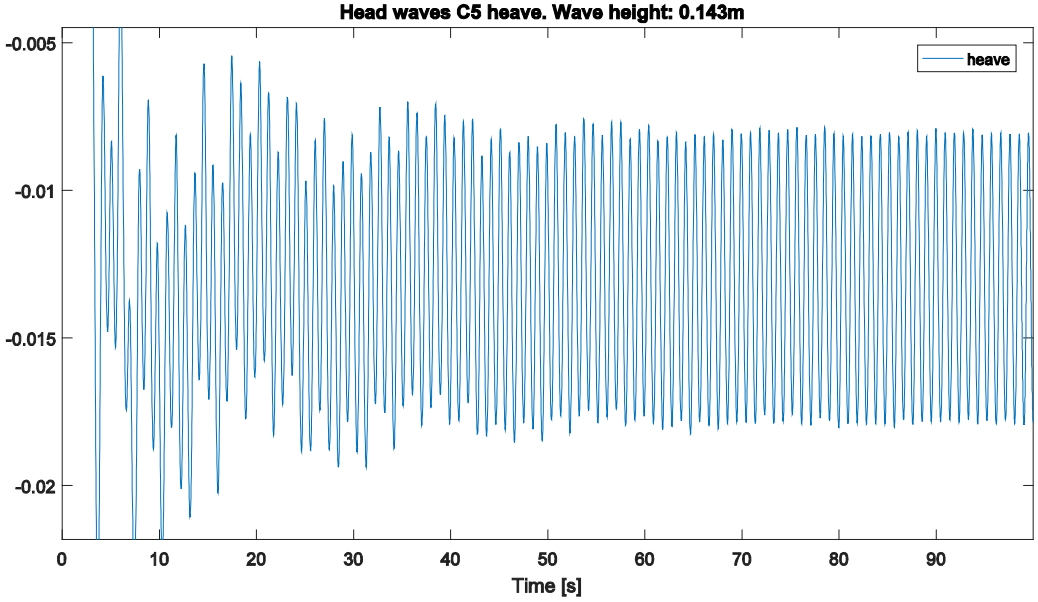
Head waves C5 heave. Wave height: 0.143m
heave
-0.005
-0.01
-0.015
-0.02
0
10
20
30
40
50
60
70
80
90
Time [s]

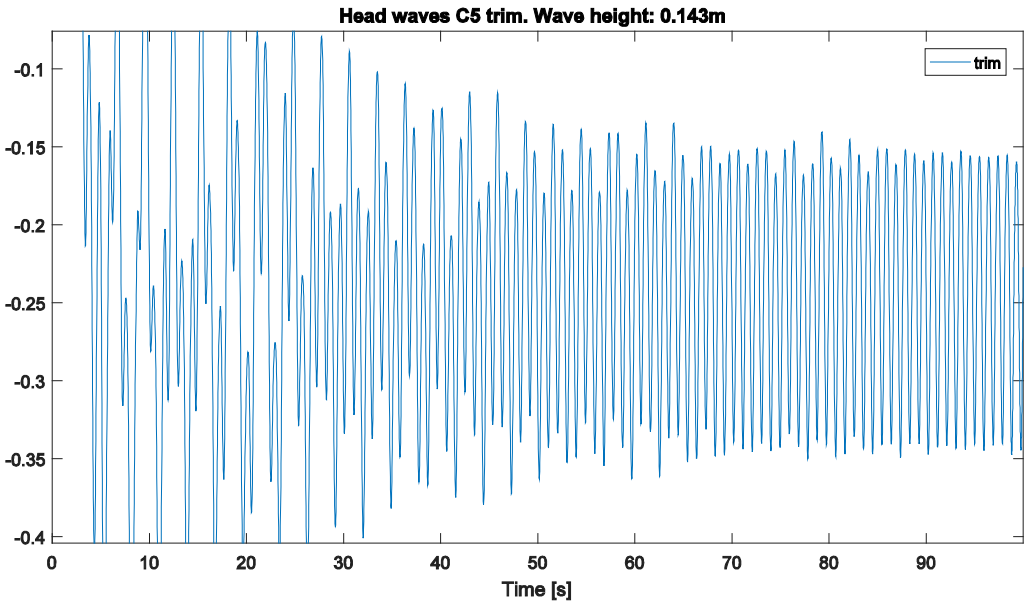
Head waves C5 trim. Wave height: 0.143m
trim
-0.1
-0.15
-0.2
-0.25
-0.3
-0.35
-0.4
0
10
20
30
40
50
60
70
80
90
Time [s]

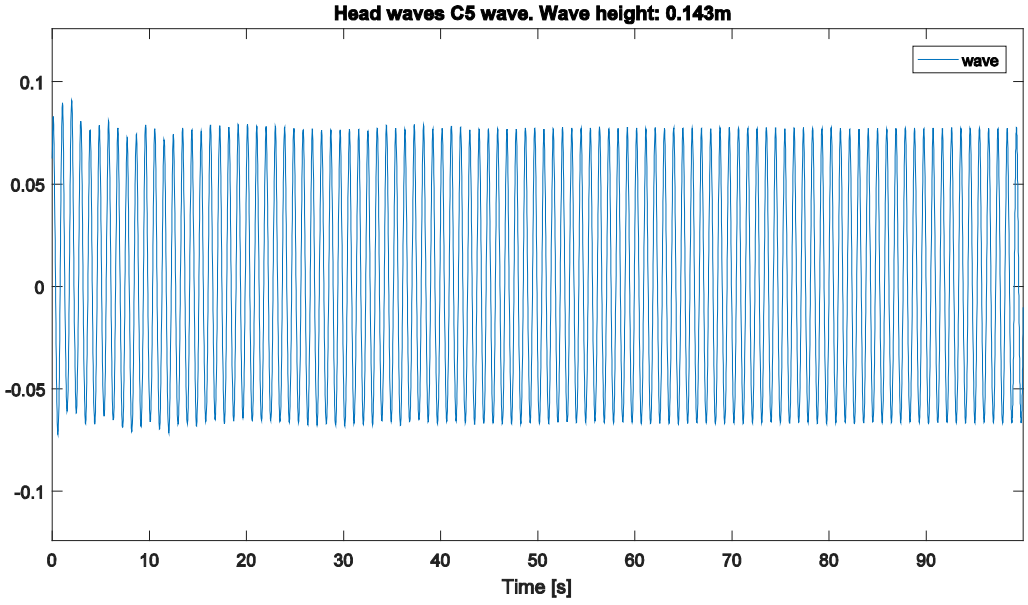
Head waves C5 wave. Wave height: 0.143m
wave
0.1
0.05
0
-0.05
-0.1
0
10
20
30
40
50
60
70
80
90
Time [s]

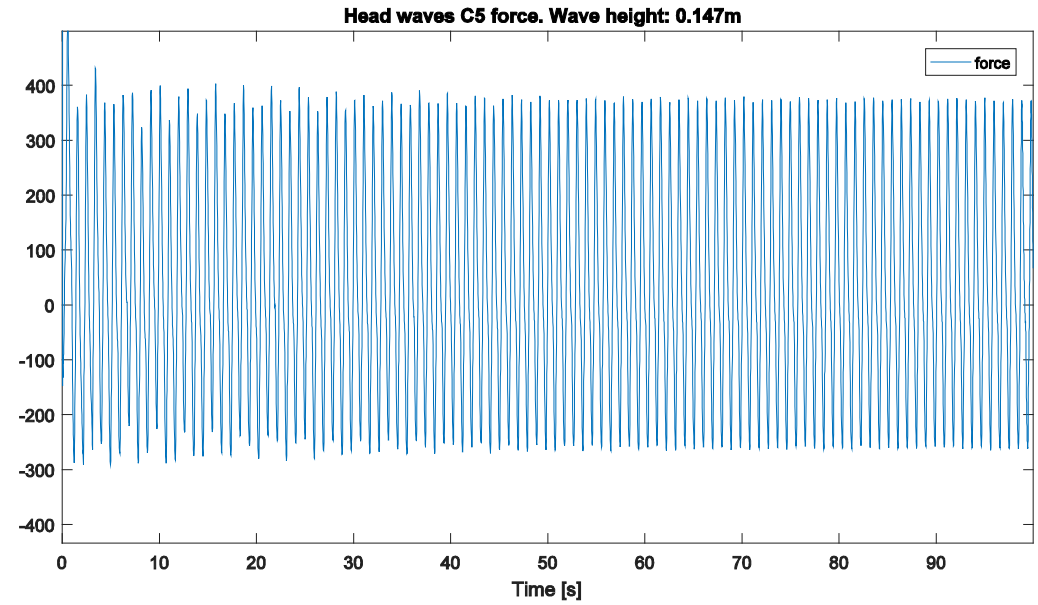
Head waves C5 force. Wave height: 0.147m
force
400
300
200
100
0
-100
-200
-300
-400
0
10
20
30
40
50
60
70
80
90
Time [s]

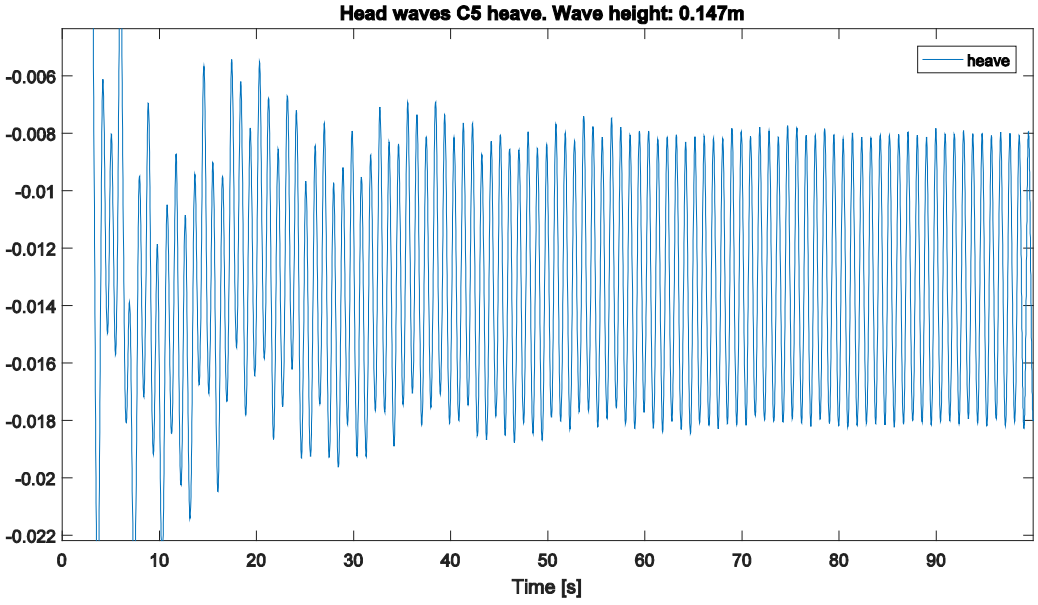
Head waves C5 heave. Wave height: 0.147m
heave
-0.006
-0.008
-0.01
-0.012
-0.014
-0.016
-0.018
-0.02
-0.022
0
10
20
30
40
50
60
70
80
90
Time [s]

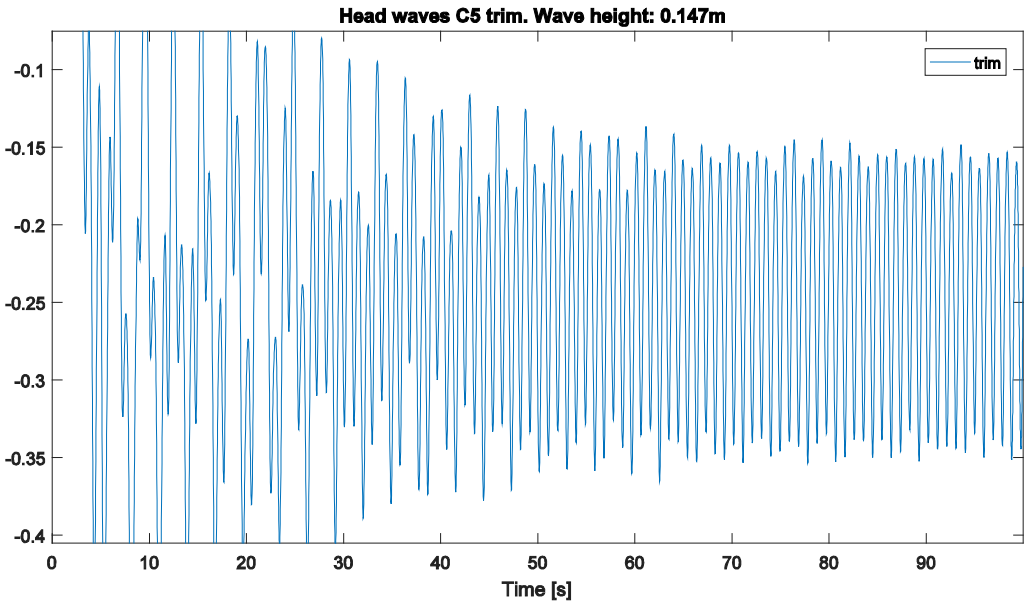
Head waves C5 trim. Wave height: 0.147m
trim
-0.1
-0.15
-0.2
-0.25
-0.3
-0.35
-0.4
0
10
20
30
40
50
60
70
80
90
Time [s]

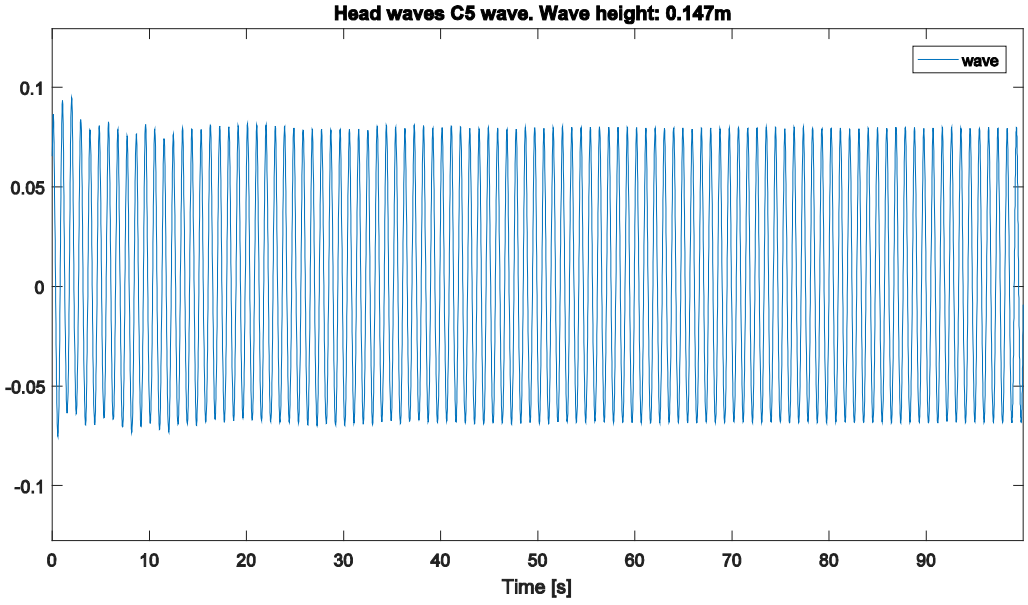
Head waves C5 wave. Wave height: 0.147m
wave
0.1
0.05
0
-0.05
-0.1
0
10
20
30
40
50
60
70
80
90
Time [s]

RAO from irregular JONSWAP head waves

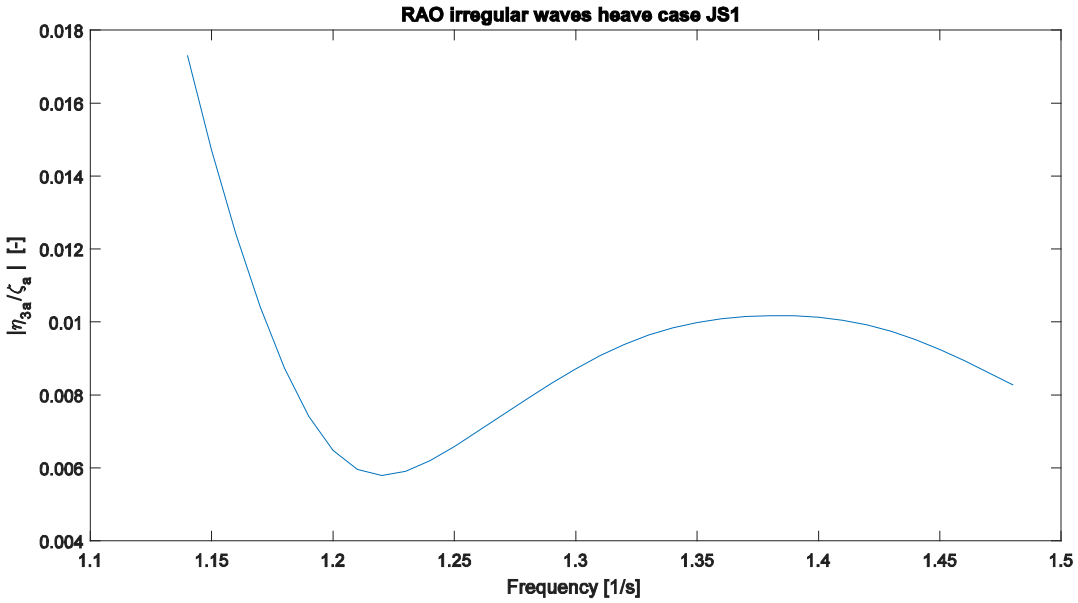

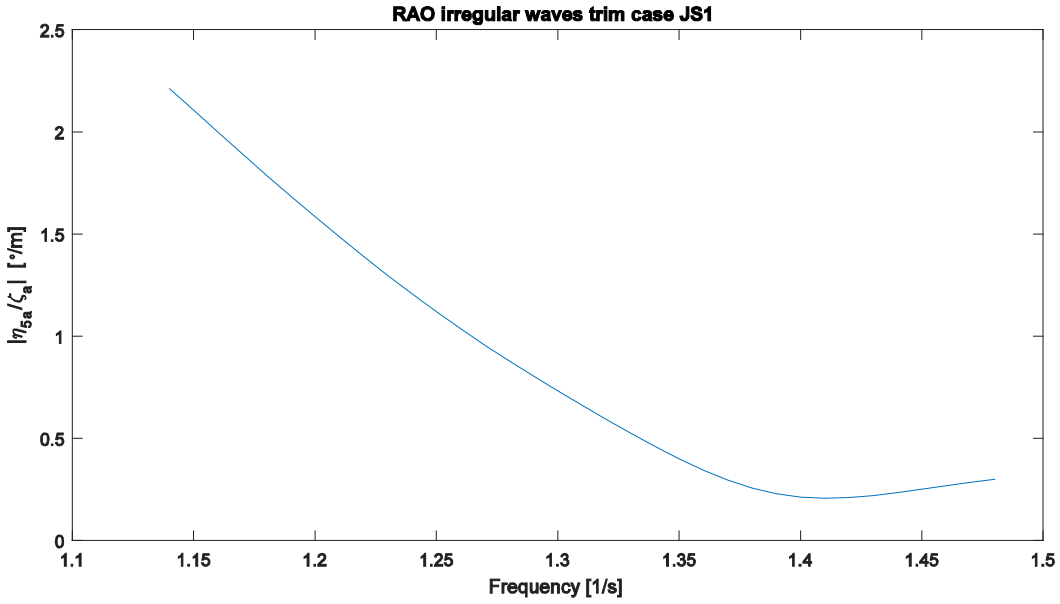

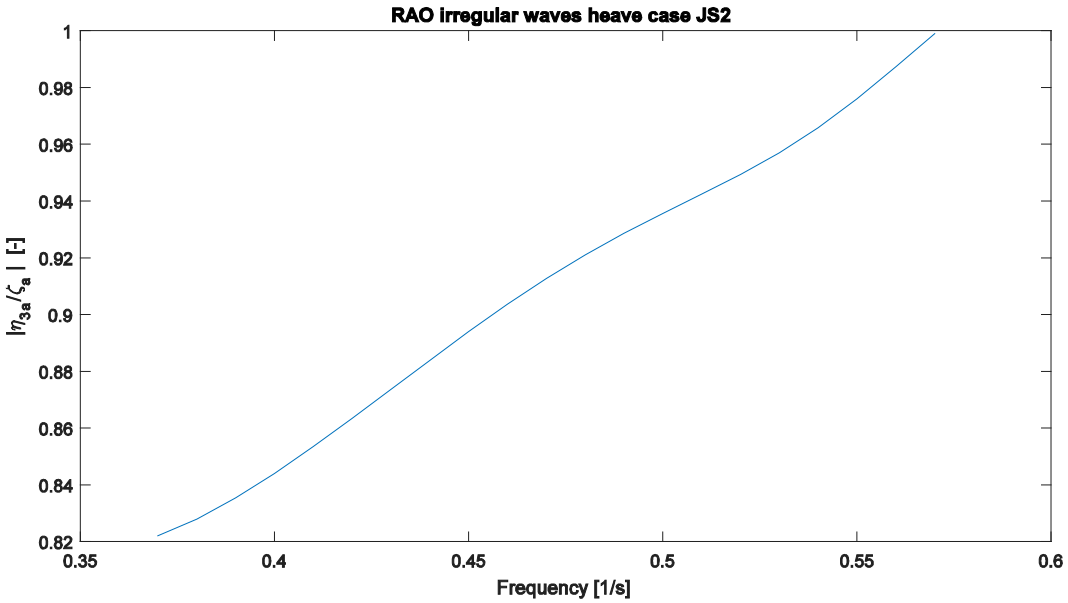
RAO irregular waves heave case JS2
1
0.98
0.96
0.94
0.92
0.9
0.88
0.86
0.84
0.82
|η3a/ζa | [-]
0.35
0.4
0.45
0.5
0.55
0.6
Frequency [1/s]

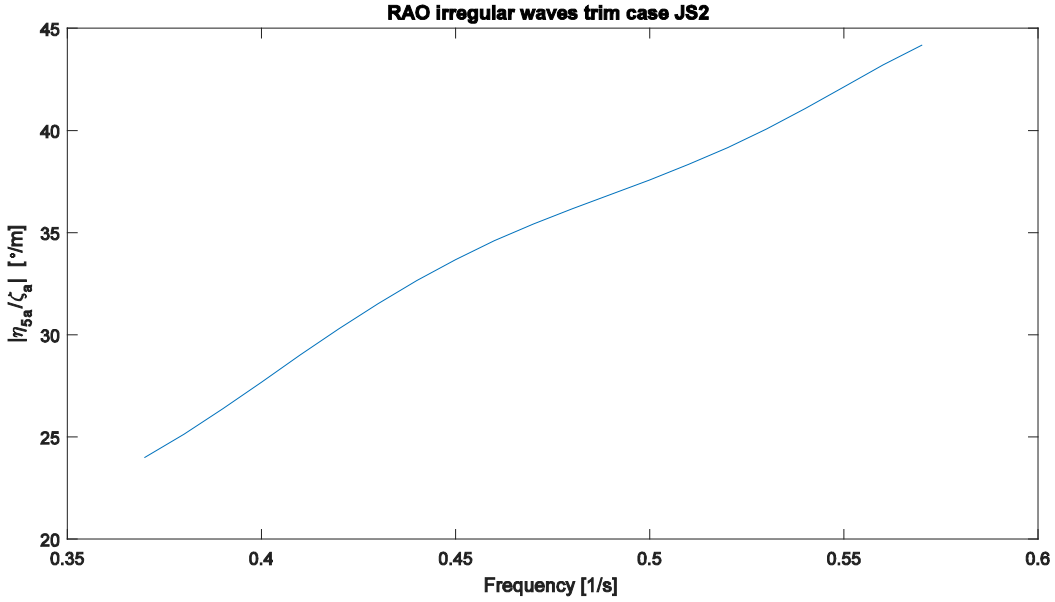
RAO irregular waves trim case JS2
45
40
35
30
25
20
|η5a/ζa| [°/m]
0.35
0.4
0.45
0.5
0.55
0.6
Frequency [1/s]